REAL TIME FLOOD MODELLING IN SOUTHERN PERIYAR RIVER BASIN USING HEC-RTS MODELLING FRAMEWORK

Director

Dr. J. V. Tyagi

Head

Dr. Sanjay Kumar Jain

Study Team:

Dr. Vishal Singh, Scientist C (PI)

Dr. Anil K. Lohani, Scientist G (Co-PI)

Water Resources System Division

National Institute of Hydrology

Roorkee – 247667

June, 2021

TABLE OF CONTENTS

LIST OF FIGURES

LIST OF TABLES

ABBREVIATIONS & ACRONYMS

IPCC	Intergovernmental Panel on Climate Change
1D	One Dimensional
2D	Two Dimensional
HEC-RTS	Hydrologic Engineering System-Real Time Simulation
RESSIM	Reservoir Simulation
HEC-HMS	HEC-Hydrologic Modeling System
HEC-RAS	HEC-River Analysis System
SWAT	Soil Water Assessment Tool
GLOF	Glacial Lake Outburst Flood
CARTOSAT	Cartographic Satellite
DEM	Digital Elevation Model
DTM	Digital Terrain Model
LISS	Linear Imaging Spectral Scanner
LiDAR	Linear Detection and Ranging
GIS	Geographical Information System
GPM	Global Precipitation Measurement
IMD	Indian Meteorological Department
cm	Centimetre
cumec	Meter cube per second
CN	Curve Number
X-section	Cross Section
CWC	Central Water Commission
m	meter
DSS	Decision Support System
TIN	Triangular Irregular Network
SMA	Soil Moisture Accounting
ET	Evapotranspiration
hr	Hour
cms	Meter Cube Per Second
FFA	Flood Frequency Analysis
RP	Return Period
RMSE	Root Mean Squared Error
MSE	Mean Squared Error
LogPT3	Log Pearson Type 3
HEs	Historical Events
km	Kilometre
Riv	River
IA	Initial Abstraction
Sub	Subbasin
RCs	Rating Curves
Q	Discharge
Tribut	Tributary
W.S.El.	Water Surface Elevation
CDF	Cumulative Density Function
RFA	Rainfall Frequency Analysis
Std. Dev.	Standard Deviation
MoM	Method of Moments
Sk C	Skewness Coefficient

CHAPTER 1: INTRODUCTION

EXECUTIVE SUMMARY

This study has been undertaken to study the flood discharge and flood inundation scenarios in the Periyar river basin, Kerala India. In India, recently severe flood disaster events occurred due to the extreme rainfall conditions such as Kerala Flood (2018), Chennai Flood (2015), Bengaluru Flood (2018) etc. The climate is changing over the last 3-4 decades and therefore, the prediction of rainfall and monsoon pattern is becoming highly uncertain in the current scenario, especially in South Asia (Hunt and Menon, 2020; Sudheer et al., 2019; Ali et al., 2019). The exponentially increasing impact of flooding has raised the profile of the practice of flood forecasting and inundation mapping. There have been significant advancements in flood inundation modelling which have been over the past few decades. The understanding of the processes controlling runoff and flood wave propagation, in simulation techniques, in uncertainty handling, and in the provision of new data sources are required to perform flood modeling.

The role of flood warning systems in flood mitigation tool is extremely important in flood prone areas, in which existing flood control infrastructure was proven insufficient to protect vulnerable areas from inundation, based on reported flood damages from severe storms in recent years. To address these inadequacies, a research study to develop a real-time, catchment-based flood modeling system on the Periyar river basin has been applied and proposed using an integrated HEC-RTS (Real Time Simulation) system with 1D and 2D flood modeling simulations. HEC-RTS is designed to integrate various HEC software including HMS, ResSim, RAS, and FIA with a flexible API (Application Programming Interface) that allows for scripting-based retrieval of observed and forecasted precipitation data and real-time production of different forecasting products.

Once the model is setup and optimized with different extreme high flood and normal conditions, including reservoir operations, the forecasted rainfall and discharge can be input to the model and model will generate the real time and stochastic scenarios of flood discharge in the selected river basin. Results showed that the integrated approach is found capable to generate historical flood events using real time hydo-meteorological datasets. Probabilistic flood inundation maps have produced based on the different return periods flood flows i.e. generated through flood frequency analysis (FFA). The hydrodynamic flood routing using 1D and 2D approaches are performed in the downstream portion of Periyar river basin to generate real time flood flows. The modelling outcomes compared with the available reference datasets and the study results well matched.

1.1 HYDROLOGICAL MODELING

A watershed is a natural unit of land from which the surface, sub-surface and groundwater runoff drain to a common/single outlet. The watershed hydrology can be defined as that branch of hydrology that deals with the integration of hydrological processes (such as precipitation, evaporation, condensation,

transpiration, the water budget, infiltration, antecedent moisture condition, time of concentration, interception, return period, environmental flow, overland flow etc.) at the watershed scale to determine the watershed response (Devia et al., 2015). The analysis of different components of water cycle oy hydrological cycle as an independent-dependent variable through advance modeling tools is referred as hydrological modeling. The hydrological modeling follows the law of conservation of mass (or continuity equation) (Devia et al., 2015; Refsgaard and Knudsen, 1996). A numbers of hydrological models with unique and common characteristics that are being developed day by day including analytical models; deterministic models; dynamic models; empirical models; heuristic models; interactive models; linear and nonlinear models; numerical models; probabilistic (stochastic) models; semi-empirical models; simulation models and theoretical models (Devia et al., 2015; Refsgaard and Knudsen, 1996). Mostly hydrological models are fed with precipitation grids at regular intervals throughout the length of the simulation. Some popular hydrological models such as SWAT, HEC-HMS, VIC, SPHY, SNOWMOD, MIKE NAM etc. have been used worldwide for various snow-eco-glacio-geo-hydrological processes (Yang et al., 2020; Sood and Smakhtin, 2015). Although, the complexities in the hydrologic modeling over large space and long times have prompted a significant need for model calibration or parameter optimization.

1.2 HYDRODYNAMIC MODELING

The space–time variation of flow and water level in the rivers are computed using St. Venant equations. The principle of hydraulic routing of river flow has been applied to many river basins worldwide. Models such as MIKE 11HD, HEC-RAS and LISSFLOD-FP have been categorized as hydraulic models, which use the above numerical methods to compute flow and water level at different grid points along the rivers (Devia et al., 2015; Refsgaard and Knudsen, 1996). The results from hydraulic or hydrodynamic models can be utilized in flood risk mapping, flood damage assessment, water resource planning, real time flood forecasting, flood related engineering, sediment transportation, floodplain ecological modeling and mapping, river system hydrology and analysis. Although, an accurate flood modelling at high spatio-temporal resolutions remains a significant challenge in any hydrologic and hydraulic studies due to the complex and chaotic nature of flooding and uncertainty associated with the conceptualization of processes. Probabilistic flood inundation maps could help in designing the flood risk management plans and their implementations. Preparedness activities and timely reply can be commenced if the forecast information comes with the level of impact of flood. In recovery and damage assessment also, the flood risk mapping can play a crucial role.

1.3 CLIMATE CHANGE IMPACTS ON RAINFALL

Changes in the atmospheric abundance of greenhouse gases and aerosols, in solar radiation and in land surface properties alter the energy balance of the climate system. In the recent time, climate extremes, warming air temperature, droughts, floods, cyclones, and GLOF (Glacial Lake Outburst Flood) revealed significant vulnerability and exposures of some ecosystems and many human systems to current climate variability. As per the IPCC reports, it is also mentioned that the frequency and

intensity of meteorological factors will be enhanced in 21st century. The drought will be more severe in the low rainfall regions and the intensity and amount of precipitation extreme event will be enhanced in the high rainfall regions around the world (Singh and Goyal, 2020; Ali et al., 2019). The negative consequences of climate change such as warmer water, more intense precipitation, and longer periods of low flow in the rainfall dependent catchment could be greater during 21st century as per the predicted emission scenarios (Ali et al., 2019; Mukherjee et al., 2018). A significant increment in rainfall intensities have been observed in most of the climate change-water studies, though their severity may higher and lower at some place and it varied from region to region (Gupta et al., 2020; Mukherjee et al., 2018).

1.4 RAINFALL EXTREME EVENTS

1.4.1 Floods

India has been categorized as one of the most flood vulnerable regions in the South Asia. The frequency of extreme flood events is on the rise in India. Although, the historical extreme flood events fall within the range of climate variability, but magnitude, frequency and extent of flooding can be increased in future due to climate change. The effects of climate change on floods may influence flood risk reduction priorities and may lead to increased flood hazard at many flood prone locations. Several recent striking examples of extreme flood events are the floods faced in Kerala (2018), Kerala (2019), Chennai (2015), Jammu and Kashmir (2014), Kedarnath (2013), Leh (2010), and Mumbai (2005) (Mohanty et al., 2020; Ali et al., 2019).

The common causes of occurrence of floods in this country are: high intensity based precipitation of shorter duration; cyclones with high speed wind velocity; urban flooding due to increasing imperviousness and blockage of natural drainages; low flow carrying capacity due to the presence of sediment within river banks for containing the high flood flows as well as silting of the river beds; landslides in hilly areas and meandering of the river water way in plain areas; drainage congestion due to many reasons; heavy rainfall and flash floods like cloudburst conditions, especially in Himalayas; dam break flood due to GLOF; floods in coastal areas; reduced velocity of flow due to tidal well as backwater effects etc (Dubey and Goyal, 2020). Many studies have shown that in future climate change will aggravate flooding problems in India as the temperatures are increasing over South Asia region.

1.4.2 Droughts

The global warming has triggered many changes to the Earth's climate resulting in changes in the characteristics of the extreme weather and climate events. Although, the impacts of the drought events are not visible initially as in the case of floods, but droughts have the potential to cause considerable changes to the ecosystem and society of a region. In recent past, the extreme drought frequency has increased considerably in many countries (Otkin et al., 2018; Mishra et al., 2018). The higher temperature in future time horizons will lead to changes in the rainfall pattern, higher rainfall

variability along with higher evaporation and evapotranspiration. The high variability in the rainfall is expected to result in water scarcity and meteorological droughts whereas an increase in evaporation because of higher temperatures may result in higher occurrences of hydrological and agricultural droughts. Many studies on droughts have shown that climate change has the potential to increase drought disasters, by subjecting various regions across the globe to much higher levels of drought frequency and severity. Droughts are usually classified into four types, viz., meteorological, hydrological, agricultural, and socio-economic droughts. The meteorological drought can be defined in terms of the magnitude of shortfall from normal rainfall and duration of the shortfall event. Agricultural drought can be linked to the meteorological drought and it occurs when the shortage of soil moisture adversely affects the agricultural production because of higher evapotranspiration losses that have not been properly met (Mishra et al., 2018). The hydrological drought is related to meteorological droughts which influence the surface water and groundwater availability. The hydrological droughts lag the meteorological and agricultural droughts. The socioeconomic drought is associated with the supply and demand of some economic goods with elements of meteorological, agricultural, and hydrological drought.

1.5 APPLICATIONS OF REMOTE SENSING AND GIS IN FLOOD MODELING

In recent past there have been a number of significant flood events have happened all around the World which have caused enormous damages both in terms of loss of life and economics. Remote sensing and GIS technologies have been enabled us to handle the complexity involved in the development and maintenance of flood management systems. The applicability and unique capabilities of remote sensing satellites to provide comprehensive, synoptic and multi-temporal coverage of very large areas at regular interval and with quick turnaround time have been very valuable in monitoring and managing flood dynamics. The flood inundation or spread areas, which can be extended from meters to several thousands of square kilometres, can be mapped very efficiently using the satellite data sets like IRS LISS3, LISS4, Landsat, CARTOSAT, SENTINEL etc. These satellite data are also useful in delineating the boundaries of flood prone zones. Digital analysis and processing the satellite data can detect changes on the sections of the inundated flood plains as well as in water quality through spectral reflectance curves. The multi temporal data sets from multiple satellites are proved to be very valuable in the identification of the site ideal for taking up structural measures to control floods.

Flood frequency analysis plays a very important role in predicting recurrence of floods thus helping in designing of structures like dams, bridges, culverts, levees, highways, sewage disposal plants etc. For evaluating whether the design specifications of hydraulic structures are optimum and to prevent under-design or over-design of these structures it is essential to estimate flood frequency and to create measurement parameters for analysing the damage caused by certain flows. Flood frequency analysis also helps in flood insurance and flood zoning. Flood plain zoning is the procedure of organization of areas responsible to floods of different frequencies in the neighbourhood of a river. These areas are then marked/delineated on large scale maps along with close contour intervals.

1.6 REPORT OUTLINE

1.6.1 Chapter 1: Introduction

1.6.2 Chapter 2: Literature Survey

1.6.3 Chapter 3: Study Area

1.6.4 Chapter 4: Materials and Methodology

1.6.5 Chapter 5: Results and Discussion

1.6.6 Chapter 6: Conclusion and Recommendation

CHAPTER 2: LITERATURE SURVEY

2.1 A REVIEW OF STUDIES ON FLOODS IN THE WORLD

Flood is the most frequent type of natural disaster among others and it occurs when an overflow of water submerges land that is usually dry. Floods are often caused by high intense rainfall, faster snowmelt GLOF and or a storm surge from a tropical cyclone or tsunami in coastal areas. Around 2000billion people worldwide. In the world, floods are usually can be defined in three types of floods.

(i) Flash floods are caused by rapid and excessive rainfall that raises water heights quickly, and rivers, streams, channels or roads may be overtaken.

(ii) River floods are caused when consistent rain or snow melt forces a river to exceed capacity.

(iii) Coastal floods are caused by storm surges associated with tropical cyclones and tsunami.

However, river based floods or riverine floods are one of the most common natural hazards, causing devastating impacts worldwide. Many studies performed across world have indicated that enhanced exposure of people and resources, as a result of population increase and economic growth, which has caused more damage due to weather-related natural disasters such as flooding (Dubey and Goyal, 2020). The impact of flooding is particularly damaging in developing countries due to low levels of flood protection.

As per the records, the Philippines in Southeast Asia has suffered from recurring flood events that caused around 100 fatalities per year between 2011 and 2013, and extended flooding in Thailand in 2011 caused serious economic losses. Many studies have evaluated the spatiotemporal characteristics of flooding and their exposure at regional and global scales under current and future climate conditions (Mohanty et al., 2020; Dubey and Goyal, 2020). Simultaneously, flood vulnerability is significantly affected by spatiotemporal changes in populations and assets.

For example, some studies indicate that unplanned urbanisation and human settlements in flood-prone regions have increased flood risk in Africa and low coastal regions (Salami et al., 2017). According to the United Nation's report (Schiermeier, 2019), floods accounted for 47% of all weather-related disasters since 1995 in USA and other countries, which are affected around 2.3 billion people, and killed around 1.57 lakhs people and incurring damages of about US$19.3 billion and US$0.83 billion in Asia and Africa, respectively. Several recent studies performed on flooding around the world have listed below in the Table 2.1.

Table 2.1: List of flood-based studies performed in the world.

Title	Report Type	Publisher	Year
A review of advances in urban flood risk analysis over China	Research Article	Stochastic Environmental Research and Risk Assessment	2015
Flood prediction using machine learning models: Literature review	Research Article	Water, MDPI	2018
A review of flood modeling methods for urban pluvial flood application	Research Article	Modeling earth systems and environment	2020
On the performance of satellite precipitation products in riverine flood modeling: A review	Research Article	Journal of Hydrology	2018
Forest operations, extreme flooding events, and considerations for hydrologic modeling in the Appalachians—A review	Research Article	Forest Ecology and Management	2007
Prediction and modeling of flood hydrology and hydraulics	Book Chapter	https://www.engr.colostate.edu/	
The Use of LiDAR-Derived DEM in Flood Applications: A Review	Research Article	Remote Sensing	2020
Numerical modeling techniques for flood analysis	Research Article	Journal of African Earth Sciences	2016
Flood risk analysis and assessment, applications and uncertainties: A bibliometric review	Research Article	Water, MDPI	2020
A review of the community flood risk management literature in the USA: lessons for improving community resilience to floods	Research Article	Natural Hazards	2019
Future flood risk estimates along the river Rhine	Research Article	Natural Hazards and Earth System Sciences	2011
Quantifying local rainfall dynamics and uncertain boundary conditions into a nested regional-local flood modeling system	Research Article	Water Resources Research	2017
A review on flood modelling and rainfall-runoff relationships	Research Article	Control and System Graduate Research Colloquium (ICSGRC)	2015
A review on applications of remote sensing and geographic information systems (GIS) in water resources and flood risk management	Research Article	Water, MDPI	2018
A Critical Review of Hydrological Modeling Practices for Flood Management	Review Article	Pramana Res. J.	2019

2.2 A REVIEW OF STUDIES ON FLOODS IN INDIA

According to the National Disaster Management Authority (NDMA) India, more than 40 million hectares of area in India is susceptible to floods out of its total area of 329 million hectares (Swain and Vyas, 2020). As per the Central Water Commission (CWC India), about 1,07,487 people died due to heavy rains and floods across India in the last 65 years from 1953 to 2018. Correspondingly, there has been damages to crops, houses and public utilities resulting in losses about Rs. 365,860 crores. Several past extreme events of floods are Kerala (2018, 19), Chennai (2015), Jammu and Kashmir (2014), Kedarnath (2013), Leh (2010), and Mumbai (2005) suffered from huge losses.

Total economic losses from flood disaster occurred in the southern state of Kerala during August 2018 have been tentatively estimated around Rupees 300 billion and claimed about 483 lives (Mohanty et al., 2020). Floods are not new to India and most India regions are prone to floods (~40mha). In India, floods occur with certain consistency and vary from region to region. The north Indian plains are more susceptible to floods than the southern ones. The flood-prone areas in the country can be generally classified into three divisions (i) the Ganga Basin, the Brahamputra, (ii) Barak Basins and the Central Indian and (iii) Deccan Rivers Basins. Based on the flood events and their mapping, it is concluded that Bihar is India's most flood-prone State, with 76% of the population in the North Bihar living under the recurring threat of flood destruction.

Around, 16.5% of the total flood affected area in India is located in Bihar, while 22.1% of the flood affected population in India lives in Bihar (Mohanty et al., 2020). Apart from Bihar, the severely affected states of the Ganga basin are West Bengal and Uttar Pradesh. Moreover, the main river Ganga, it tributaries such as Sarada, Rapti, Gandak, Saryu and Ghagra causes flood in eastern part of Uttar Pradesh. The Yamuna is responsible for flooding Haryana and Delhi, especially during extreme high rainfall event in the upstream basin and monsoon time. Assam experiences massive dangerous flood every year due to Brahmaputra and their tributaries. Several recent studies performed on flooding in India in different aspects have listed below in the Table 2.2.

Table 2.2: Details of research highlights on relevant topics.

Title	**Report Type**	**Publisher**	**Year**
Flood management in India: A focussed review on the current status and future challenges	Research Article	International Journal of Disaster Risk Reduction	2020
Climate change, flooding in South Asia and implications	Research Article	Regional environmental change	2011
Impacts of land use–land cover change and urbanization on flooding: A case study of Oshiwara River Basin in Mumbai, India	Research Article	Catena	2016
Study of cloudburst and flash floods around Leh, India, during August 4–6, 2010	Research Article	Natural hazards	2013
Satellite images for extraction of flood disaster footprints and assessing the disaster impact: Brahmaputra floods of June–July 2012, Assam, India	Research Article	Current Science	2013
Floods in a changing climate: hydrologic modeling	Book	books.google.com	2012
A comparative assessment of flood susceptibility modeling using multi-	Research Article	Journal of Hydrology	2019

criteria decision-making analysis and machine learning methods			
Hydroclimatological perspective of the Kerala flood of 2018	Research Article	Journal of the Geological Society of India	2018
Challenges in developing urban flood resilience in India	Research Article	Transactions of the Royal Society A	2020
Analysis of persistence in the flood timing and the role of catchment wetness on flood generation in a large river basin in India	Research Article	Theoretical and Applied Climatology	2020
Waterlogging and flood hazards vulnerability and risk assessment in Indo Gangetic plain	Research Article	Natural hazards	2010
Flood risk assessment of Srinagar city in Jammu and Kashmir, India	Research Article	International Journal of Disaster Resilience in the Built Environment	
Calibration of HEC-RAS model on prediction of flood for lower Tapi River, India	Research Article	Modeling Earth Systems and Environment	2011
Glacier recession and glacial lake outburst flood studies in Zanskar basin, western Himalaya	Research Articl Research Article e	Journal of Hydrology	2018
Rain gauge network design for flood forecasting using multi-criteria decision analysis and clustering techniques in lower Mahanadi river basin, India		Journal of Hydrology: Regional Studies	2015

2.3 RECENT FLOOD DISATSTERS AND THEIR CAUSES ACROSS INDIA

In recent few years India has been witnessed of some extreme high flood events such as Kerala (2018), Chennai (2015), Jammu and Kashmir (2014), Kedarnath (2013), Leh (2010), and Mumbai (2005) are a very few of the regularly increasing flood events in India. Many studies reported that climate change has played a significant role in occurrence of more frequent shorter duration and high intensity-based rainfalls, that majorly caused these flood events.

A very few researchers elaborated that the foremost causes of floods in India are changes in the monsoon pattern and resultant rainfall, reduction in the river channel carrying capacity for high flows due to bank exploitation for agricultural needs, riverbank erosion and the siltation of channel beds, poor and blocked natural drainages in flood prone areas and urban areas, cloudbursts and several other meteorological factors in Himalaya (Mohanty et al., 2020). Figure 2.1 clearly shows that during recent few years the extremity of floods in India has enhanced (Mohanty et al., 2020).

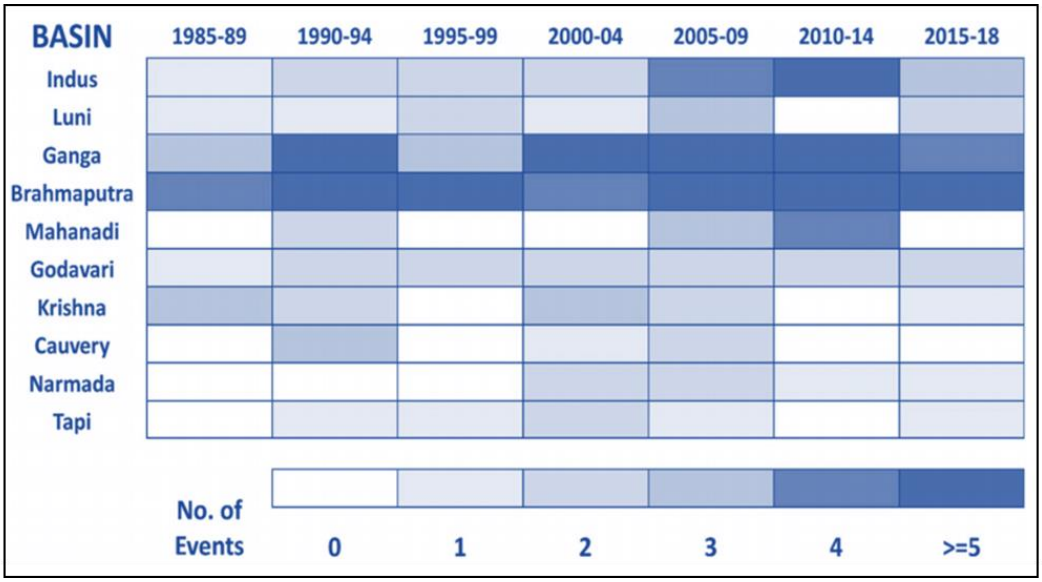

Figure 2.1: Increasing trend of flood events in India during 1985-2018 (source: Mohanty et al., 2020).

Additionally, in last few decades, rapid urbanization and changes in the land use/land cover (LULC) pattern have given rise to urban floods. In Himalaya, especially in eastern Himalayan region part of Brahmaputra basin faces frequent earthquakes and landslides which affects the natural regime of streamflow (Mohammed et al., 2017). Various options include flood forecasting, flood plain zoning, flood proofing, and disaster preparedness. India has majorly focused on structural measures of flood control and overlooked flood preparedness. To address these inadequacies, a research study to develop a real-time, catchment-based flood warning system on the Periyar river basin has been proposed using a 2D HEC-RTS (Real Time Simulation) platform. HEC-RTS is designed to integrate various HEC software including HMS, ResSim, RAS, and FIA with a flexible API (Application Programming Interface) that allows for scripting-based retrieval of observed and forecasted precipitation data and real-time production of different forecasting products. The realtime and forecasted rainfall and discharge will be utilized to generate the real time and stochastic scenarios of flood discharge in the selected river basin.

2.4 OBJECTIVES

The present research work shall explore the flood discharge and their inundation in the Southern river basin. During extreme high rainfall events, the frequency of flood events increases. The high amount of flood discharge may cause severe flood conditions in the downstream portion of the river basin. A destructive flood hazard has been recently happened in the Kerala state of India (2018) during monsoon season. Therefore, the purpose of this research work is to provide the advance research and engineering guidelines as per the adopted approaches and methodologies for the hydrological and hydrodynamic assessment of the flood discharge and inundation in the Southern river basin under extreme scenarios. Based on current research needs, following are the research objectives defined:

1) To process and accuracy assessment of the rainfall dataset over the selected river basin by utilizing satellite-based rainfalls (e.g. TRMM+GPM) and measured rainfalls (e.g. IM gridded rainfalls).

2) Construction of the hydrological model (i.e. HEC-HMS) to generate streamflows at different sections of the river channels.

3) Reservoir simulation of historical flood event (HEs) (i.e. Kerala Flood event 2018) using HEC-RESSIM and applying same rules and optimized parameters to construct other HEs.

3) Generation of flood discharges at different sections of rivers using HMS and the development of flood inundation maps in a stochastic manner including multiple return periods (e.g. 20 years, 50 years, 100 years, and 200 years) using steady state simulation.

4) Construction of the 1D and 2D Flood model, inundation maps and other hydrodynamic variables by the coupling of hydrological model (i.e. HEC-HMS) and hydrodynamic model (i.e. HecRAS) named as HEC-RTS framework.

CHAPTER 3: STUDY AREA

3.1 STUDY REGION

The Periyar river basin is a part of Central Kerala. Its location lies between 9°15'30" N to 10°21'00" N latitudes and 76°08'38" E to 77°24'32" E longitudes (Figure 3.1). It covers the districts of Idukki, Thrissur and Ernakulum. The districts of Idukki and Ernakulum are mostly dependent on this river for their drinking, navigation and irrigation needs. A number of dams and power stations lie on this river. It also plays a very important role in the agricultural, industrial and commercial development of the state. The plantation and forest area which is predominant in the basin was at 75% in 1997, but reduced to 73% till 2005. On the other hand, built up area percentage increased from 7% to 13%. There was also an observed increase of 8% in the conversion of plantation and barren land into built up area.

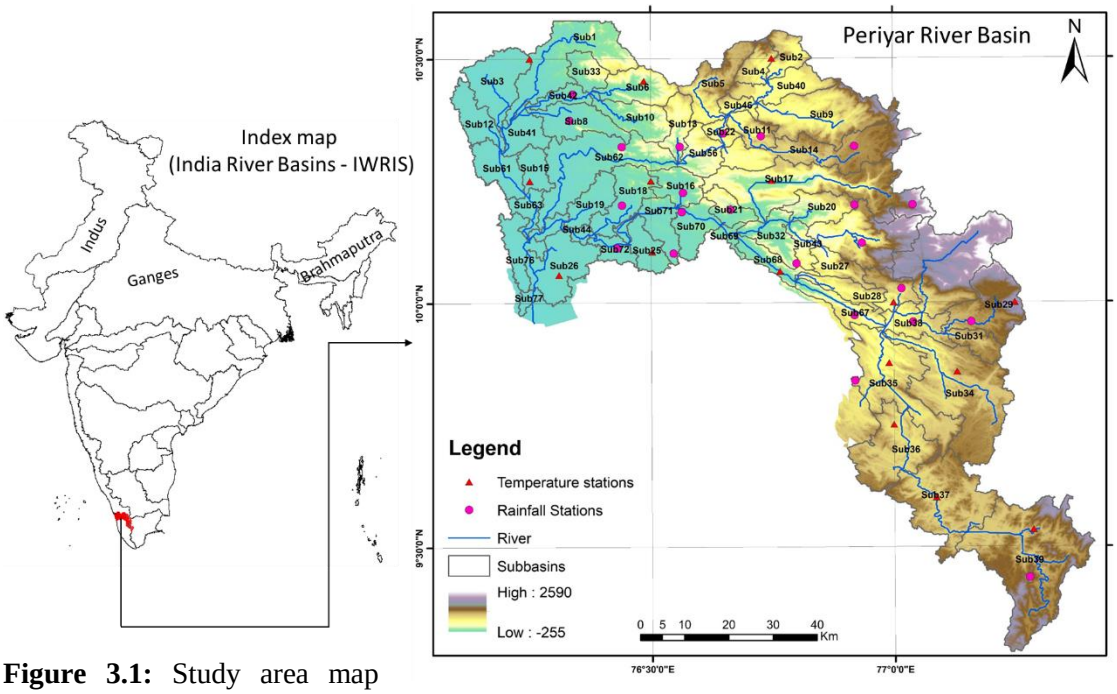

Figure 3.1: Study area map (Periyar river basin) showing elevation and other watershed characteristics.

3.2 HYDRO-CLIMATOLOGY OF THE PERIYAR RIVER BASIN

Kerala is known for its humid tropical rainforest climate. It also experiences cyclones from time to time.

(a). Rainfall: The Periyar river basin experiences tropical humid climate. The average rainfall received by this area over a time period of 20 years is 2809 mm, out of which 1785 mm is received from June to August (during the Southwest monsoon) whereas the remaining 704 mm is received from September to November (during the Northeast monsoon).

(b). Temperature: The maximum temperature experienced by the basin is 32°C; the minimum temperature experienced is 10°C whereas the mean is around 27°C.

(c). Humidity: The basin has a very high humidity of 83% at 8-30 hrs. and 75% at 17-30 hrs.

CHAPTER 4: MATERIALS AND METHODOLOGY

4.1 DATA SETS USED

4.1.1 Geospatial and Thematic Data Sets

The main thematic data layers such as digital elevation model (DEM), landuse/land cover (LULC) map and soil map have been utilized. In this study, the applicability of various freely available DEMs such as SRTM DEM (30m), ASTER DEM (30m), CARTOSAT DEM (30m) and ALOS PALSAR (12.5m) have been tested and then finally ALOS PALSAR, which is having finest resolution among all DEMs, has been selected for the analysis. The SOIL map and LULC map of the study area are mainly used to derive the curve numbers and for the computation of other hydrologic and hydrodynamic parameters. LULC map was obtained from the GLOBE Cover (2009 version) (https://land.copernicus.eu/global/products/) and soil map was used from the FAO soil map version 2 (2014) (http://www.fao.org/soils-portal/en/). The watershed boundary, sub-catchments (or subbasins), slope, flow direction, flow accumulation and streams were delineated using DEM. All these thematic data inputs were used as input datasets for HEC-HMS and HEC-RAS models.

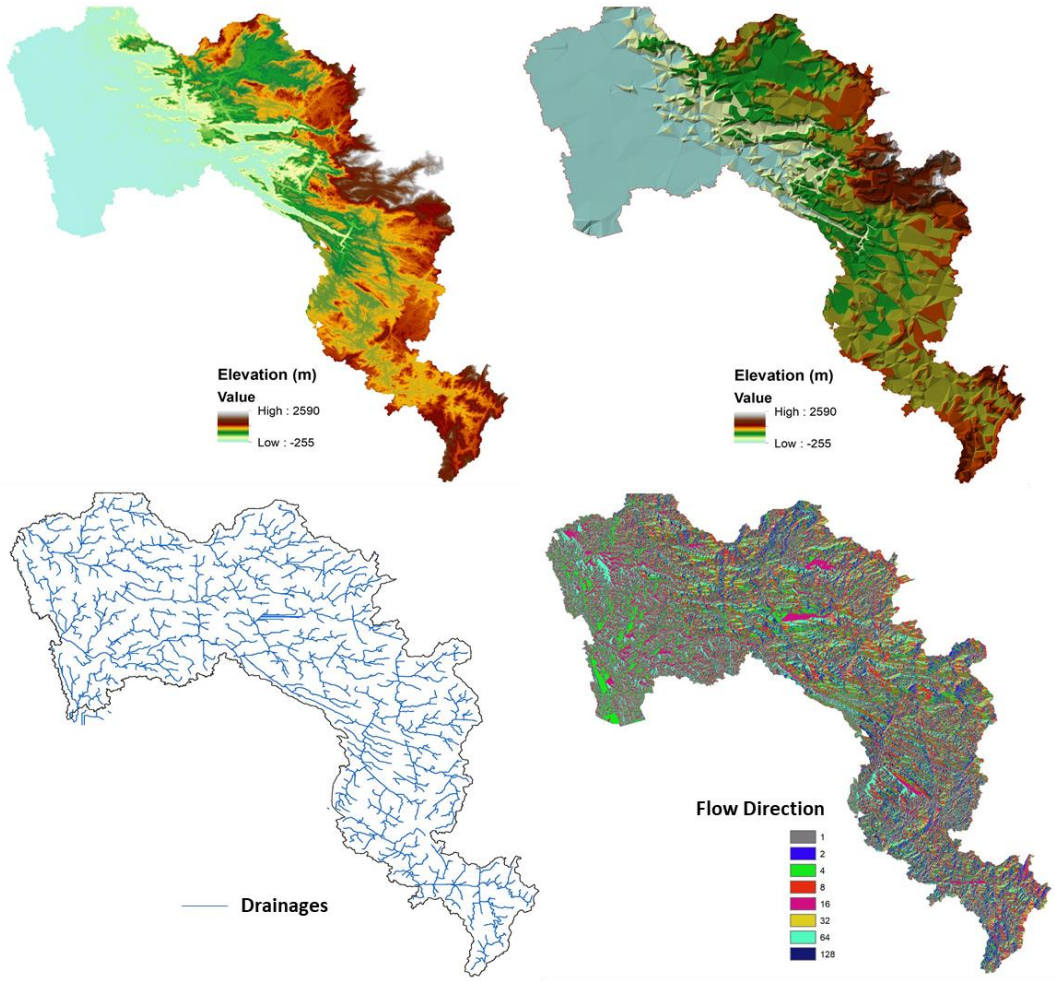

Figure 4.1: DEM derived watershed components.

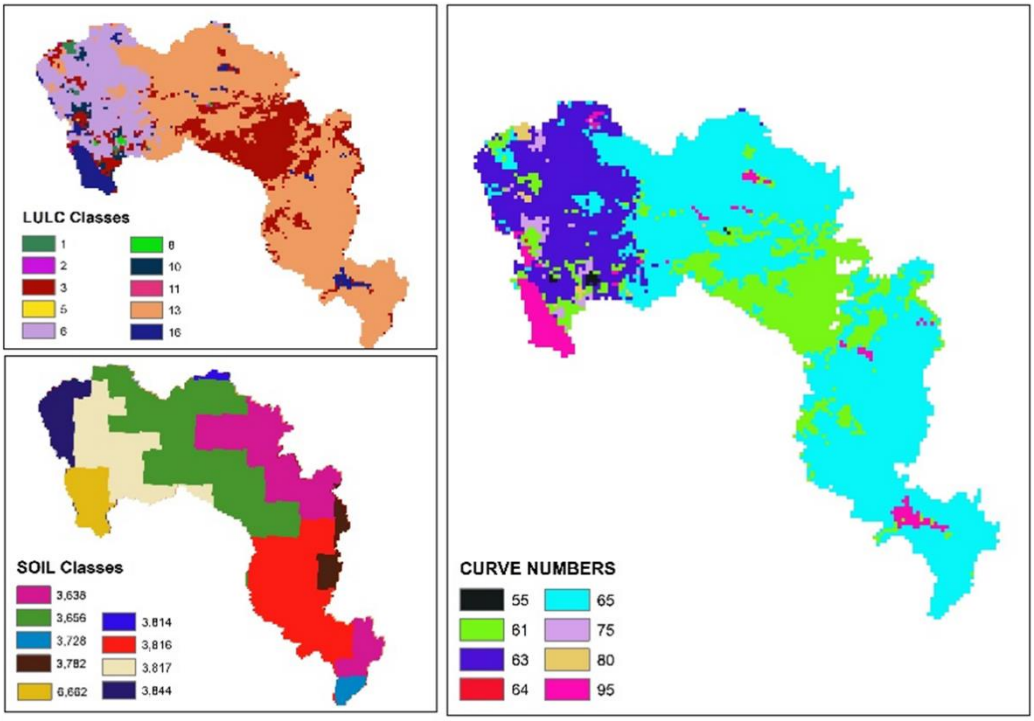

Figure 4.2: Thematic maps such as LULC, Soil and CNs map.

4.1.2 Hydro-observation and Meteorological Datasets

The hydro-observation and meteorological datasets such as 3-hourly rainfall (Aug 1 to Aug 22, 2018) from TRMM+GPM (gridded rainfall at 25km^2), daily rainfall from 1991 to 2018 (gridded rainfall at 12 km^2) were used for the flood frequency analysis and flood modeling. TRMM+GPM datasets are freely available (https://earthdata.nasa.gov/learn/articles/tools-and-technology-articles/trmm-to-gpm). Whereas IMDAA based IMD reanalysis data are downloaded from the National Centre for Medium Range Weather Forecasting (NCMRWF) web portal (https://rds.ncmrwf.gov.in/) (Ashrit et al., 2020). The daily gridded minimum and maximum temperature datasets from 1991-2018 (at 25km^2) were obtained from the NASA NEXGDDP (at 25km^2) historical datasets (https://www.nccs.nasa.gov/services/data-collections/land-based-products/nex-gddp). The temperature data from IMD data was available at 1º scale and therefore it is used for the bias correction of NASA NEXGDDP data sets. These hydro-meteorological variables are used as inputs to models. The observed discharge during Kerala most disastrous flood event, happened during Aug 1 to Aug 22, 2018, were available at CWC and thus obtained to calibrate and validate historical flood event simulation, also utilized to calibrate and validate other hydrodynamic flood modeling outcomes. Apart from this, daily average flow data (2007-2010) from CWC is also available at Neeleswaram gauge and therefore used in this study mainly for calibration and validation daily flood flows.

4.1.3 Hydrological, Hydrodynamic Variables and Other Datasets

For event wise hydrological analysis and to generate the boundary conditions flood flows at different sections of the study area, various hydrological variables such as curve number CN, ratio to peak, time of concentration, delayed flow, baseflow are computed/obtained using the available data inputs as discussed above and also collected from the literature surveys. Similarly, for continuous simulation, various hydrological parameters (as referred to Table 4.1) were computed empirically and some parameters are optimized using automated calibration process in HEC-HMS. For reservoir simulation in HEC-RESSIM, the storage, area, capacity and discharge tables are collected from different sources such as CWC, a published report on Kerala Flood Event 2018 by CWC, standard journals (Mohanty et al., 2020; Hunt and Menon, 2020; Sudheer et al., 2019) and other literatures.

Cross sections (or X-section) are the cross-sections are mostly delineated from the ALOS PALSAR DEM. Although, few cross sections are available at Neeleswaram gauge from Central Water Commission (CWC) and hence utilized to correct the DEM's delineated cross sections and also used in the study. Initially the manning's n value has been utilized as a standard global value suggested by HEC-RAS manual based on the channel condition (i.e. 0.015 to 0.025). Finally, the manning's n values have been optimized as 0.013-0.015 through a trial and error basis manual calibration process. For the unsteady flow computations, the implicit weighting factor is taken between 0.7 to 0.8. This value generally varies from 0.6 to 1, where 1 recommended for more stable condition but less accurate results. The other hydrodynamic variables such as water surface calculation tolerance (m), storage area elevation tolerance (m), max error in water surface solution (m) and maximum number of iterations are taken as 0.006, 0.006, 30.0 and 20, respectively.

4.2 PROCESSING OF RAINFALL AND TEMPERATURE DATASETS

In this study, 3-hourly and daily rainfall datasets have been utilized. For 3-hourly rainfall datasets, the TRMM+GPM satellite based open sources rainfall data have been used. Total 14 grids which are falling near to/inside the study area being considered. The event based analysis mainly done with the daily observed IMD rainfall data datasets. However, during the flood events, the hourly IMD rainfall datasets were missing and thus we went for the daily rainfall and other sources such as TRMM+GPM rainfall. A few studies mentioned that while using the daily rainfall data, the actually flood extremity (or peaks) can be lost (Gupta et al., 2020; Sudheer et al., 2019). Therefore, we took TRMM+GPM 3-hourly rainfall data and then TRMM+GPM rainfall averaged on a daily scale, mainly for the bias correction purpose. Then we compute the average bias in daily averaged TRMM+GPM at each rainfall station with reference to daily IMD rainfall. After that the computed bias was divided into 3-hourly steps with respect to the ratio of 3-hourly TRMM+GPM rainfall and accordingly the bias ratio is added to the 3-hourly TRMM+GPM rainfall datasets (Gupta et al., 2020). The comparison of Kerala flood event (i.e. July-August, 2018) constructed by bias corrected TRMM+GPM 3-hourly rainfall datasets has been done with respect to the flood event computed by daily rainfall datasets, mainly to highlight the variations in extreme peaks.

4.3 INTEGRATED HYDROLOGICAL-HYDRODYNAMIC MODELING USING HEC-RTS

4.3.1 HEC-DSSVue

HEC Data Storage System Visual Utility Engine (HEC-DSSVue) is a Graphical Unser Interface (GUI) which is designed to view, edit and manipulate large database files which can be linked to the HEC-HMS, HEC-RESSIM and HECRAS tools. This tool is mainly useful to store and organize various amount of time series and event based information at a single place and all the database which is stored in the HECDSSVue can be called directly from HEC-HMS, HEC-RESSIM and HEC-RAS tools. Therefore, this tool makes process easier to handle large amount of datasets in performing integrated hydrological and hydrodynamic modeling. In HEC-DSSVue, one can rename, delete, duplicate, and copy data in HEC-DSS files and can also compare data sets and whole files to determine differences as well as search for values within files. A figure 4.3 has shown some general utilities of organizing and maintaining database in HECDSSVue. In Figure 4.3 (a) shows the GUI interface of HECDSSVue, (b) shows the format of data storage system in HEC-DSSvue, (3) a geo-spatial data of rainfall can be visualized and (d) a tabular information of any time series datasets can be visualized.

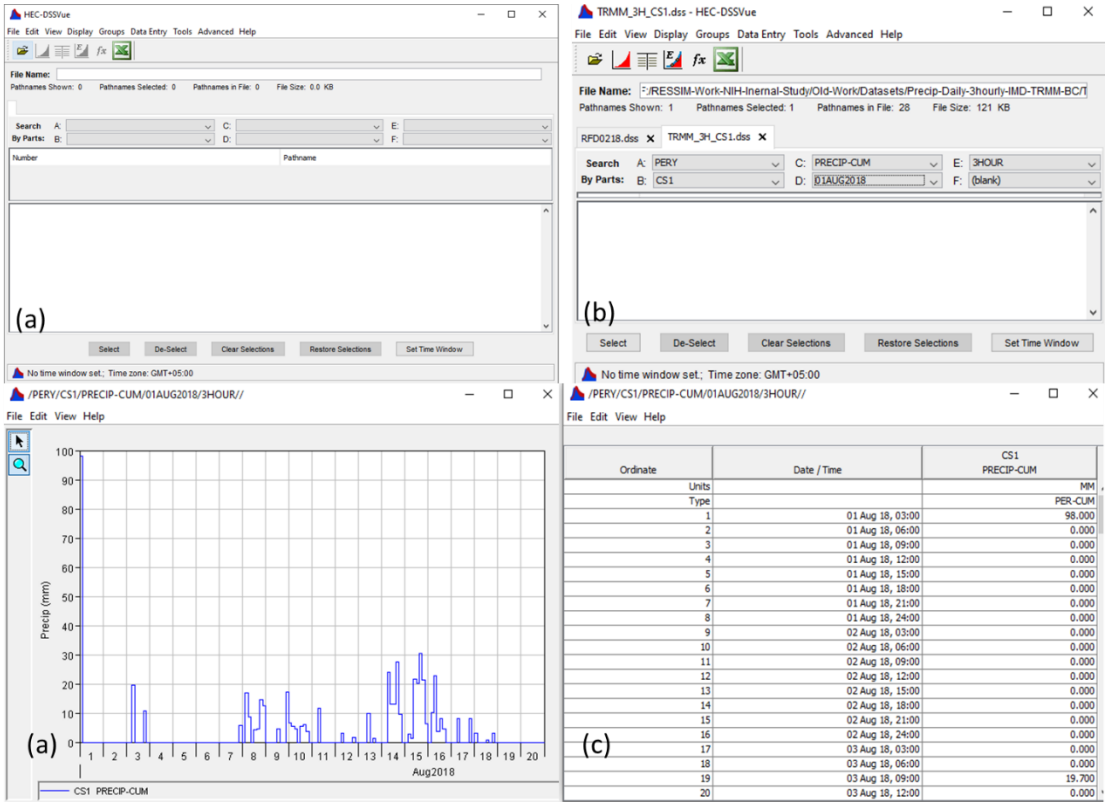

Figure 4.3: The Schematic representation of HEC-DSSVue.

4.3.2 Meteorological Data Processing (HEC-METVue)

In HEC-RTS system, HEC-Meteorological Visualization Utility Engine (HEC-METVue) has been designed to view and edit meteorological datasets by performing a variety of computations and analyses. HEC-METVue supports HEC-DSS, PRISM, ESRI ASCII GRID formats to read the datasets. HEC-MetVue also provides a variety of Triangular Irregular Network (TIN) image editing tools to resize and to change the image orientation. HEC-METVue computes and visualizes an aggregate basin average layer and permits to write the basin average time series into HEC-DSS output file.

4.3.3 HEC-HMS Hydrological Model

The Hydrological Modeling System (HMS) from HEC has been developed to compute the flood discharge at different portions and sections of the river basin. In HEC-HMS, two types of simulation can be performed i.e. (i) event-based simulation of flood flows and (ii) continuous simulation of flood flows. In HEC-HMS, various hydrologic process such as canopy storage, surface storage, loss, transform, baseflow, snowmelt, evapotranspiration (ET), and hydrologic routing can be performed by adopting various methods (Thakur et al., 2017). HEC-HMS is basically a lumped parameter model and in HEC-HMS different hydrologic processes are solved independently on one another.

4.3.3.1 Data inputs to HEC-HMS

In HEC-HM, seven hydrological data processing components are available such as (ii) Basin model manager – for creating basin and subbasin characteristics like junction, node and reach, (ii) Meteorological model manager – deals with precipitation, temperature and other meteorological variables, (iii) Control specification manager – to define the model run time steps, (iv) Time-series data manager – deals with gauge, discharge and other time series based hydro-observation datasets, (v) Paired data manager – for reservoir details and to define the relationships between area, elevation, discharge and capacity, (vi) Grid data manager – deals with spatial gridded rainfall and other meteorological datasets and (vii) Terrain data manager – to delineate basin boundary, subbasin

boundary, drainage, longest flow path, time of concentration, slope and other physical parameters of river basin and subbasins.

4.3.3.2 Methods used for event and continuous simulation

This study performed event wise simulation to construct the historical flood events and continuous simulation to generate the long-term flood flows for the computation of multiple return period flood flows. Total seven historical flood events have been identified based on the extreme rainfall. First, we identified the wet and dry years during 2001 to 2018 using probabilistic rainfall analysis (as per annual IMD report). Then based on the extreme threshold of rainfall (min 7 days' max rainfall for a given year), the seven historical events (HEs) have been identified as HE-1 (Jul 25 to Aug 20, 2002), HE-2 (Jun 15 to Jul 7, 2003), HE-3 (Jul 25 to Sep 20, 2004), HE-4 (Jul 25 to Aug 20, 2008), HE-5 (Jun 5 to Jun 25, 2013), HE-6 (Jun 8 to Jul 5, 2017) and HE-7 (Aug 8 to Aug 22, 2018). For the HEs, SCS CN has been taken as a loss method (Sudheer et al., 2019), SCS unit hydrograph has been adopted for the transformed method (Zema et al., 2017), constant monthly baseflow has been used to compute the baseflow and Muskingum method was used for the hydrological routing of stream flows (Sudheer et al., 2019). The SCS CNs for a given watershed can be calculated as a function of LULC, soil and antecedent moisture conditions (AMC), using a published table by the SCS USA. Previous researchers elaborated that India represents mostly AMC II type of moisture conditions. Therefore, the current study area has followed the AMC II type of moisture condition (Grimaldi et al., 2020). AMC I stands for very dry soil moisture conditions and AMC III stands for very wet soil conditions. The imperviousness is calculated using LULC map by extracting the area of settlement within the study area. For the mathematical expression of the event based methods, a well theoretical document is available on the HEC-HMS web portal (*https://www.hec.usace.army.mil/confluence/hmsdocs/hmstrm*).

For continuous simulation, soil moisture accounting (SMA) based loss method has been adopted, which is more suitable for the continuous time series simulation as suggested by previous researchers (Maneshdavi et al., 2018). HEC-HMS continuous simulation was performed during 2002 to 2018 by adopting daily hydro-meteorological datasets. The SMA method simulates the movement of water through and storage of water on vegetation, in the soil profile, on the soil surface, and in groundwater layers. As per the specified precipitation and potential evapotranspiration (ET), the model computes surface runoff, groundwater flow, losses due to ET, and deep percolation over the entire basin. SMA method deals with number of parameters such as canopy (%), soil (%), surface (%), canopy storage (mm), surface storage (mm), maximum infiltration (mm), soil storage (mm), imperviousness, tension storage, soil percolation (mm/hr), groundwater storages (mm) and groundwater percolations (mm/h). These parameters can be computed empirically (Maneshdavi et al., 2018).

4.3.3.3 Calibration and parameterization

For model calibration and parameters optimization in Periyar river basin, an automated calibration tool, which is an inbuilt function of HEC-HMS, has been performed. Initially, for the model setup and simulation, the standard global values suggested by HEC-HMS theoretical document and also suggested in previous studies performed in the same domain have been adopted. Then automated calibration has been done in HEC-HMS during continuous simulation step and optimized parameters values were computed to generate the final modeling outcomes. During optimization of hydrological variables (or parameters), the simplex method has been used (Cheng et al., 2021; Wang et al., 2018). The goal is set to minimize the errors in the final modeling outcomes. For event based simulations, the manual calibration was utilized to adjust the CNs, ratio to peak, and routing K and x. For event-based simulation, the manual calibration is preferred in some studies (Ouédraogo et al., 2018). The observed discharge has been used for both event and continuous calibration. The "Sum of Squared Residuals" has been taken as the main objective function (Cheng et al., 2021; Wang et al., 2018). The details about the optimization of input parameters for event-based simulation methods and continuous simulation

methods have been comprehensively discussed in the results and discussion section (Chapter 5). For continuous model simulation, the suggested parameters as per SMA method has shown in Table 4.1

Table 4.1: Calibration and modeling parameters for SMA method in HEC-HMS.

Parameter	Value	
	Min	**Max**
Canopy %	0	5
Surface %	0	5
Soil %	60	90
Groundwater 1 %	20	60
Groundwater 2 %	60	90
Canopy storage, mm	1.5	5.5
Surface storage,mm	0.5	4
Maximum infiltration, mm	4	70
Imperviousness	0	100
Soil storage, mm	400	500
Tension storage, mm	50	180
Soil percolation, mm/hr	0.1	2.5
Groundwater 1 storage (mm)	75	200
Groundwater 1 percolation (mm/h)	0.1	2
Groundwater 1 coefficient (h)	50	200
Groundwater 2 storage (mm)	75	200
Groundwater 2 percolation (mm/h)	0.1	5
Groundwater 2 coefficient (h)	0.1	3

4.3.4 HEC-RESSIM Model

The Reservoir System Simulation (HEC-RESSIM) has mainly developed to model rule-based reservoir operations for a single reservoir or multiple reservoirs including variety of operational goals and constraints. RESSIM is mostly used for the flood management studies including irrigation water supply, hydropower generation, drinking water supply and flood mitigation. HEC-RESSIM is part of HEC-RTS system, and it takes inputs from HEC-HMS (e. g. discharge at various locations) and provides regulated and optimized floods to HEC-RAS for further hydrodynamic computations of flood flows. Although, HEC-RESSIM can also be utilized independently (i. e. not a part of integrated HEC-RTS) similar to HEC-HMS and HEC-RAS tools.

In this study, the reservoir simulation has been done during the Kerala flood event (i.e. HE-7) for Mullaperiyar Dam which is situated upstream of the selected river basin and Periyar Dam is situated below the Mullaperiyar Dam. For the reservoir simulation of HE-7 event, the 3-hourly rainfall datasets (i.e. the bias corrected TRMM+GPM) at multiple locations (14 nos.) have been utilized. After the 3-hourly reservoir simulation (which is initially independently done in HEC-RESSIM) and optimization for HE-7 event, the same adopted parameter such as elevation-area-capacity-discharge curves were re-input to the HEC-HMS for the event based analysis of HEs (historical flood events) utilizing the daily IMD based observed rainfall datasets. HEC-RESSIM has basically three important components such as watershed network, reservoir setup and simulation modules as described below.

4.3.4.1 Watershed network

In HEC-RESSIM, a watershed or river basin can be represented as a georeferenced catchment, river channels, reservoir locations, reaches (i.e. required for routing), stream junctions (e.g. to connect rivers and reaches), and diversions. In watershed network included creating new watersheds, defining

watershed configurations, describing watershed's physical features and viewing schematic elements which are created. This study mainly corresponded with two major reservoirs such as Mullaperiyar and Idduki. Mullaperiyar is situated at the upstream portion, while Idukki is situated just downstream of the Mullaperiyar.

At the downstream of Idukki reservoir, a gauge site namely Neeleswaram is available. In the watershed network, the inflows, local flows and regulated flows released from reservoirs can be linked or accumulated at an element namely Junction. In watershed network, reaches transport water from one junction to another junction. For routing water through reaches in HEC-RESSIM, this study utilized Muskingum method. However, for very short reaches, NULL routing was used. The optimal values of X and K parameters were identified by manual calibration (e.g. trial and error basis). The watershed setup module for the Periyar river basin, during HE-7 (Kerala flood event August 2018) has shown in Figure 3.1

4.3.4.2 Reservoir setup

Once a reservoir network is constructed, the connection between network elements is allowed. Although, a good model design includes junctions at key locations to identify and manage inflow data effectively across various alternatives. Depending on the objectives of the model, rating curves (stage-discharge relationship) may be important to the operation of the reservoirs for downstream controls. The physical and operational data that describe an operation plan or scheme upon which it can base its decision are provided into model using these elements. An operation set (Figure 4.1) consists of three basic features: Zones, Rules and the identification of the Guide Curve. Decision logic of the program is related with zones, rules and guide curve.

(i) Zones are operational subdivisions of the Reservoir Pool. Each zone is

defined by a curve describing the top of the zone.

(ii) Rules represent the goal and constraints upon the releases.

(iii) Guide Curve is the target elevation.

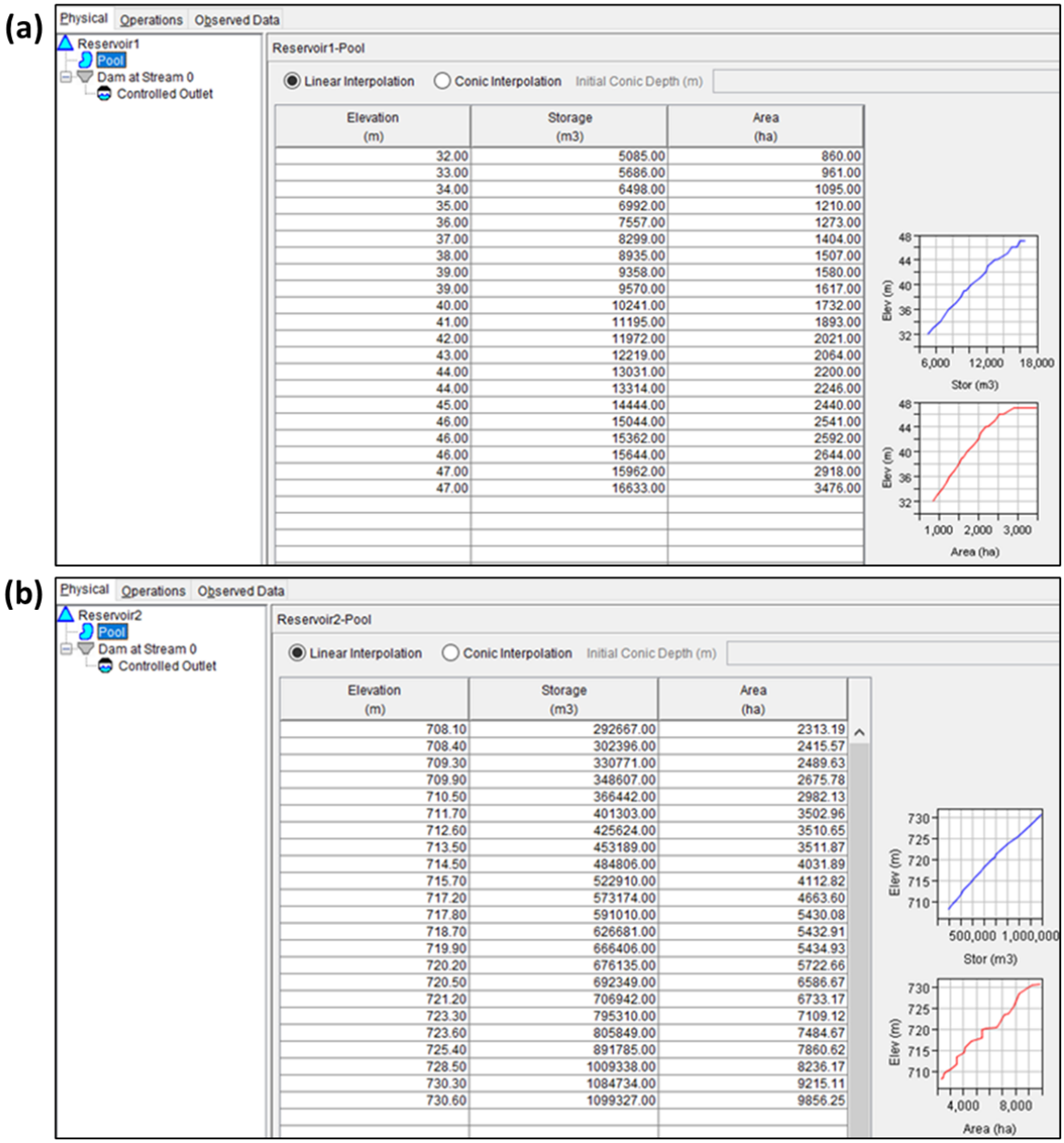

Figure 4.4: Elevation-Storage-Area curves for (a) Mullaperiyar dam and (b) Idukki dam considered to perform the reservoir operations during HE-7 event (Kerala flood, August 2018).

To setup the reservoir related parameters, elevation-area-capacity curve must be defined (Figure 4.1). Based on this, water level readings can be converted to current water capacity and lake surface area. In HEC-RESSIM, reservoir releases to the downstream of the river channel are made by spillways and outlet works. Spillways provide the capability to release high flow rates during major floods without damage to the dam and appurtenant structures.

Spillways are designed in a way to allow flood inflows to safely flow over or through the dam, irrespective of the reservoir contains flood control storage capacity. Spillways can be uncontrolled or gated. A controlled spillway provides with crest gates with other facilities that permit the outflow rate to be modified (Sudheer et al., 2019).

Reservoir Operation Rules

Reservoir 1 - Mullaperiyar

Flood Control Zone

Maximum Release Rule		
Date	**Time**	**Release, cms**
01-Jan	1000	50
02-Aug	800	50
03-Aug	1100	50
04-Aug	1100	40
05-Aug	800	40
06-Aug	1100	50
07-Aug	1400	75
08-Aug	1100	1000
09-Aug	2100	2000
10-Aug	2100	500
11-Aug	2100	1000
12-Aug	2100	500
13-Aug	2100	1000
14-Aug	2100	1000
15-Aug	2100	1500
16-Aug	2100	1500
17-Aug	2100	1000
18-Aug	2100	1500
19-Aug	2100	2000

Conservation Zone

Minimum Release Rule		
Date	**Time**	**Release, cms**
01-Jan	0	100
06-Aug	300	100
07-Aug	2100	100
08-Aug	2100	200
10-Aug	2100	200
11-Aug	2100	200
12-Aug	2100	200
14-Aug	2100	500
16-Aug	2100	200
17-Aug	2100	500
19-Aug	2100	500

Storage Zone	Flood Control
Function of	Date & Time
Top Elevation	53.6 m

Reservoir 2 - Idukki

Flood Control Zone

Maximum Release Rule		
Date	**Time**	**Release, cms**
01 Jan	0000	50
10Aug	0600	1000
12Aug	0600	1800
14Aug	0900	2000
16Aug	0300	4500
18 Aug	0300	4500

Conservation Zone

Date	Time	Release, cms
01 Jan	0000	50
10Aug	0600	1000
12Aug	0600	1200
14Aug	0900	1200
16Aug	0300	1200
18 Aug	0300	1400

Storage Zone	Flood Control
Function of	Date & Time
Top Elevation	710.0 m

Figure 4.5: Reservoir rules for the optimization of flood flows during HE-7.

In this study, the reservoir rules are defined as per the maximum and minimum release rule as a function of date and time, which provides to control channel capacity through the downstream channel. The rule limit is only effective since the amount of water will be released within the guide curve range. Alternatively, HECRESSIM provides 'Specified Rule Types' which eliminates Guide Curve and release the desired amount of water although the target elevation is not achieved. It could also be noted that; ordering of rules is important in terms of execution priority. Figure 4.5 has shown the HEC-RESSIM reservoir network module.

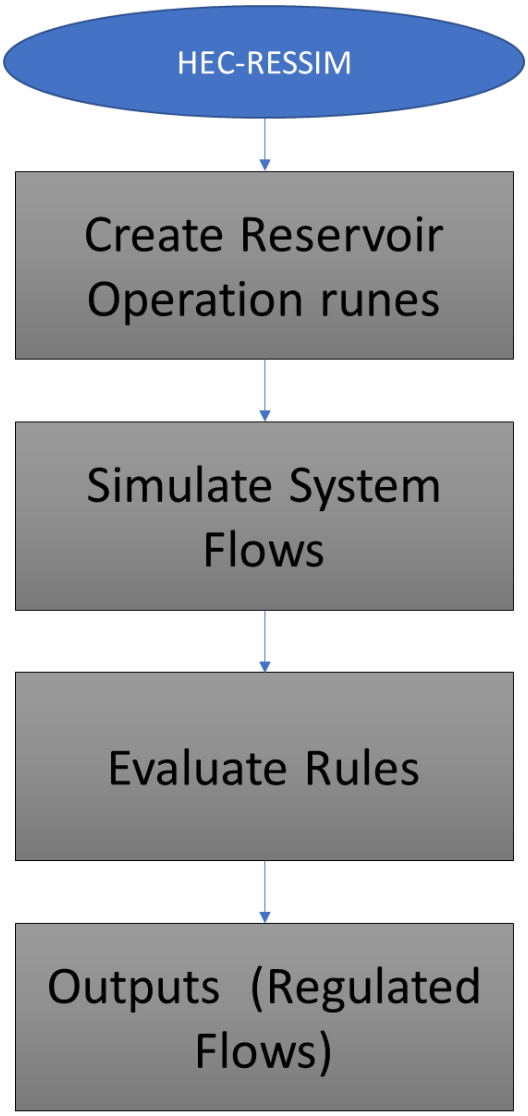

Figure 4.6: Components involved in HEC-RESSIM.

4.3.4.3 Simulation

HEC-RESSIM has been developed for both short-term and long-term operations. In HEC-RESSIM, the simulations can be performed on a daily and hourly time steps. In this study, we performed our study on the three-hourly steps as per the availability of rainfall and discharge datasets. In this study, the reservoir operation (for HE-7 event) has been simply applied with a simple simulation model by dividing the total reservoir storage area capacity into designated pools. The input and reservoir rules have shown in Figure 4.5.

The whole mechanism of reservoir simulation in HEC-RESSIM has shown in Figure 4.6. For the validation of HEC-RESSIM based flood discharge during HE-7 event, the comparison between observed and modelled flows have been done and coefficient of determination (R^2) was selected as an objective function to evaluate the model performance.

4.3.5 HEC-GeoRAS AND HEC-RAS Hydraulic Model

4.3.5.1 HEC-RAS data processing using HEC-GeoRAS

HEC-GeoRAS is a GUI based tool that works in the ArcGIS software platform. It is basically developed to process geospatial data and generate the data input layers (or geometric data) for HEC-RAS. HEC-GeoRAS basically creates the geospatial data layers such as stream centreline, banks, flow paths and cross sections, which are the important parameters to setup 1D HEC-RAS model. For creating these layers, HEC-GeoRAS requires DEM which must be converted into digital terrain model (DTM) in the ArcInfo TIN format. Water surface profile data and velocity data exported from HEC-RAS simulations may be processed by HEC-GeoRAS for GIS analysis for floodplain mapping, flood damage computations, ecosystem restoration, and flood warning response and preparedness.

4.3.5.2 HEC-RAS mapper and geometric data information

The HEC-GeoRAS based created geometric data layers can be imported in HEC-RAS through geometric data and RAS mapper. However, in the latest version of HEC-RAS (i. e. >5.0.4), HEC-RAS dependability on HEC-GeoRAS has been ended. Now these geometric data layers can also be created in the latest versions of HEC-RAS through RAS mapper tool. For this, a DEM in ".TIF" format can be added and then it can be converted into DTM. After this, the new geometry layers can be created.

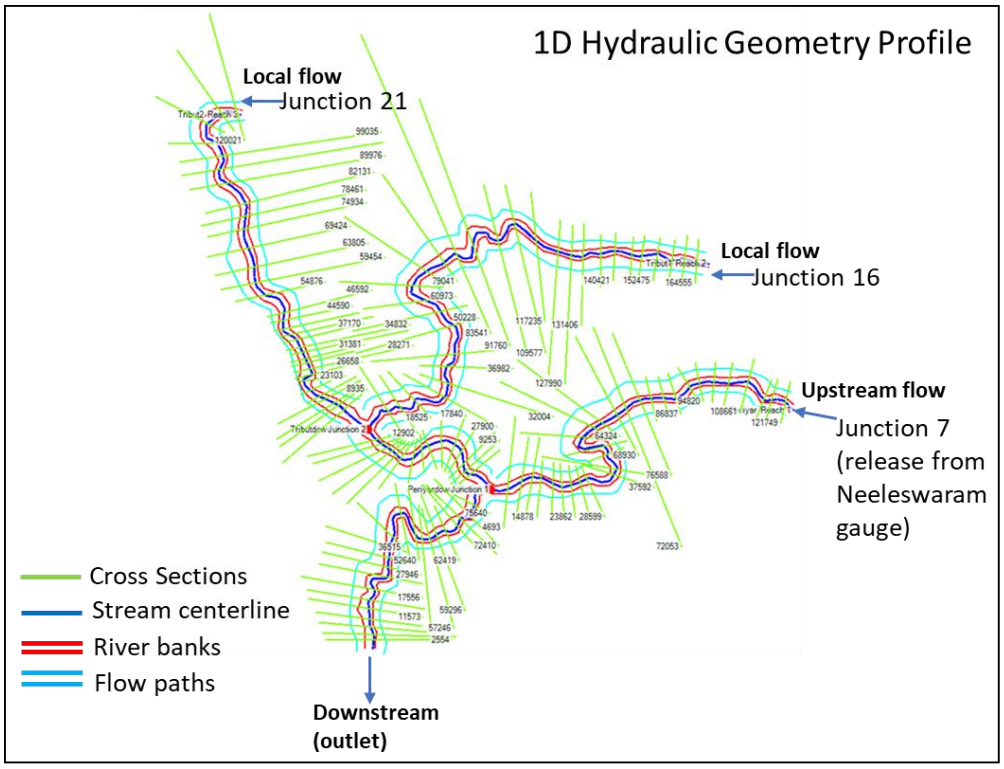

Figure 4.7: 1 D Hydraulic geometry profile to setup HEC-RAS model prepared in HEC-GeoRAS.

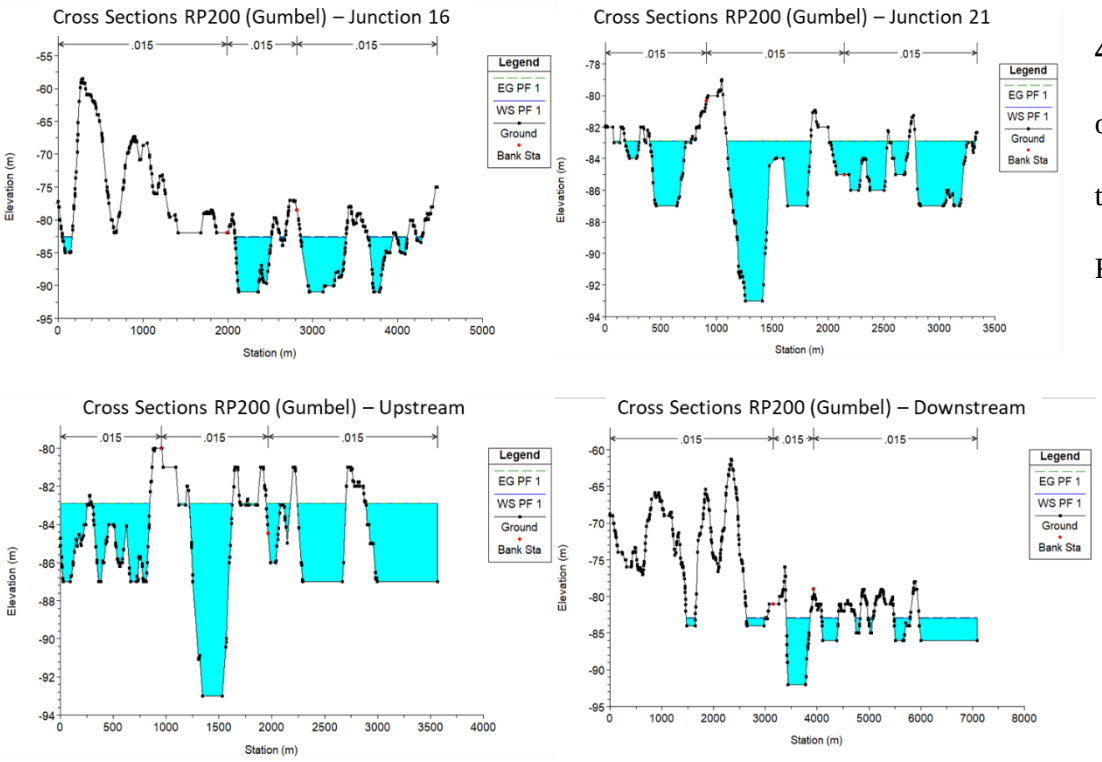

Figure 4.8: An example of Cross-sections to setup-HEC-RAS 1D steady and Unsteady flow simulations.

In HEC-RAS, the stream centerline is used to establish the river reach network. The river network must be digitized from upstream to downstream (in the direction of flow). Unique river and reach name are assigned using river reach ID tool. Connectivity, length of each river and reach is calculated from starting station to end station. The bank lines layer is used to identify the main channel conveyance area from that of the overbank floodplain areas. The flow path lines layer is used to determine the downstream reach lengths between cross section in the channel and overbank areas.

A flow path line should be created in the center-of-mass of flow in the main channel, left overbank, and right overbank for the water surface profile of interest. Flow path lines are digitized in the downstream direction, following the movement of water. The cross sections must be located perpendicular to the direction of flow (Figure 4.6). The cross-section lines must cover the entire extent area of the flood plain to be modelled. The typical structure of cross sections at different sections within the study area has been shown in Figure 4.7. The elevation for each cross-section is extracted from the terrain model. The Manning's n value must be defined for each cross-section. The geometry data layers have shown in Figure 4.7.

4.3.5.3 1D steady and unsteady flows simulation methods

The unsteady flow computational program in HEC-RAS uses the same hydraulic calculations (cross section properties, bridge and culvert hydraulics, weirs, gated structures, etc.). In this study, both steady and unsteady (1D) and unsteady 2D modelling have been performed.

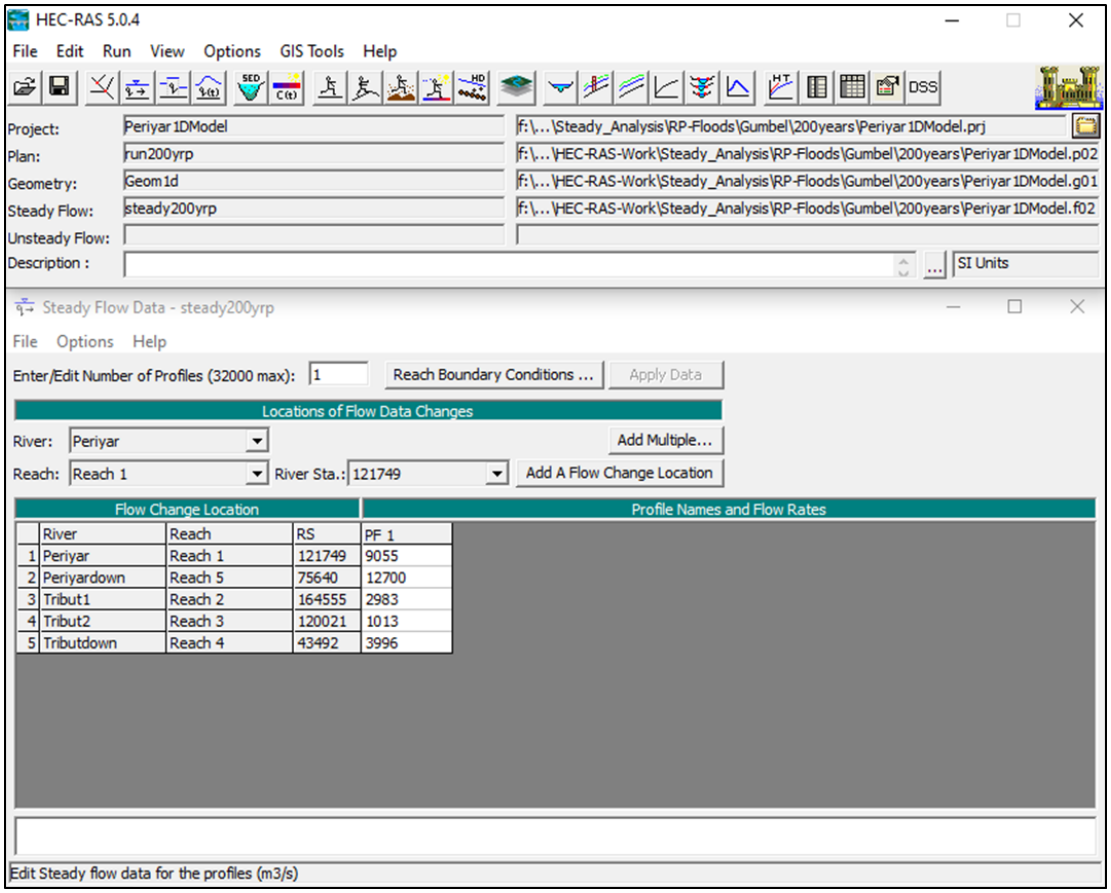

Figure 4.9: HEC-RAS setup for 1D steady state flow simulations.

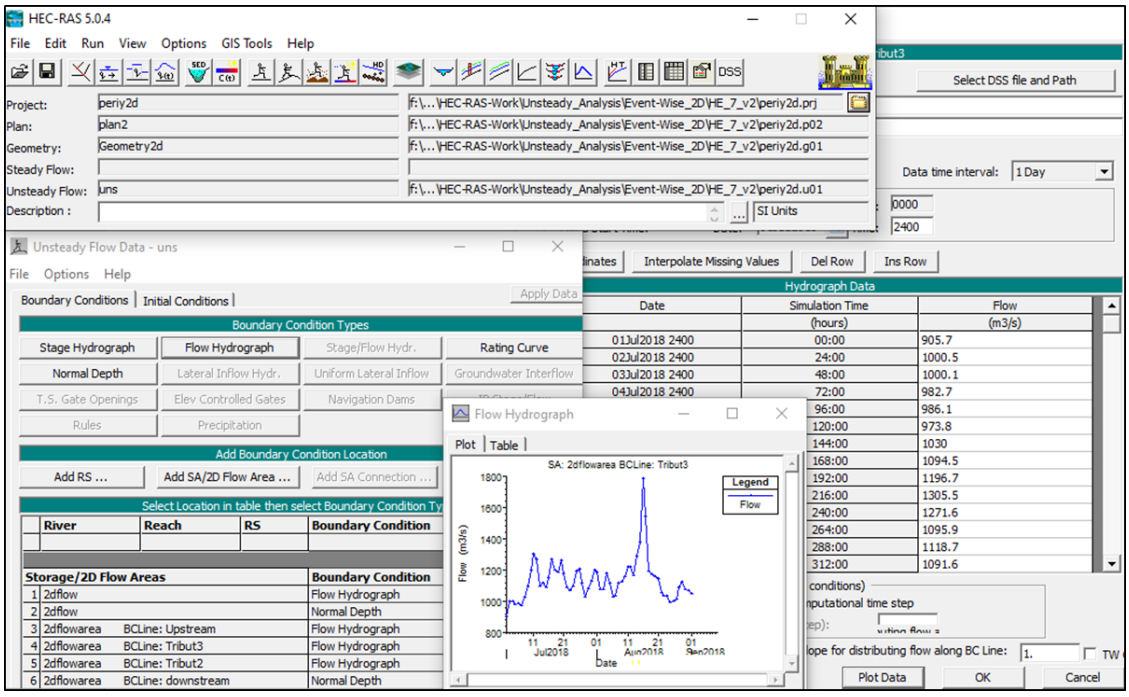

Figure 4.10: HEC-RAS setup for 1D unsteady state flow simulations.

For 1D steady state modelling, flood frequency analysis has been performed and multiple return period floods such as 50years, 100 years and 200 years utilizing Gumbel and Log Pearson Type 3 extreme value distribution models (Figure 4.9). For 1D unsteady flow analysis, seven historical flood events (HEs) were identified and for few flood events, unsteady flood flows routing was performed. Unsteady flow data is comprised with initial and boundary conditions. In unsteady flow analysis, the boundary conditions must be specified for each upstream, downstream and local tributary where flow enters the system. In this study, for the upstream and tributaries, flow hydrograph (i.e. at Neeleswaram gauge, Junction 16 and Junction 21) and for the downstream condition, normal depth (taken as 0.001) options are considered. Because for the downstream point, the energy slope is unknown, and thus it approximated by using the slope of the channel bottom. For each HE and return period event, various hydraulic variables such as flood depth, velocity, longitudinal water profile, flooded area and rating curves have been generated. Initial conditions are also necessary and consist of flow and stage information at each of the cross sections as well as elevations for any storage areas defined in the system. The HEC-RAS windows for entering steady flow and unsteady flow data have shown in Figures 4.9 and 4.10.

In HEC-RAS, for the case of steady flow calculations, the model calculates stages throughout the interior points, while discharge is constant. While in case of unsteady flow computations, the HEC-RAS performs computation of discharge and stages throughout the interior points. Under steady flow, the calculated discharge-stage ratings are unique, i.e., kinematic (Ouédraogo, 2018). The steady-state computes water levels at discrete cross-sections using the return period flood flows. On the other hand, under unsteady flow, the model calculates dynamic looped discharge-stage ratings according to the variabilities of the flow. HEC-RAS unsteady flow model uses the St. Venant equations (Ouédraogo, 2018).

$$\frac{\partial A}{\partial t}+\frac{\partial \phi Q}{\partial x_c}+\frac{\partial (1-\phi)Q}{\partial x_f}=0$$

$$\frac{\partial Q}{\partial t}+\frac{\partial}{\partial x_c}\left(\frac{\partial \phi^2 Q^2}{A_c}\right)+\frac{\partial}{\partial x_f}\left(\frac{(1-\phi)^2 Q^2}{A_f}\right)+gA_c\left(\frac{\partial z}{\partial x_c}+S_c\right)+gA_f\left(\frac{\partial z}{\partial x_f}+S_f\right)=0$$

Where, **A**: cross-sectional area, **Q**: Discharge, **S**: frictional slope, **z**: water depth, **x**: distance along the flow, **f**: fraction to determine channel versus floodplain discharge, **t**: time

(i) 1D Profile

The water surface profile in HEC-RAS is computed by using the basic form of energy equation. The goal is to find the head loss between two cross-sections to the water surface at the upstream cross-section can be found by adding the head loss to the downstream water surface elevation.

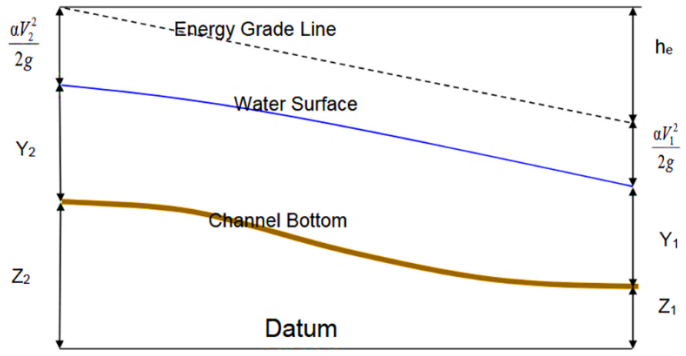

$$h_e = L\bar{S}_f + C\left|\frac{a_2V_2^2}{2g}-\frac{a_1V_1^2}{2g}\right| \qquad \frac{V_1^2}{g}+h_e$$

In which, $\mathbf{h_e}$: head loss, **V**: velocity, **g**: gravitational acceleration, **L**: reach length, **a**: velocity coefficient.

(ii) Flow conveyance and Frictional Slope

Computation of flow conveyance (K) and frictional slope (S_f) is based on Manning's n values. Thus Manning's n or roughness coefficient plays a critical role in hydraulic modeling.

$$Q = KS_f^{1/2} \longrightarrow S_f = \left(\frac{Q}{K}\right)^2$$

$$K = \frac{1.486}{n} AR^{2/3}$$

$$\bar{S}_f = \left(\frac{Q_1 + Q_2}{K_1 + K_2}\right)^2$$

4.3.5.4 2D unsteady flow simulation method

This study also performed the 2D unsteady flood analysis for the HEs as similar to 1D unsteady flow analysis in Periyar river basin. In 2D unsteady flow analysis, the 2D flow area (in form of polygon) can be computed/digitized based on the DTM in form of mesh grid with an appropriate grid size. Each grid contains a computation points and for each grid manning's n need to be defined.

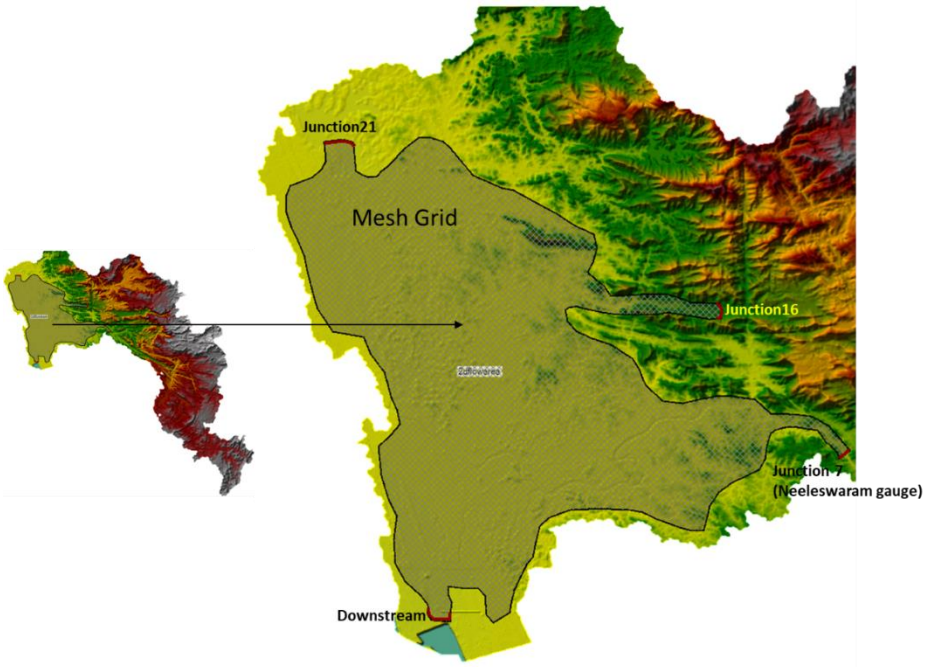

Figure 4.11: HEC-RAS represents 2D mesh boundary to setup 2D flood flow simulation.

The size of the mesh grid will depend on the resolution of the DTM. The finer grid will provide more precise outcomes, but the time of computation will be enhanced. In 2D flow area, boundary cells may vary in shape and size to follow the detailed boundary (or polygon). After defining the 2D flow area, the inlet flows, local flows, and downstream conditions can be defined as similar to 1D unsteady flow. The 2D mesh pre-processor computes a detailed elevation-volume relationship for each cell. HEC-RAS 2D unsteady flow computation can be performed using diffusion wave or full momentum 2D equations.

In this study, full momentum equations were used with Implicit Finite Volume solver (Reference). The 2D mesh grid representation has shown in Figure 4.11.

4.4 RAINFALL AND FLOOD FREQUENCY ANALYSIS (FFA)

Extreme high volume flood estimates are needed for conditions where the reservoir inflow peak discharge is superior than the maximum spillway capacity, the reservoir has a large, carry-over storage, and/or the reservoir has dedicated flood control space. Flood hydrographs include peak, volume and timing, and integrate the drainage basin and channel response to precipitation, given some initial, variable state of moisture throughout the watershed. To conduct risk analyses and dam safety evaluations, extreme floods and probability estimates (i.e. FFA) are required. Flood frequency analysis was conducted using peak-flow, historical and paleo flood data within the watershed. In this study, the objective is to perform FFA mainly to improve the 1D and 2D flood flow simulations with the spatially distributed watershed model that includes physically-based and relevant hydrologic and hydraulic processes to simulate extreme floods on large watersheds.

In this study, Flood Frequency Analysis (FFA) has been performed to generate extreme rainfall and flow values corresponding to specific return periods. Initially, three different distribution methods were used for the frequency analysis - Gumbel method, Normal Distribution method and Log Pearson Type 3 (LogPT3) method. After evaluation of these three distribution methods using MSE and RMSE, the Log Pearson Type 3 and Gumbel are the most fit method for calculating flood frequency of an extreme event. For this, annual maximum of rainfall datasets (2002-2018) at different rainfall stations (23) and simulated discharge data (2002-2018) at the sub-catchments outlets were taken and calculations were performed for multiple Return Periods (T) 20, 50, 100, 200, 500. We have also highlighted the variations in Gumbel and LogPT3 methods.

4.4.1 GUMBEL Extreme Value Distribution Method

The Gumbel method used annual maximum value (e.g. Rainfall and Flow), which can be defined as the largest or extreme high value for the given year. The general characteristics of the Gumbel extreme-value distribution are; the mean flow occurs at the return period of Tr = 2.33 years, which shows a positive skewness (i.e., it is skewed towards the high flows or extreme values). Despite the positive skew of the Gumbel distribution, it has some drawbacks that it does not account directly for the computed skew of the data. Although, it predicts the high flows reasonably well. The entire curve fit is not much better than that obtained with the normal distribution, indicating that the peak flow series is not distributed according to the double-exponential distribution equation. The equation used for this distribution to calculate the peak discharge (in cfs) was:

$$x_T = \bar{x} + k.\sigma_x$$

where $\bar{x} = \sum_{i=1}^{n} x_i$ = mean of the sample size

$\sigma_x = \sqrt{\frac{1}{(n-1)}\sum_{i=1}^{n}(x-\bar{x})^2}$ = standard deviation of the sample size

$\text{Yt} = -\left[\ln.\ln\left(\frac{T}{T-1}\right)\right]$ = reduced variate

$\text{k} = \frac{Y_t - \bar{Y}_n}{S_n}$ = frequency factor

The values of $\bar{Y}_n$ and S_n were taken from Gumbel's Extreme Value Distribution.

4.4.2 LOG-PEARSON TYPE 3 Extreme Value Distribution Method

Log Pearson Type III is also a 3 parameter distribution belonging to the Exponential/Pearson type family. The 3 parameters are skew coefficient, mean and standard deviation. In this method, log of the annual average discharge data was calculated from which all the parameter values were calculated.

The equation for the log of peak discharge value in Log Pearson Type 3 distribution is given below from which the peak discharge (m^3/s) was calculated by taking the antilog of the log peak values:

$$\log Q_j = \bar{x} + K_j \sigma_y$$

where $\bar{x}$ = mean of the sample size

K_j= Frequency factor

σ_y = standard deviation of the sample

The frequency factor was calculated using the Probability of exceedance and the Skewness coefficient, C_{sy} and was obtained from the Frequency factor table.

The formulas used to calculate mean, standard deviation and Skewness coefficient were:

$$\bar{x} = \frac{1}{n}\sum_{i=1}^{n} X_i$$

$$\sigma = \left[\frac{1}{(n-1)}\sum (x_i - \bar{x})^2\right]^{1/2}$$

$$C_{sy} = \frac{n\sum_{i=1}^{n}(x_i - \bar{x})^3}{(n-1)(n-2)\sigma^3}$$

4.5 FLOOD INUNDATION MAPPING AND PROBABILISTIC FLOOD MODELING

4.5.1 Return Period Based Flood Inundation Mapping

The return period based flood inundation mapping has been performed in HEC-RAS 1D model. As per FFA, the return periods based flood values have been computed by performing Gumbel and LogPT3 distribution methods. The Rainfall frequency analysis has been performed at each station/grid and then probabilistic return period extreme rainfall such as 20years, 50years, 100years, and 200years were generated. These return periods rainfall can be used to generate the probable maximum flood and then the flood spread area and depth can be computed. Similarly, multiple return period flood flows such as 20years, 50years, 100years, and 200years have been generated at different locations over the selected study area.

HEC-HMS has been used to generate the flood discharge at the outlets and each sub-catchment and thus different return period floods were computed corresponding to each sub-catchment outlet. Additionally, at three locations such as Neleswaram gauge, Junction 16 and Junction 21, the accumulated flood flows are computed, which actually represent the three main tributaries. Thus, different return period floods are computed mainly to highlight the real flood scenario if such event happened in the future. Finally, the steady state analysis was carried out in HEC-RAS to generated the flood volume, depth, water surface elevation, and other hydrodynamic variables with respect to each return period floods. The flood inundated maps generated for the different return periods at different sections can be further used to characterize the flood plain zones.

4.5.2 Event Wise Flood Inundation Mapping

The main aim of the constructing historical flood events (HEs), to present an integrated approach which could be able to generate more accurate future extreme flood scenarios if such events repeat in the future

(Table 4.2). Therefore, the long-term rainfall data has been taken and then the probabilistic dry and wet year were identified. First, we calculated the mean of all-time series, mainly to consider high-rainfall duration (i. e. mostly monsoon time). Then the percent of departure of rainfall is calculated for each year and if rainfall exceeds for any given year >20-30% so that year may be treated as wet year. The for the wet years, the maximum rainfall or extreme high rainfall events are identified and selected. Then based on this high rainfall based HEs, the HEC-HMS modelling was performed, and corresponding floods (Q in m^3/s) have been generated at differ. Total seven HEs have been identified and the greatest magnitude event was identified as HE-7 (July-Aug, 2018) i.e. referred as Kerala flood event.

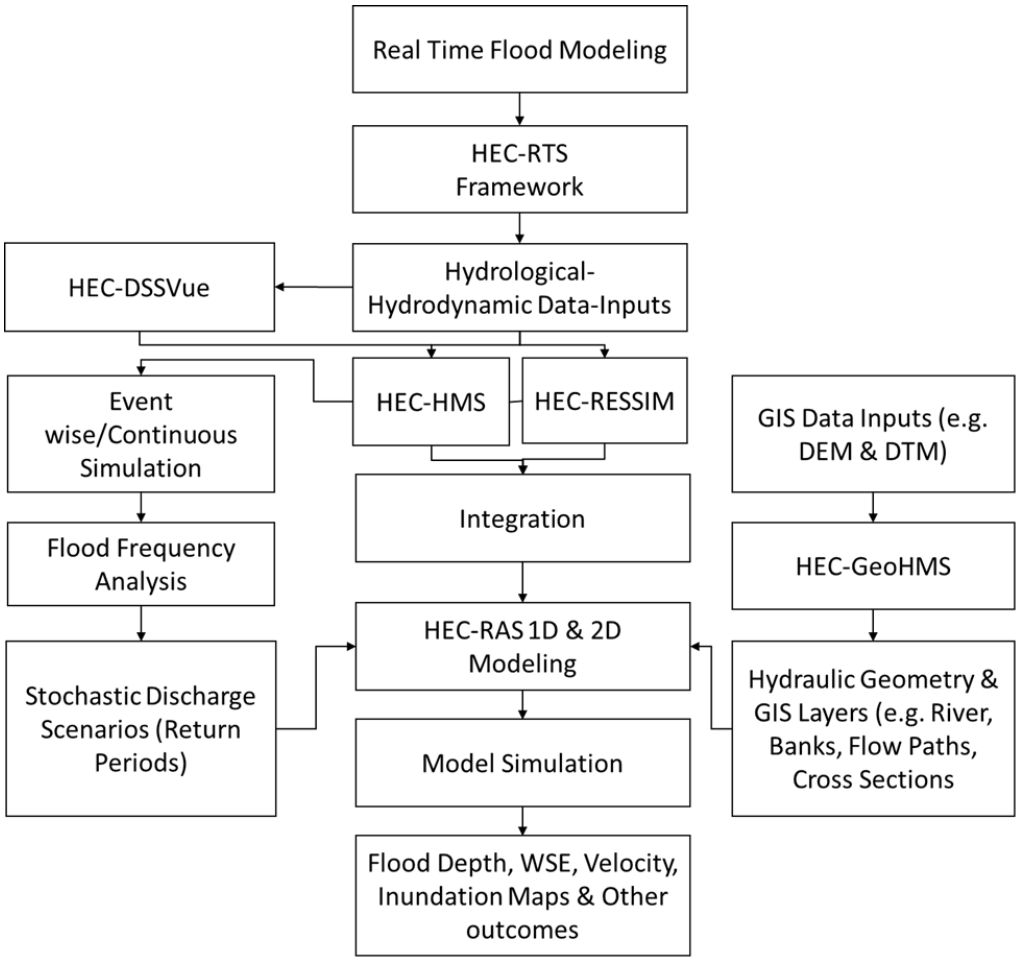

Figure 4.12: Overall integrated modeling framework in HEC-RTS system.

Based on the simulation, calibration and optimization of the HE-7 event, the optimized parameter values were used to model the other HEs in HEC-HMS and then finally extreme high flood discharge was generated at different locations. Using the same flood flows as per each HE, the 1D and 2D unsteady flow analysis were performed in HEC-RAS and flood inundation maps were generated for different HEs. The validation of HEs, especially for HE-7 (i.e. Kerala flood event 2018) was performed while comparing the observed vs modelled discharge. The spread area and calculated depth for the HE-7 event also validated with real time satellite dataset and other thematic flood maps that are published online through different journals and web portals. The overall integrated modeling framework in HEC-RTS system has shown in Figure 4.12.

Table 4.2: Event wise and continuous modeling details.

SI No.	Event IDs	Structured/Virgin Flow Condition	Simulation Step	Method	From	To
1	HE_1	Structure	Event wise	CN - Method	25/7/2002	20/8/2002
2	HE_2	Structure	Event wise	CN - Method	15/6/2003	7/7/2003
3	HE_3	Structure	Event wise	CN - Method	25/7/2004	20/09/2004
4	HE_4	Structure	Event wise	CN - Method	25/7/2008	20/8/2008
5	HE_5	Structure	Event wise	CN - Method	5/6/2013	25/6/2013
6	HE_6	Structure	Event wise	CN - Method	8/6/2017	5/7/2017
7	HE_7	Structure	Event wise	CN - Method	1/7/2018	31/8/2018
8	WR_1	Virgin Flow Condition	Continuous	SMA Method	1/1/2002	31/12/2018

CHAPTER 5: RESULTS & DISCUSSION

5.1 GENERATION OF BIAS FREE RAINFALL AND TEMPERATURE DATASETS ACROSS THE STUDY AREA

This study performs integrated hydrological and hydrodynamic real time flood modeling through HEC-RTS tools such as HEC-DSSVue, HEC-HMS, HEC-RESSIM and HEC-RAS in the Periyar river basin. For flood modeling, the event wise and continuous simulation have been performed. To generate the historical flood events (total seven) and continuous simulations, daily rainfall (23 stations) and temperature datasets (14 stations) were processed, and bias corrected. For Kerala floods (2018) i.e. HE – 7, the 3-hourly bias corrected rainfall (TRM+GPM) was used and then the optimized elevation-area-capacity-discharge curves were re-used in HEC-HMS to perform the event wise and continuous simulations using daily rainfall datasets (2002-2018).

Figures 5.1 and 5.2 show the station wise scenarios of daily rainfall and temperature, respectively. The annual average across all stations is calculated around 100 mm to 2500 mm. The maximum rainfall events mostly corresponded between 80 mm to 490 mm, considering all stations (Figure 5.1). The mean temperature (daily average) ranges from 20^{O}C to 32℃ (Figure 5.2). Table 5.1 shows the statistics of bias corrected rainfall (TRMM+GPM) across 14 stations distributed over the Periyar river basin. The bas correction methodology of rainfall is already explained in the methodology section. During Kerala flood event (HE-7), it was observed that while doing the reservoir simulation using daily rainfall, some rainfall extremity was lost during the high rainfall events. Therefore, initially, the HEC-RESSIM was setup with 3-hourly rainfall to get the best possible outcome variables and then again we improved the daily rainfall with respect to hourly rainfall and then event wise simulation was carried out in HEC-HMS.

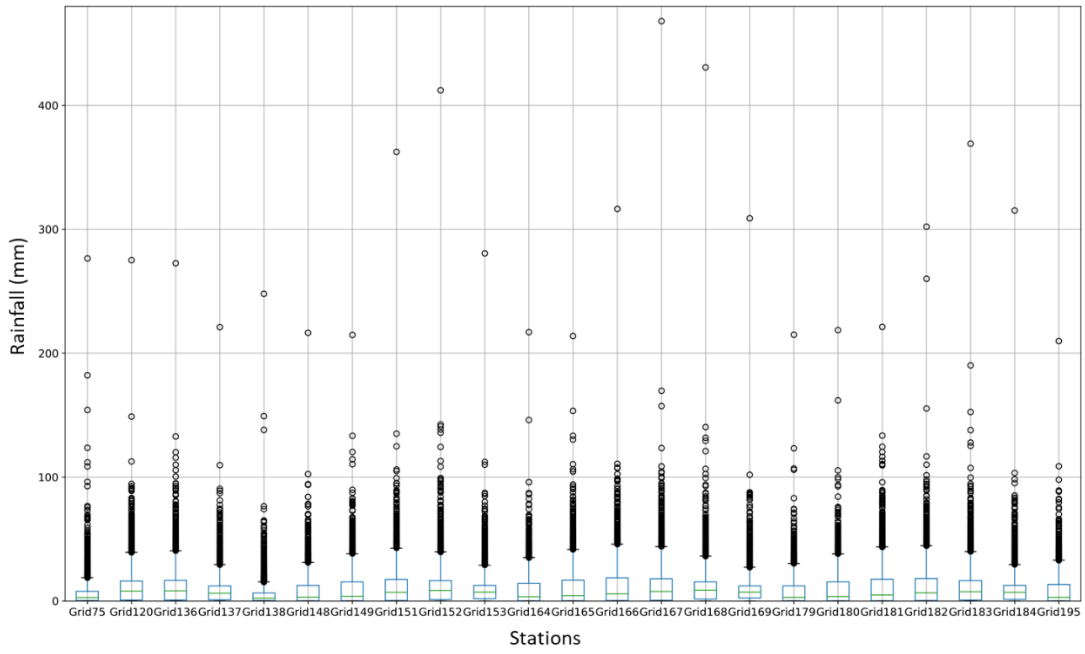

Figure 5.1: Daily Rainfall Data (23 stations) Across the Study Area (2002-2018).

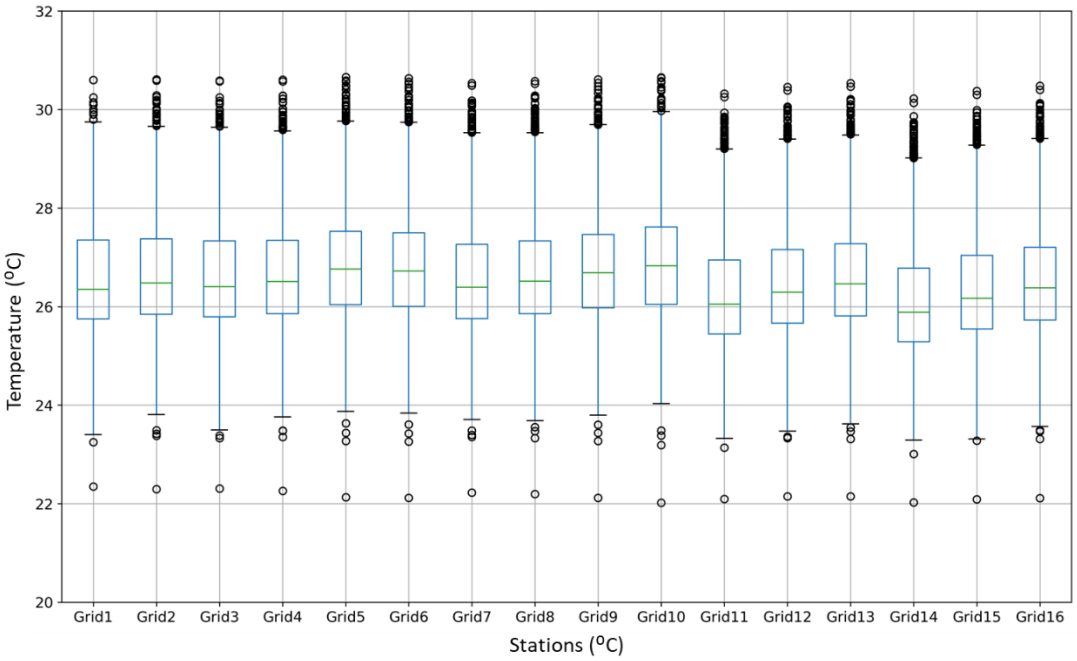

Figure 5.2: Daily Mean Temperature Data (16 stations) Across the Study Area (2002-2018).

Table 5.1 shows a significant improvement in the 3-hourly bias corrected rainfall. There is significant improvement can be noticed between Sum of IMD and Sum of (TRMM+GPM) corrected rainfalls across all 14 stations.

Table 5.1: Event wise bias corrected 3-hourly rainfall (TRMM+GPM).

Stations	Sum of-IMD	Sum of-TRMM+GPM	Sum of -(TRMM+GPM) corrected	St. Dev of -(TRMM+GPM) corrected	Max of -(TRMM+GPM) corrected
CS1	656.48	570.93	626.11	9.21	98.00
CS2	339.90	274.50	325.42	5.28	65.40
CS3	516.30	471.55	530.58	5.82	55.40
CS4	389.18	339.60	365.62	4.98	55.00
CS5	496.93	478.93	492.74	5.08	33.59
CS6	1140.51	542.68	1512.49	22.52	177.89
CS7	343.40	321.66	346.59	3.26	17.13
CS8	1086.42	248.12	1232.74	16.30	92.40
CS9	587.90	246.74	651.46	11.08	80.56
CS10	343.71	244.03	469.76	5.51	29.84
CS11	1361.70	328.75	1552.05	18.41	91.37
CS12	1177.42	493.26	1495.48	19.66	105.20
CS13	745.43	187.67	788.26	17.81	147.84
CS14	1025.77	175.87	1040.89	19.23	125.00

5.2 HEC-HMS MODEL SETUP, SIMULATION, CALIBRATION AND PARAMETERIZATION RESULTS

As explained in the methodology section, HEC-HMS model has been used to generate the flows (or discharge values) at different portions (e.g. at different outlets including up-streams and down-streams). First, an event based analysis has been performed to generate flood flows for different historical events (HEs) and then continuous simulation was performed to generate flood flows at each sub-catchment. In HEC-HMS, the watershed characteristics including subbasin, rivers, reaches, junctions and outlet were derived from ALOS PALSAR DEM (12 m). The subbasin wise watershed parameters such as area, longest flow path, slope of the basin, basin relief, drainage density, and curve numbers (CNs) have been simulated and their details have been provided in Table 5.2. For the hydrologic routing (e.g. between two subbasins from upstream to downstream though various Reaches and Junctions), the Muskingum method has been utilized. The details of Muskingum parameters for each Reach have been provided in Table 5.3.

Table 5.2: Subbasin wise watershed parameters computed in HEC-HMS.

Subbasin	Area (km2)	Longest Flowpath Length (km)	Basin Slope	Basin Relief (m)	Drainage Density (km/km2)
Sub39	523.9	63.68005	0.00827	1126	0.13262
Sub37	307.8	53.83883	0.00267	744	0.12027
Sub36	223.93	38.59119	0.00867	785	0.10006
Sub34	405.82	61.21518	0.01115	1130	0.12676
Sub35	285.97	46.84816	0.01294	1141	0.09994
Sub29	189.1	36.50604	0.02249	1853	0.12923
Sub31	57.801	18.22829	0.02085	582	0.04743
Sub23	333.91	44.92861	0.03022	2114	0.10028
Sub30	64.794	19.8144	0.03384	1386	0.08277
Sub38	89.576	27.13019	0.02616	924	0.25225
Sub67	81.724	32.28418	0.02606	936	0.30816
Sub28	66.708	27.66739	0.02377	1088	0.18673
Sub24	201.25	33.60501	0.04591	2155	0.08729
Sub27	63.321	21.19204	0.04381	1129	0.07083
Sub20	88.794	22.95914	0.04402	1201	0.0875
Sub43	44.01	19.01882	0.02916	834	0.2401
Sub17	396.14	63.52382	0.02386	2610	0.12443
Sub68	63.813	25.99705	0.02153	789	0.30588
Sub32	89.726	24.12288	0.00761	850	0.18084
Sub21	58.295	19.28968	0.02772	749	0.02396
Sub69	22.683	11.03817	0.00503	377	0.23206
Sub70	90.12	16.59064	0.00032	616	0.14454
Sub16	78.054	16.41018	0.00284	552	0.05114
Sub71	97.831	35.20164	0.00011	375	0.2271
Sub25	70.638	15.81007	0.00172	122	0.01387
Sub18	123.14	36.74219	0.00107	398	0.14028
Sub72	46.015	18.644	0.00043	83	0.25781
Sub19	80.726	22.53804	0.00106	139	0.11102
Sub9	269.17	46.08639	0.01656	1423	0.0975
Sub40	106.2	27.04938	0.01287	845	0.09945
Sub2	65.812	25.36526	0.01414	1019	0.11109
Sub4	57.644	15.88673	0.05829	1092	0.04168
Sub11	62.566	17.74371	0.02299	923	0.06552
Sub46	30.675	11.53088	0.01673	734	0.28847

Sub5	134.61	39.13654	0.01567	1033	0.15645
Sub14	256.84	63.48644	0.01453	1963	0.16545
Sub22	31.134	11.06944	0.00251	625	0.33831
Sub56	81.164	18.30749	0.02177	844	0.19064
Sub13	71.29	22.06283	0.02906	1015	0.10196
Sub62	293.09	63.19209	0.00146	669	0.20469
Sub6	112.07	26.33858	0.01337	1119	0.12412
Sub10	106.64	30.11024	0.00309	1039	0.16792
Sub33	59.811	19.51553	0.00676	800	0.02179
Sub8	118.63	32.25542	0.00149	409	0.10859
Sub42	43.882	21.93827	0.00076	147	0.46608
Sub1	261.52	58.55508	0.00238	898	0.16683
Sub3	152.38	32.85466	0.00008	93	0.12408
Sub12	87.453	26.03809	0.00072	99	0.07099
Sub41	79.121	29.26241	0.00027	99	0.21926
Sub61	98.126	24.98647	0.00043	99	0.1554
Sub15	58.316	17.64173	0.0006	99	0.00436
Sub63	46.642	22.15779	0	99	0.35745
Sub44	44.956	25.5707	0.00068	99	0.54117
Sub26	163.72	32.91342	0.00073	115	0.10123
Sub76	84.317	26.32034	0.00015	102	0.19811
Sub77	17.295	9.99992	0.00053	104	0.46655

The computation of various watershed variables/parameters at each subbasin scale as shown in Table 5.2 are necessary to calculate the different hydrological processes for both event and continuous simulations. Total 56 subbasins have been delineated in the selected Periyar river basin. The subbasin (Sub) area varies from ~ 17.295 km^2 (i.e. Sub77) to 523.9 km^2 (i.e. Sub39). In case of hydrologic routing Muskingum K and x parameters were adjusted using manual calibration. The Muskingum K varies from 0.3 to 2.5 and the Muskingum x values was taken as 0.5, considering extreme high flood conditions. Here, K is the travel time of a flood wave passing through the Reach and x is a measure of the degree of storage (x= 0 means a level-pool reservoir or maximum storage, x = 0, means a pure transmission reach in which there are no storage effects, and x range between 0 and 0.5).

Table 5.3: Details of Muskingum routing parameters at each Reach in HEC-HMS.

Reach	Method	Muskingum K	Muskingum x	No of Subreaches
Riv18	Discharge = Inflow	1	0.5	1
Riv 38	Discharge = Inflow	0.8	0.5	1
Riv 39	Discharge = Inflow	1.5	0.5	1
Riv13	Discharge = Inflow	1	0.5	1
Riv12	Discharge = Inflow	1.1	0.5	1
Riv33	Discharge = Inflow	1	0.5	1
Riv29	Discharge = Inflow	1.2	0.5	1
Riv24	Discharge = Inflow	0.9	0.5	1
Riv11	Discharge = Inflow	1.1	0.5	1
Riv10	Discharge = Inflow	1	0.5	1
Riv35	Discharge = Inflow	0.8	0.5	1
Riv30	Discharge = Inflow	0.7	0.5	1
Riv20	Discharge = Inflow	0.8	0.5	1
Riv19	Discharge = Inflow	0.9	0.5	1
Riv9	Discharge = Inflow	0.5	0.5	1

Riv8	Discharge = Inflow	1.4	0.5	1
Riv7	Discharge = Inflow	0.5	0.5	1
Riv6	Discharge = Inflow	0.5	0.5	1
Riv5	Discharge = Inflow	0.5	0.5	1
Riv4	Discharge = Inflow	1.8	0.5	1
Riv32	Discharge = Inflow	1.3	0.5	1
Riv28	Discharge = Inflow	0.55	0.5	1
Riv27	Discharge = Inflow	1.4	0.5	1
Riv22	Discharge = Inflow	0.9	0.5	1
Riv16	Discharge = Inflow	1.4	0.5	1
Riv3	Discharge = Inflow	2.5	0.5	1
Riv37	Discharge = Inflow	0.8	0.5	1
Riv36	Discharge = Inflow	2.4	0.5	1
Riv25	Discharge = Inflow	2.2	0.5	1
Riv23	Discharge = Inflow	0.3	0.5	1
Riv21	Discharge = Inflow	1.3	0.5	1
Riv17	Discharge = Inflow	2.2	0.5	1
Riv15	Discharge = Inflow	2	0.5	1
Riv2	Discharge = Inflow	2	0.5	1
Riv1	Discharge = Inflow	1.2	0.5	1

5.2.1 Event Based Simulation Results

The main purpose of this study is to compute the flood flows and optimization of various parameters related to flood discharge and reservoir simulation during extreme climate conditions. Therefore, seven HEs were reconstructed to fulfil the above objective. The selection process of seven HEs has already been explained in the methodology section. For the construction of the seven HEs in HEC-HMS through event wise simulation, the CN method has been used to compute the losses and SCS Unit Hydrograph method were selected to transform the actual runoff (Sudheer et al., 2019). Table 5.4 shows the parameterization of loss method. The Initial Abstraction IA (mm) has been taken as 5 mm as suggested in few studies (Ouédraogo et al., 2018). The CN values for each subbasin has been calculated using SCS curve number method using LULC, soil maps and rainfall based antecedent moisture conditions (taken 5 days prior rainfall) as previously computed in few studies (Ouédraogo et al., 2018). The CN for each subbasin has shown in Table 5.4, which are aggregated from the CNs grid generated for this study basin (Figure 4.2). In this study area, the CN varies from 60 (representing towards low runoff conditions) to 95 (representing towards high runoff conditions).

The soil imperviousness (%) is an important component in the computation of infiltration losses and overland flow. If the soil surface area is 100% imperviousness, then, runoff will be extremely high (almost 100% except ET and canopy losses) and there will be no infiltration. In this study, the imperviousness (%) has been calculated based on the settlement area computed in LULC map (referred to Figure 4.2). Each subbasin wise imperviousness (%) has shown in Table 5.4. The imperviousness (%) varies from 0 to 40. The downstream subbasins are corresponded with high imperviousness (%) that means these areas are having high settlement densities and can also be seen in LULC map (Figure 4.2). Basin lag, tp shows the response of rainfall to runoff in time and majorly depends on slope of the basin. If the slope is high, the tp will be short or less. Figure 5.3 shows the subbasin wise response of tp and slope.

Table 5.4: Loss method parameters.

Subbasin	Area	IA, mm	CN	Imperviousness, %
Sub39	523.9	5	75	2
Sub37	307.8	5	80	5
Sub36	223.93	5	85	2
Sub34	405.82	5	78	0
Sub35	285.97	5	78	2
Sub29	189.1	5	70	5
Sub31	57.801	5	70	4
Sub23	333.91	5	63.5	2
Sub30	64.794	5	63	6
Sub38	89.576	5	67	2
Sub67	81.724	5	60	1
Sub28	66.708	5	60	5
Sub24	201.25	5	60	2
Sub27	63.321	5	60	2
Sub20	88.794	5	63.5	1
Sub43	44.01	5	63.5	0
Sub17	396.14	5	63.5	2
Sub68	63.813	5	60	11
Sub32	89.726	5	63.5	2
Sub21	58.295	5	63.5	1
Sub69	22.683	5	63.5	6
Sub70	90.12	5	63.5	2
Sub16	78.054	5	67	1
Sub71	97.831	5	63.5	10
Sub25	70.638	5	63.5	30
Sub18	123.14	5	63.5	22
Sub72	46.015	5	63.5	30
Sub19	80.726	5	63.5	23
Sub9	269.17	5	74	3
Sub40	106.2	5	67	0
Sub2	65.812	5	67	5
Sub4	57.644	5	67	2
Sub11	62.566	5	67	0
Sub46	30.675	5	67	0
Sub5	134.61	5	67	2
Sub14	256.84	5	81	2
Sub22	31.134	5	70	0
Sub56	81.164	5	70	0
Sub13	71.29	5	63	0
Sub62	293.09	5	63.5	20
Sub6	112.07	5	63.5	2
Sub10	106.64	5	63.5	1
Sub33	59.811	5	63.5	0
Sub8	118.63	5	60	20
Sub42	43.882	5	67	0
Sub1	261.52	5	67	25
Sub3	152.38	5	69.3	35

Sub12	87.453	5	63.5	40
Sub41	79.121	5	63.5	40
Sub61	98.126	5	74	20
Sub15	58.316	5	67	20
Sub63	46.642	5	74	15
Sub44	44.956	5	77.5	25
Sub26	163.72	5	78.7	35
Sub76	84.317	5	77.5	15
Sub77	17.295	5	95	15

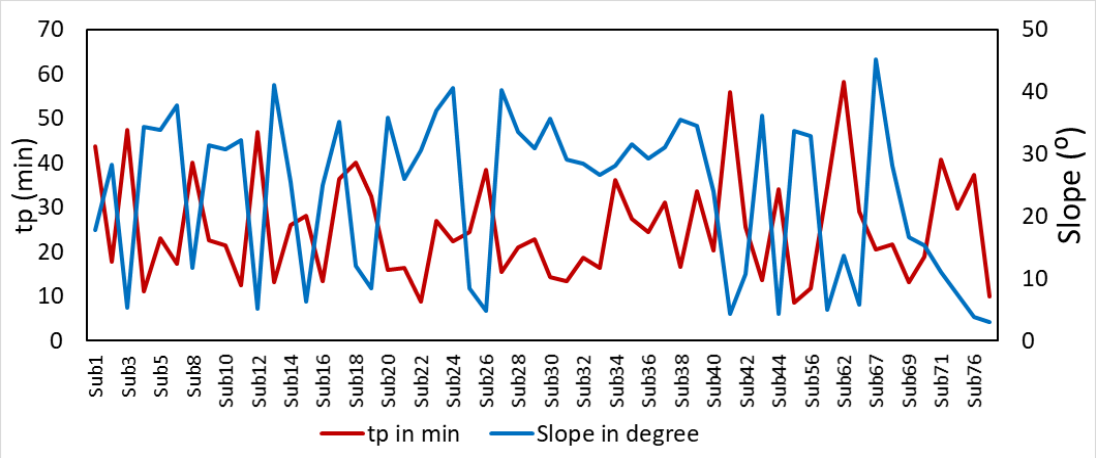

Figure 5.3: Subbasin wise basin lag and slope.

For event-based analysis, first the greatest historical flood event among others i. e. HE-7 (Kerala flood, 2018) was simulated in HEC-HMS. For event wise simulation, the two main reservoirs situated at the upstream areas are also taken into consideration. To analyze the effect of reservoirs in floods, for example flood peak attenuation, the reservoir parameters such as elevation (m) vs area (km^2) and elevation (m) vs Q (m^3/s) curves are prepared and used as input parameters for Mullaperiyar and Idukki dams (Figure 5.4). In new versions of HEC-HMS, the reservoir simulation can be effectively performed (Bekele et al., 2021; Srinivas et al., 2018). Based on these curves, the regulated flood flows are computed in the downstream portion. Similarly, other HEs are also computed based on the optimized parameters (including hydrological processes and reservoirs related parameters). Figure 5.6 shows the information of inflows/outflows (m^3/s) and storage (1000 m^3) vs elevation (m) relationship during HE-7 (Kerala Flood, July-August, 2018). In Figure 5.6, a significant reduction in flood peaks (peak attenuation) can be observed.

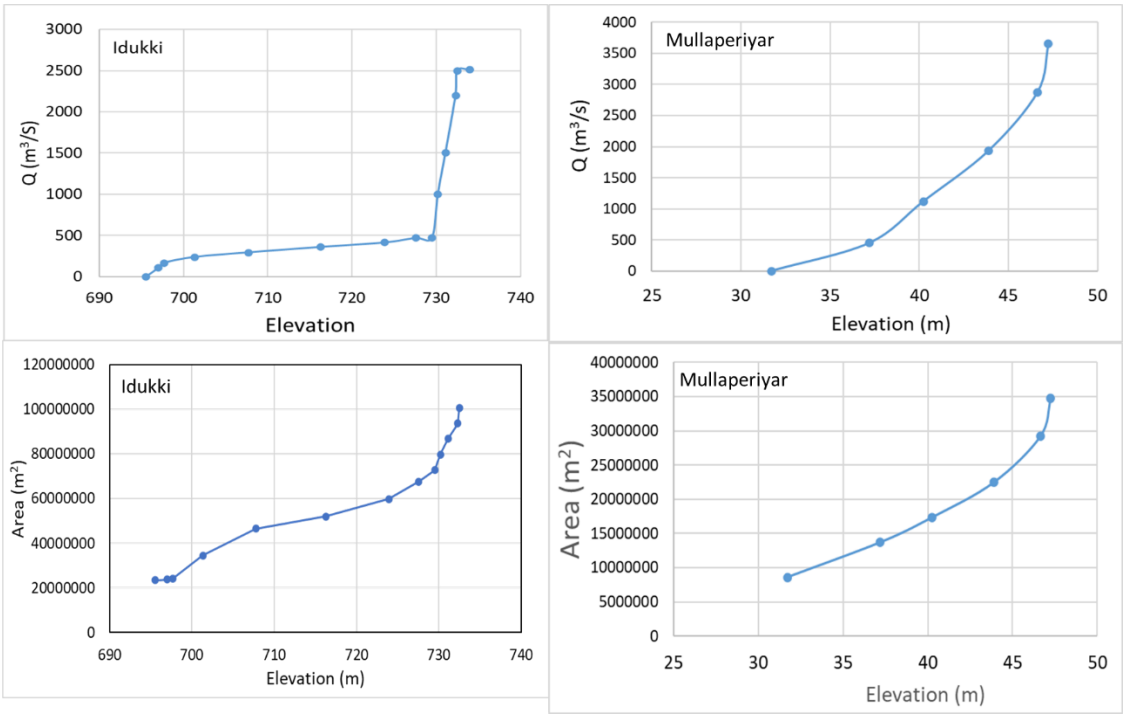

Figure 5.4: Area-Elevation-Discharge curves to simulate flood flows through Mullaperiyar and Idukki dams in HEC-HMS.

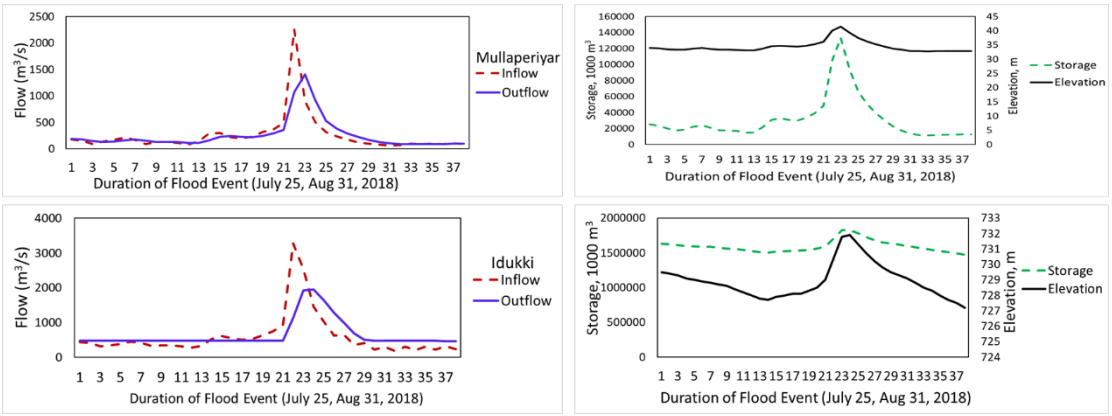

Figure 5.5: Information of inflows/outflows (m^3/s) and storage (1000 m^3) vs elevation (m) relationship during HE-7 (Kerala Flood, July-August, 2018).

The resultant flood flows simulation for the HE-7 event including reservoirs incorporation, the simulated flood discharge was calibrated and compared at Neeleswaram gauge, at the downstream of Idukki reservoir, with reference to the observed discharge (during July 25 to August 22, 2018). Figure 5.7 (a) shows the line diagram, which compares the simulated flood flows vs observed flood flows on the daily scale during July 25 to August 22, 2018. The line diagram shows a well matching in both high and low peaks, except 2/3 events (days). As compared to peaks, the modelled flood discharge found able to capture extreme high peaks, however it is slightly overestimated as compared to observed discharge (Figure 5.7a). However, both scenarios are compared on a daily scale therefore a slight variation in peaks (underestimation/overestimation) can be expected. Figure 7(b) shows the regression plot that highlights the correlation (coefficient of determination R^2) between observed and modelled discharge during the HE-7 event. The R^2 is computed as 0.80, which shows a good match between modelled and observed flood discharge.

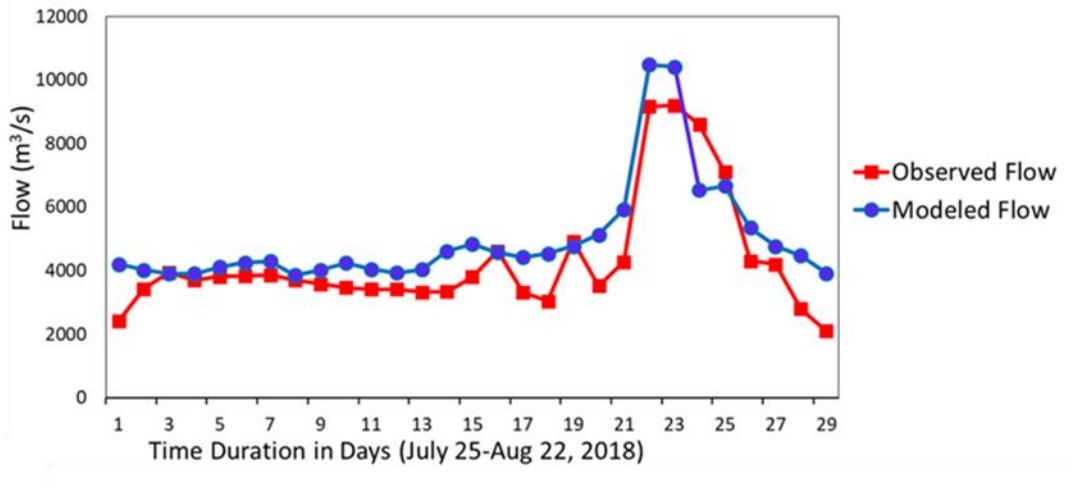

Figure 5.6: Line diagram shows the comparison of flood flows between modelled and observed flood discharge during HE-7 event.

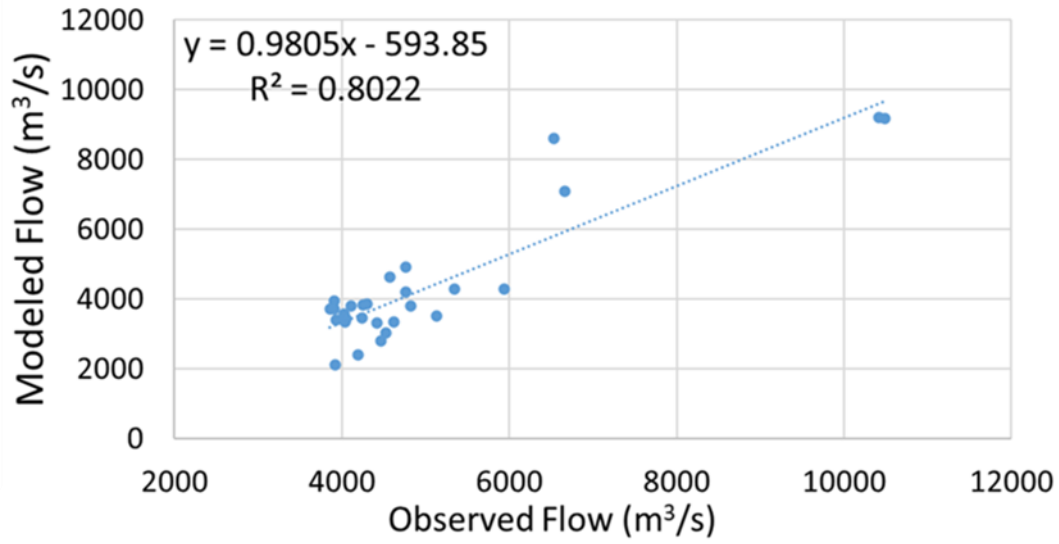

Figure 5.7: Regression plot shows the comparison of flood flows between modelled and observed flood discharge during HE-7 event.

Figure 5.8 shows the information of inflows/outflows (m^3/s) and storage (1000 m^3) vs elevation (m) relationship for HEs such as HE-1, HE-2, HE-3, HE-4, HE-5 and HE-6 at Mullaperiyar dam computed in HEC-HMS by adopting same parameters and reservoir datasets (i. e. elevation vs area and elevation vs discharge) after calibrating the flood discharge for the HE-7 at the Neeleswaram gauge. In all HEs (Figure 5.8), a significant lag (or peak attenuation) between inflows and outflows peaks can be observed. This shows the reservoir storage effect in the minimization of flood discharge during extreme high flood conditions. Similarly, Figure 5.9 shows the information of inflows/outflows (m^3/s) and storage (1000 m^3) vs elevation (m) relationship for HEs such as HE-1, HE-2, HE-3, HE-4, HE-5 and HE-6 at Periyar dam computed in HEC-HMS by adopting same parameters and reservoir datasets after calibrating the flood discharge for the HE-7 at the Neeleswaram gauge. The storage vs elevation effect can be understood here in these HEs (Figures 5.8 and 5.9). In HEC-HMS the storage vs elevation computes at each step or (event). This curve defines the storage as a volume of water stored in the reservoir. If the reservoir has capacity, then more flood volume can be stored and in this case the outflow can be constant and cannot be released more than the inflow. Such effect can be visualized in case of Idukki for few HEs (Figure 5.9), which allow to mitigate flood effect. However, when reservoir capacity is full then additional flood discharge cannot be stored.

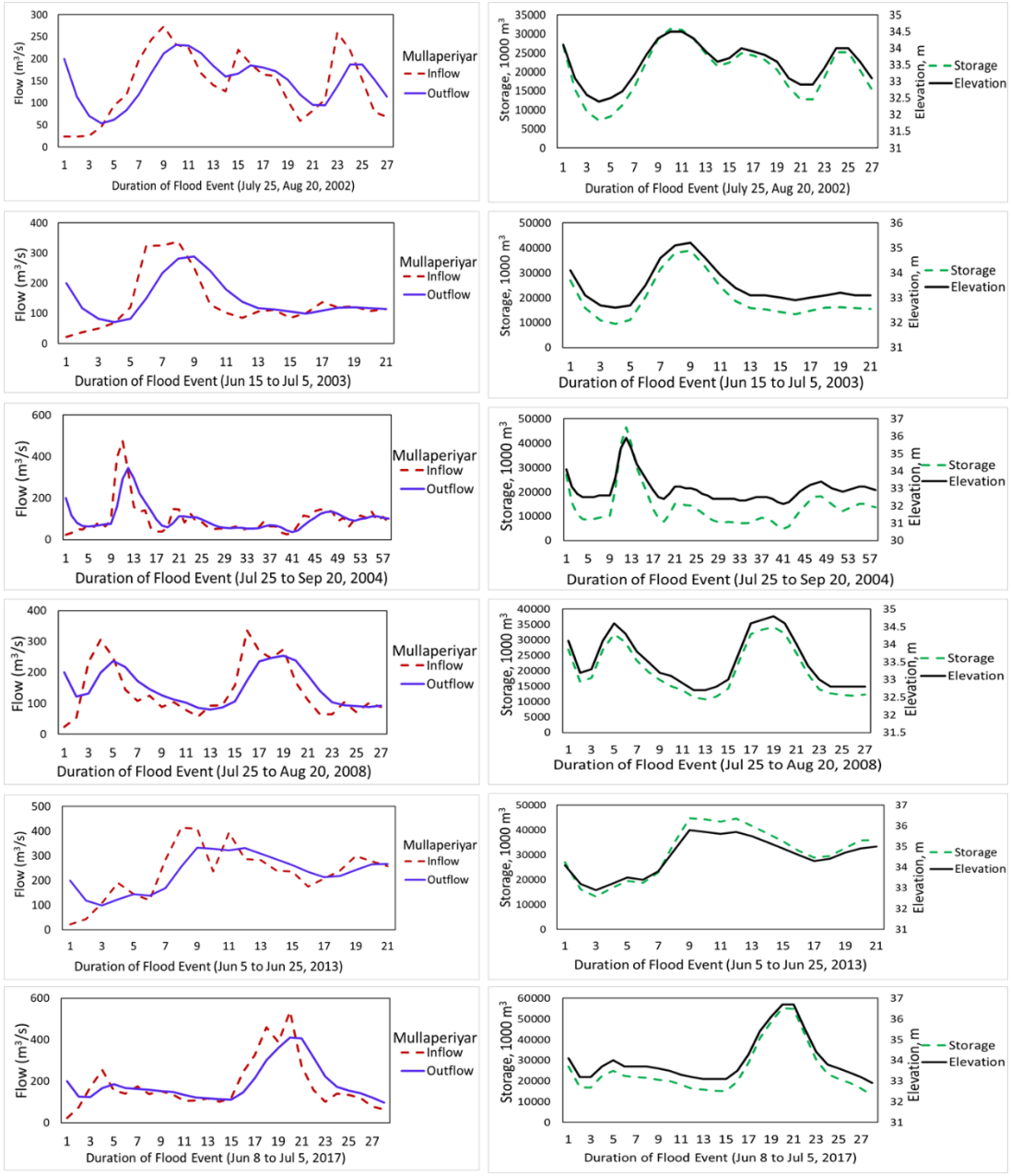

Figure 5.8: Information of inflows/outflows (m^3/s) and storage (1000 m^3) vs elevation (m) relationship for HEs such as HE-1, HE-2, HE-3, HE-4, HE-5 and HE-6 at Mullaperiyar dam.

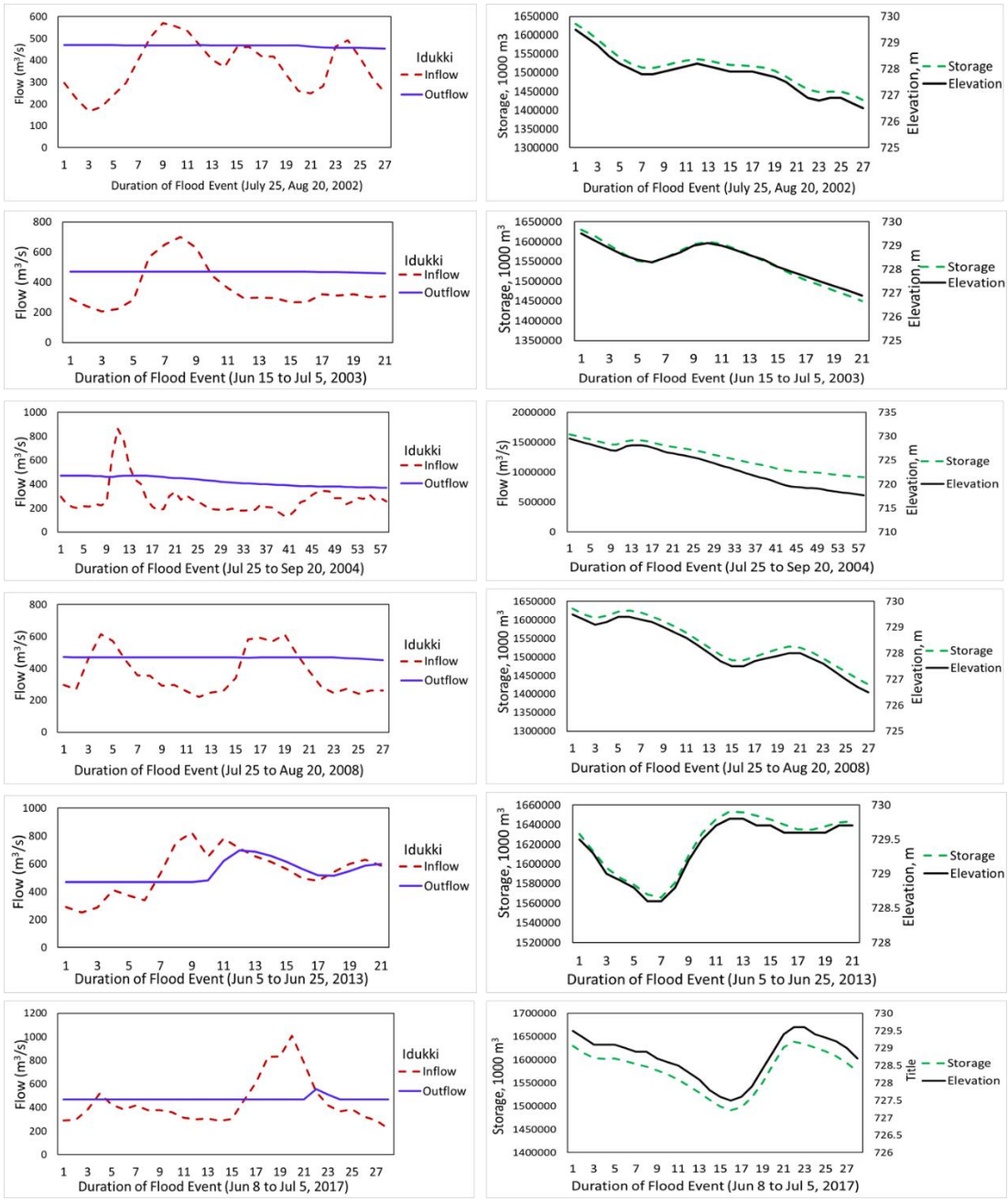

Figure 5.9: Information of inflows/outflows (m^3/s) and storage (1000 m^3) vs elevation (m) relationship for HEs such as HE_1, HE_2, HE_3, HE_4, HE_5 and HE_6 at Periyar dam.

After successful simulation of each HE in HEC-HMS, the flood discharge has been computed at different subbasins and junctions. In subbasin, the flood discharge can be computed for that subbasin only; while at each Junction, the cumulative discharge can be computed for the Junction's upstream area. In HEC-RAS, the hydrodynamic or hydraulic flood routing is setup at the downstream of Neeleswaram gauge.

Therefore, the to fulfil the boundary conditions in HEC-RAS for 1D and 2D unsteady flood modeling of HEs, the flood discharge is calculated at Junction 7 (i. e. the just downstream of Neeleswaram gauge), Junction 16, Junction 21 (considering two major tributaries of main Periyar river basin) and each subbasin. Figure 5.10 shows the unsteady daily flood discharge at Neeleswaram gauge (or Junction 7), Junction 16 and Junction 21 corresponding to each HE. In box plots (Figure 5.10), the flood extremity for each HE can be seen (at y-axis). At each location (i. e. Neeleswaram gauge, Junction 16 and Junction

21), the flood extremity varies corresponding to each location, which highlights the variations in rainfall across the basin during extreme high flood event. For example, In case of HE_1, the high flood discharge was computed at Junction 16, while in other HEs the maximum discharge is mostly corresponded to Neeleswaram gauge. However, these variations are not equal corresponding to each location.

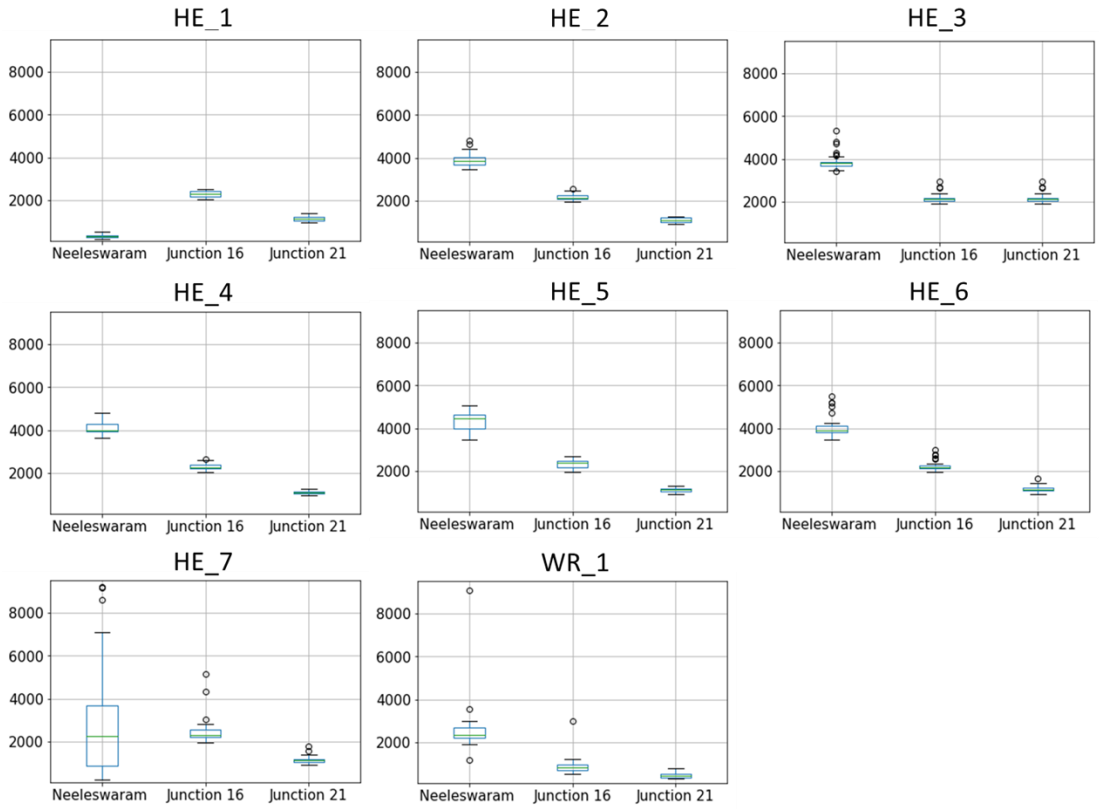

Figure 5.10: Flood discharge computation at three locations namely Neeleswaram gauge (Junction 7), Junction 16 and Junction 21 for the HEs HE_1, HE_2, HE_3, HE_4, HE_5, HE_6, HE_7 and continuous time series (2002-2018) WR_1.

Figure 5.11 shows the HEC-HMS based computed flood flows at subbasin scale corresponding to each HE and for the long-term historical time series (i. e. WR_1). In the Box plot (Figure 5.11), the x-axis highlights the information of HEs and continuous simulation (2002-2018) and y-axis shows the range of daily flood flows. In Figure 5.11, one can observe that the maximum high flood events (or values) corresponding to HE-7 and WR_1. They include the 2018 event duration i.e. found equivalent to the 100 years return period (Hunt and Menon, 2020; Sudheer et al., 2019).

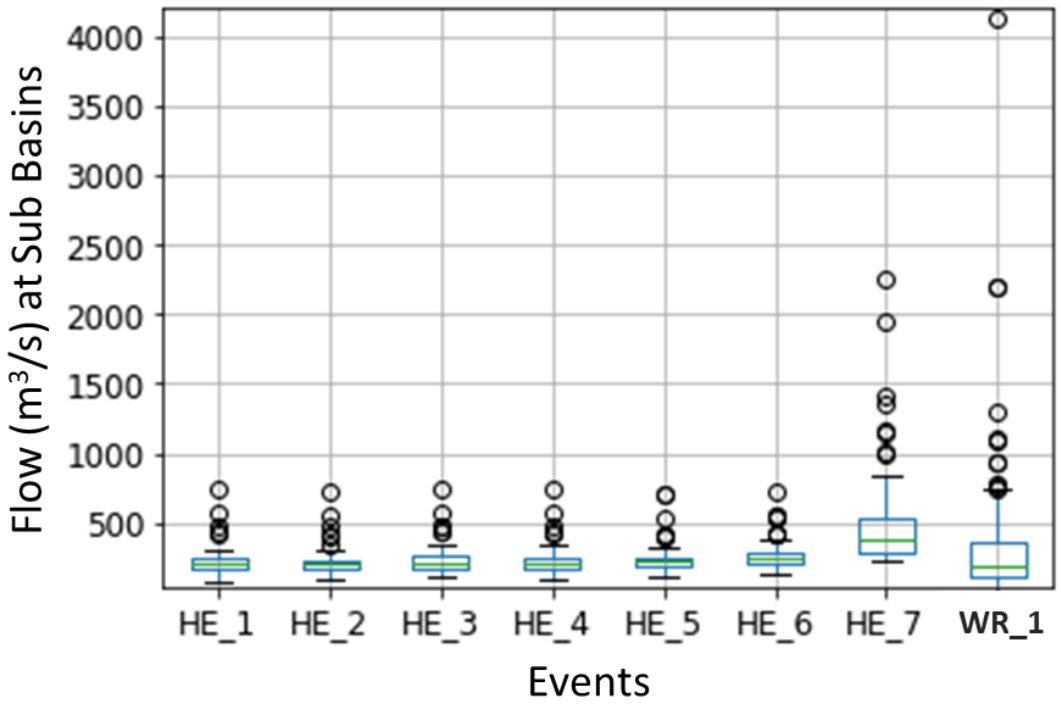

Figure 5.11: Box plot highlighting subbasin wise flood discharge computation for the HEs HE_1, HE_2, HE_3, HE_4, HE_5, HE_6, HE_7 and continuous simulation time series (2002-2018) WR_1.

5.2.2 Continuous Simulation Results

In HEC-HMS, the continuous simulation has been performed to generate long-term time series (2002-2018) discharge at each subbasin. The main purpose of the continuous simulation of discharge is to generate return period flood maps through flood frequency analysis and hydrodynamic simulations in HEC-RAS. For continuous simulation, the Soil Moisture Accounting (SMA) method has been performed as suggested in previous studies (Ouédraogo et al., 2018). In the continuous simulation, the reservoir simulation is not taken into the consideration, because the restricted flood volume may produce uncertain flood peaks during extreme high rainfall events as also suggested in few previous studies (Sudheer et al., 2019). For the computation of return period floods, the virgin flow conditions should be preferred. The details of initial and optimized parameters relevant to the SMA method has shown in Table 5.5.

Table 5.5: Calibration and optimization of SMA related parameters detail in HEC-HMS.

Subbasin	Parameters	Unit	Initial	Optimized
Sub39	Recession - Ratio to Peak		0.15	0.38213
Sub37	Recession - Ratio to Peak		0.15	0.29826
Sub36	Recession - Ratio to Peak		0.15	0.29849
Sub34	Recession - Ratio to Peak		0.15	0.38117
Sub35	Recession - Ratio to Peak		0.15	0.40738
Sub70	Recession - Ratio to Peak		0.15	0.42326
Sub21	Recession - Ratio to Peak		0.15	0.24544
Sub39	Soil Moisture Accounting - Max Infiltration	MM/HR	69	69.195
Sub37	Soil Moisture Accounting - Max Infiltration	MM/HR	58	57.322

Sub70	Soil Moisture Accounting - Max Infiltration	MM/HR	59	59.986
Sub21	Soil Moisture Accounting - Max Infiltration	MM/HR	43	43.639
Sub16	Soil Moisture Accounting - Max Infiltration	MM/HR	43	42.236
Sub39	Soil Moisture Accounting - Soil Storage	MM	499	477.38
Sub37	Soil Moisture Accounting - Soil Storage	MM	495	468.36
Sub36	Soil Moisture Accounting - Soil Storage	MM	495	481.73
Sub70	Soil Moisture Accounting - Soil Storage	MM	471	465.16
Sub21	Soil Moisture Accounting - Soil Storage	MM	495	461.17
Sub39	Soil Moisture Accounting - Soil Percolation	MM/HR	0.4	0.3762
Sub37	Soil Moisture Accounting - Soil Percolation	MM/HR	0.4	0.37516
Sub36	Soil Moisture Accounting - Soil Percolation	MM/HR	0.4	0.3344
Sub38	Soil Moisture Accounting - Soil Percolation	MM/HR	0.4	0.44095
Sub70	Soil Moisture Accounting - Soil Percolation	MM/HR	0.4	1.0959
Sub21	Soil Moisture Accounting - Soil Percolation	MM/HR	0.4	1.0811
All Subbasins	Soil Moisture Accounting - Soil Storage Scale Factor		1	1.6448
All Subbasins	Soil Moisture Accounting - Soil Percolation Scale Factor		1	1.5349
All Subbasins	Soil Moisture Accounting - Max Infiltration Scale Factor		1	1.4698
All Subbasins	Soil Moisture Accounting - GW1 Storage Scale Factor		1	1.3852
Sub68	Soil Moisture Accounting - Initial GW1 Content	%	40	52.964
Sub39	Soil Moisture Accounting - Initial GW1 Content	%	40	52.188
Sub37	Soil Moisture Accounting - Initial GW1 Content	%	40	51.241
Sub36	Soil Moisture Accounting - Initial GW1 Content	%	40	51.069
Sub28	Soil Moisture Accounting - Initial GW1 Content	%	40	49.861
Sub70	Soil Moisture Accounting - Initial GW1 Content	%	40	46.291
Sub23	Soil Moisture Accounting - Initial GW1 Content	%	40	43.801
All Subbasins	Soil Moisture Accounting - Initial GW1 Content Scale Factor		1	1.0474

Figure 5.12 shows the time series plot which compares the modelled vs observed discharge computed during continuous simulation (2007-2010) on a monthly time scale. In Figure 5.12, the modelled discharge found comparable to the observed plot. Figure 5.13 shows the regression plot, which demonstrate the R^2 between modelled and calibrated discharge on a monthly scale at the Neeleswaram gauge. The R^2 is computed around 0.68 which shows a reasonable match between modelled and calibrated discharge.

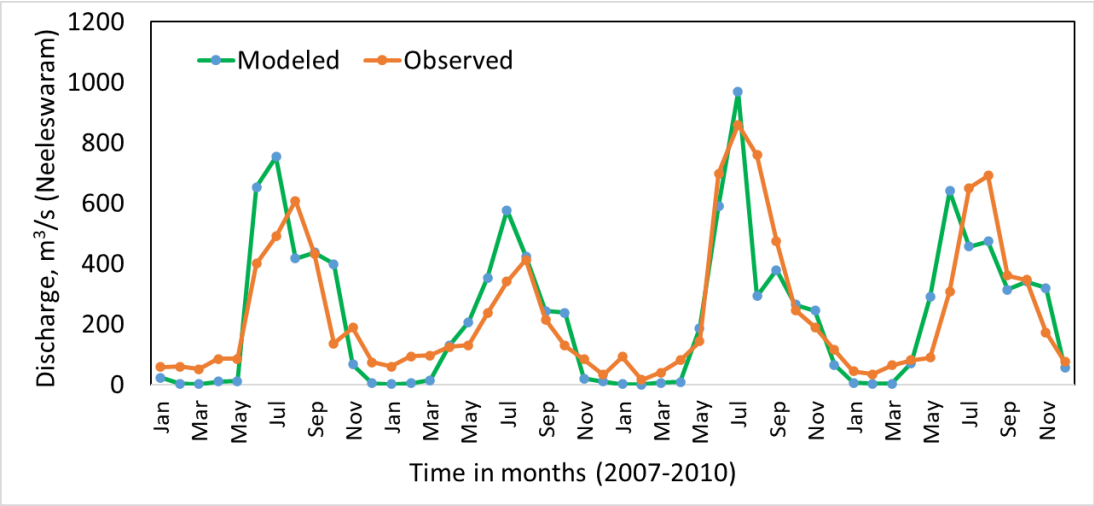

Figure 5.12: Time series plot shows the monthly comparison between observed and modelled discharge at Neeleswaram gauge during 2007 to 2010 as per SMA method.

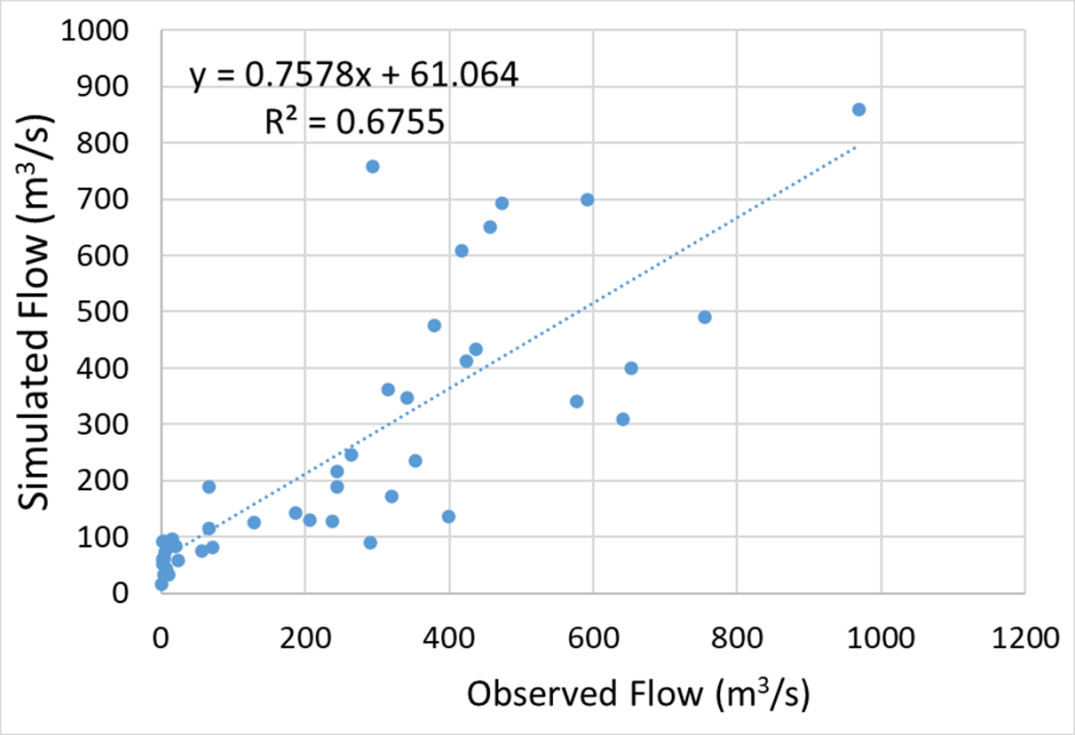

Figure 5.13: Regression plots between monthly simulated and observed flow at Neeleswaram gauge during 2007-2010 in a continuous simulation method.

The calibration has been done at Neeleswaram gauges utilizing the observed daily discharge from the year 2007 to 2010. The automatic calibration and optimization method inbuilt in HEC-HMS has been performed. The explanation of optimization procedure and processes have already made in the

methodology section. For the optimization of SMA parameters, an optimization process has been setup for the individual subbasin and for all subbasins. After getting the satisfactory match between the observed and modelled discharge, the optimization was stopped, and the optimized parameters were re-input to the HEC-HMS model and run the simulation again to get the final modeling outcomes. Around 10 parameters were optimized at different subbasins.

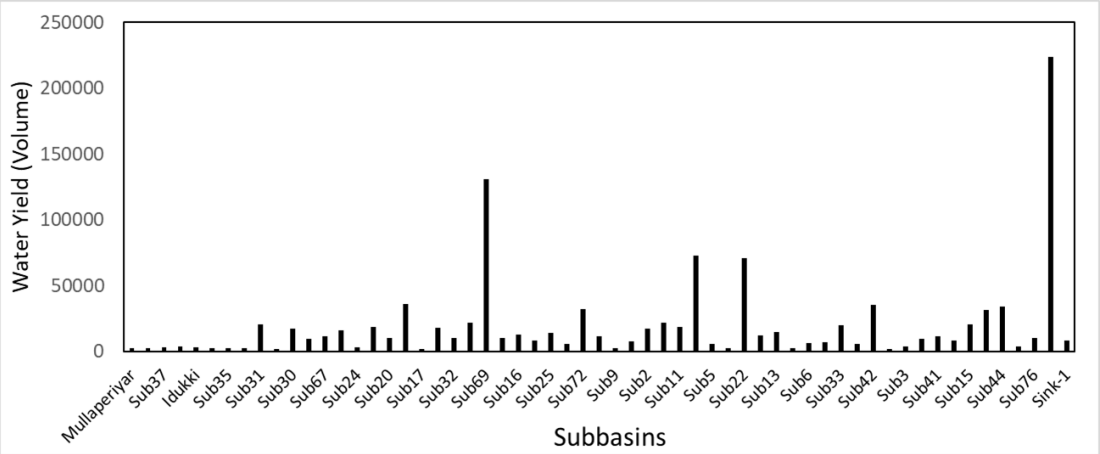

Figure 5.14: Computation of max water yield (volume in mm) at each sub-catchment scale as per SMA continuous simulation method in HEC-HMS.

Figure 5.14 shows the computation of max water yield (volume in mm) at each sub-catchment scale as per SMA continuous simulation method in HEC-HMS. Here in the time series plot (Figure 5.14), the maximum water yield on a given day (during the years between 2002 and 2018) has shown and it elaborates the contribution of maximum water corresponding to each subbasin. In this calculation, the virgin flow conditions were analyzed. Based on these water yield, the subbasin specific discharge (m^3/s) has been calculated to perform the flood frequency analysis (FFA). The subbasin specific discharge has already been shown in Figure 5.11 (WR_1). The subbasin specific discharge computed for HEs compared with the WR_1 and it has been noticed that the HEs based computed discharge at each subbasin is slightly underestimated, because HEs based computation includes the reservoir components and then some flows are regulated. Therefore, the extreme high peaks as per HEs found slight less than WR_1 based procedure (it does not include reservoirs and the generated flows are totally non-regulated).

5.3 RESERVOIRS SIMULATION RESULTS USING HEC-RESSIM FOR KERALA FLOOD EVENT (HE-7) (JULY-AUGUST, 2018)

HEC-RESSIM is a part of HEC-RTS integrated system, although it can be used independently too like HEC-HMS and HEC-RAS. In this study, the HEC-RESSIM is basically applied to re-construct the reservoir simulations during extreme historical flood event (HE-7) that was happened in July-August, 2018 in Periyar river basin Kerala. For this simulation, the inflows and other local flows were generated in HEC-HMS utilizing 3-hr rainfall datasets. The main purpose of this simulation is to generate the reservoir modeling parameters for extreme flood conditions.

Figure 5.15 shows the 3-hr inflows (Aug1 to Aug 21, 2018) for three reservoirs such as Mullaperiyar, Idukki and Idamalayar computed in HEC-HMS. The area-capacity-discharge-elevation curves along with other variables, which are necessary to setup the HEC-RESSIM, obtained from the CWC and some datasets were collected through the published reports (Mohanty et al., 2020; Sudheer et al., 2019). The minimum and maximum release-based reservoir rules are formulated to construct the HE-7 flood event. The details of reservoir rules and area-capacity-discharge-elevation curves have already explained in

methodology section. In this HEC-RESSIM, the two major reservoirs situated at the upstream portion on the mainstream, are taken into the consideration.

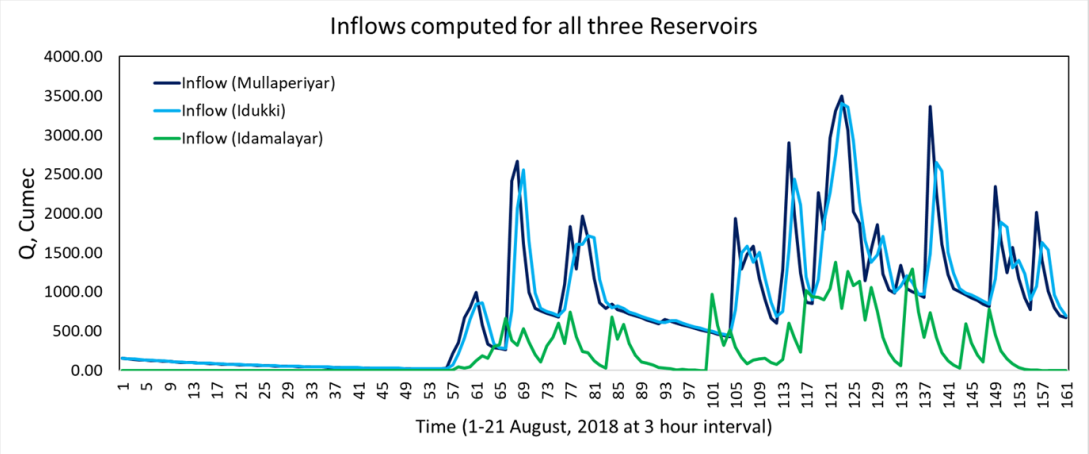

Figure 5.15: Inflows to setup HEC-RESSIM during the HE-7 flood event.

Figures 5.16 (a and b) show the inflows and outflows at Mullaperiyar and Idukki reservoirs. The Mullaperiyar dam is situated at the upstream portion and Idukki is situated at the downstream of Mullaperiyar dam. The reservoirs rule curves i. e. maximum and minimum release rules are defined only for the extreme high flood events (Aug 1 to Aug 21, 2018). The elevation-area-capacity curves and flow releases are separately defined for Mullaperiyar and Idukki dams. For the reservoir simulation and optimization, the total reservoir area is categorized into three zones such as (i) flood control zone, (ii) conservation zone and dead storage zone for both reservoirs and accordingly the maximum and minimum release. The details of reservoir parameters such as dead storage level, full reservoir level (FRL) and highest flood level (HFL), design discharge of spillway have been collected for both reservoirs. All this information about reservoir related parameters were collected from reports published by various agencies.

Generally, rule curves at target levels to be maintained in the reservoirs throughout the year under varied conditions of inflows. In this study, DAM pre-release concept has been adopted. After that the maximum and minimum release rules are adjusted only for the extreme high flood condition during August 2018 based on the available flow conditions at Neeleswaram gauge by following the continuity equation. First, the inflows were provided to the upper dam and then the water level is defined for each zone. As per the event time (happened in July and August), the reservoir level is almost full and therefore the release from the reservoir is pre-set as per the occurrence of flood discharge at each day (average of 3-hr floods) during the event. The maximum release is set to the Flood Control Zone and the minimum release is set for the Storage Zone to maintain the reservoir storage and to attenuate the extreme high flood peaks. In HEC-RESSIM, the Storage zone can be set as a function of Date and Time. Similar, rules and strategies are followed for the downstream situated reservoirs i. e. Idukki dam. The release rules for Idukki dam is adjusted as per the released flood flows from the upstream reservoir i.e. Mullaperiyar, contribution from local flows and the availability of flood flows at Neeleswaram gauge.

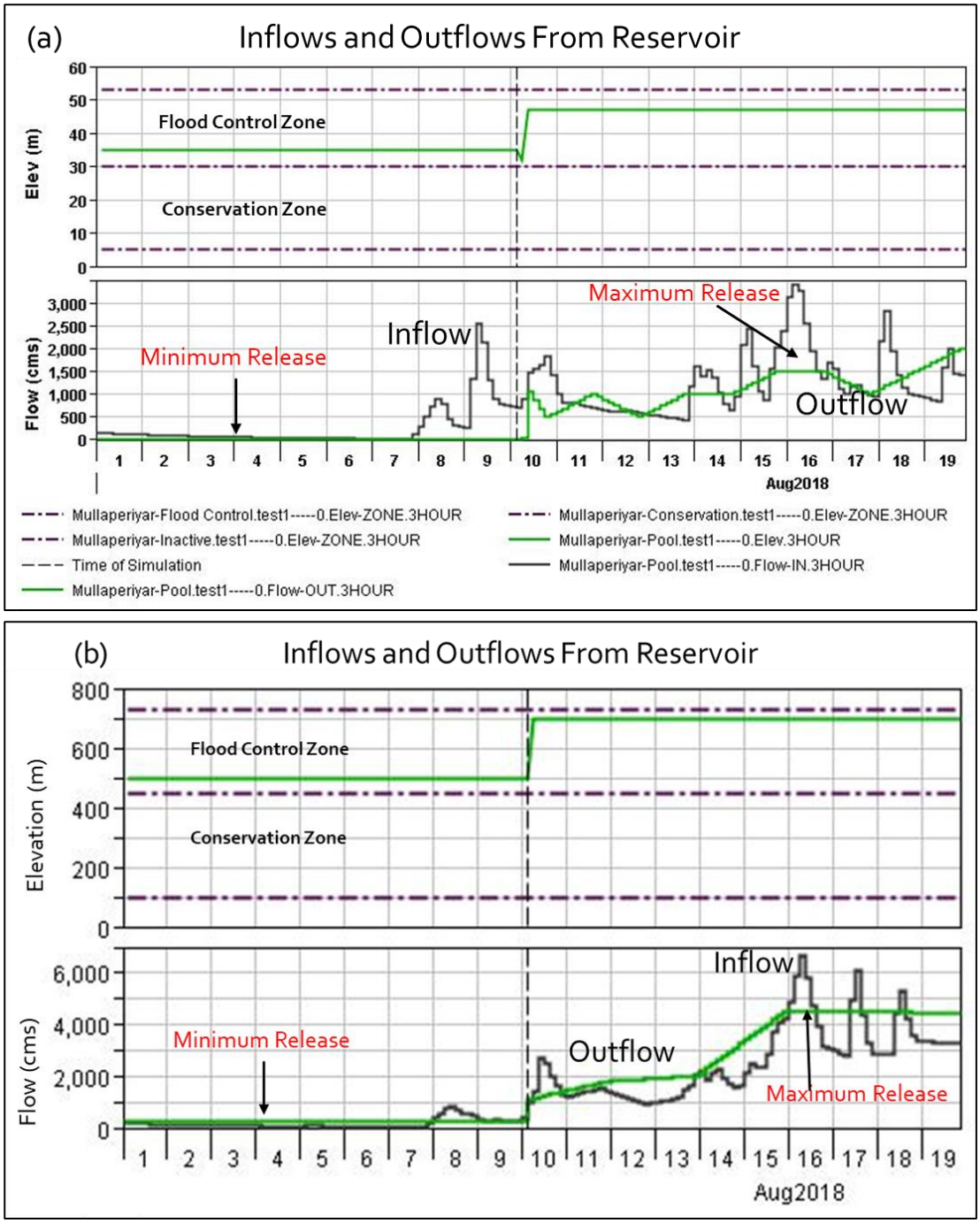

Figure 5.16: Inflows and outflows details released from (a) Mullaperiyar and (b) Idukki reservoirs with different reservoir capacity zones.

In Figure 5.16 (a), a significant reduction in the outflows can be seen as compared to the inflows. In this figure, the effect of storage of flood volume between conservation and flood control zone can be visualized. Similar observations can also be seen in case of Idukki reservoir, where outflow peaks are minimized as compared to inflows. However, in case of Idukki dam, the difference between the extreme high peaks considering inflows and outflows is found less than Mullaperiyar. Because due to the high rainfall that is occurred in previous days (July and first weak of August, the reservoir was already full at the FRL and thus whatever the floods were coming that are released immediately. Here, the rules are made in such a way so that the gaps (time) between the two peaks have been utilized to release the more flood water and additional flood water can be stored for some time in the reservoir as per the occurrence of next extreme high flood peak. In this way, flood peaks can be attenuated, and the effect of flood can

be minimized. This kind of observation can be seen in the Figure 5.16. Therefore, prior rainfall information or forecasted rainfall is needed to handle such kind of flood event even the reservoirs are fully devoted to flood mitigation and management.

The availability and occurrence of flood flows is then aggregated at Neeleswaram gauge during the HE-7 (i.e. Kerala flood event 2018) after performed the reservoir operation in HEC-RESSIM and the result of this HE-7 event has been compared with the study report published by CWC. As per Figure 5.17, this study results are found comparable as per the CWC report. The flood discharge is released around 6000 to 7000 m^3/s during extreme flood event days from Idukki reservoir and the total flood flows is modelled around 9800 m^3/s, which is found slightly overestimated as compared to flood flows recorded by CWC (i. e. ~9000 m^3/s) at Neeleswaram gauge (Sudheer et al., 2019). These results are basically derived from the 3-hr bias corrected rainfalls so some difference in extreme high peaks can be expected.

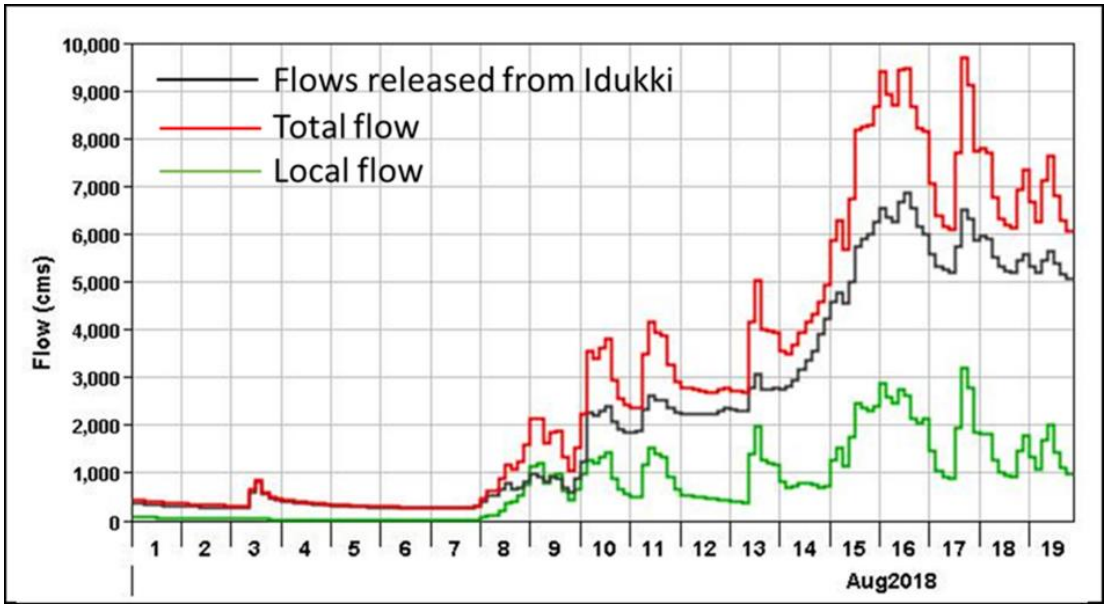

Figure 5.17: Floods at the Neeleswaram during HE-7 event (Kerala flood, August 2018) generated in HEC-RESSIM analyzed independently.

5.4 PREPARED GEOMETRIC DATA INPUTS USING HEC GEO-RAS

In this study, the geometric layers to setup 1 D unsteady and steady flow models, the HEC-GeoRAS has been utilized. The HEC-GeoRAS works with ArcGIS interface. The DEM is required to calculate the HCE-RAS geometry. In this study, the ALOS PALSAR 12.5-meter DEM has been used for the generation of 1D geometric layers.

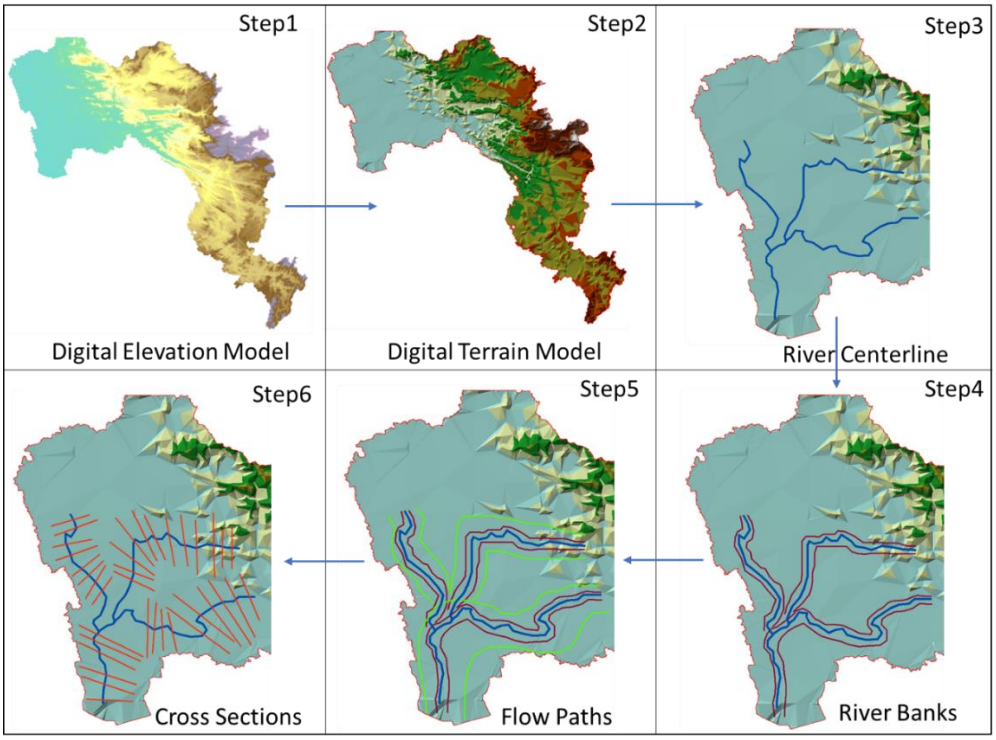

Figure 5.18: All the geometric layers computed in HEC-GeoRAS to setup 1D HEC-RAS. model.

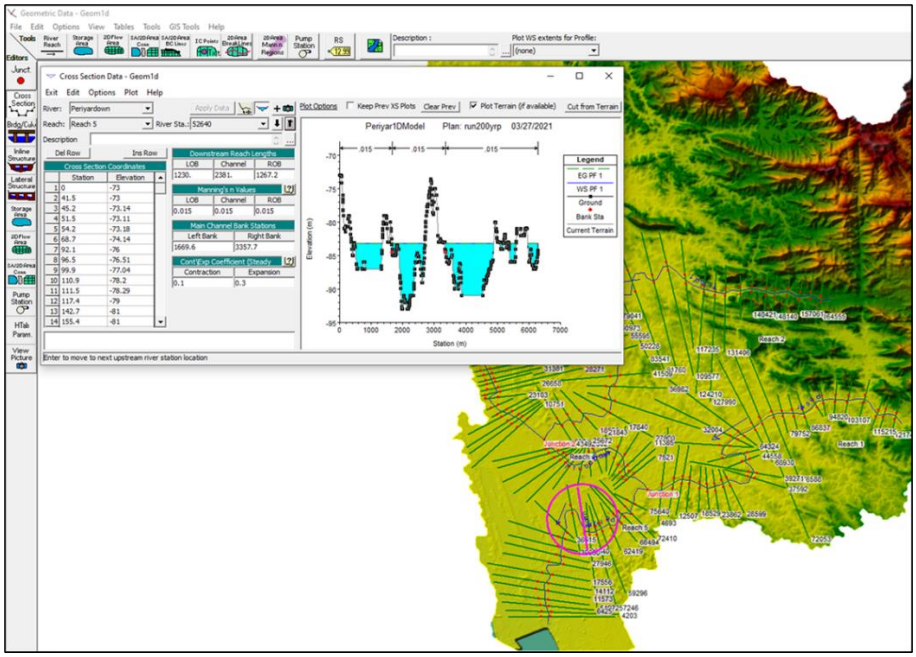

Figure 5.19: **T**he geometry of 1D HEC-RAS model imported in HEC-RAS from HEC-GeoRAS model.

First, we removed the sinks in DEM and then DEM has been converted into digital terrain model (DTM). DTM is the primary input to HEC-GeoRAS. After that, the project setup has been done and stream centreline, river-banks, flow paths and cross sections were derived. The delineation methodology of the 1D geometric layers in HEC-GeoRAS has already been discussed in the methodology section. Figure 5.18 has shown all the geometric layers computed in HEC-GeoRAS to

setup 1D HEC-RAS model. Once the layers and their attributes are successfully generated then all GIS layers can be exported as per the prescribed format of HEC-RAS. After exporting the HEC-RAS files, they can open in HEC-RAS geometry section. Figure 5.19 has shown the geometry of 1D HEC-RAS model.

5.5 HEC-RAS MODEL OUCOMES AS PER 1D STEADY, 1D UNSTEADY AND 2D UNSTEADY FLOWS

After creating geometric layers, the 1D steady and 1D unsteady state simulations have been performed in HEC-RAS model. For 1D steady flow analysis, the different return period (RP) flood flows (e. g. 50years, 100 years and 200 years) generated at three sections such as Neeleswaram gauge (or Junction 7), Junction 16 (tributary 1) and Junction 21 (tributary 2) (total 5 reaches were created) from two methods namely Gumbel and Log Pearson Type 3 (LogPT3) were utilized. The methodology for the generation of different return period flood flows utilizing the Flood Frequency Analysis (FFA) has already been elaborated in the methodology section. In steady flow analysis, the flood flows from different return periods (e.g. 50years, 100 years and 200 years) computed as per Gumbel and LogPT3 models were used to define the steady state boundary conditions and then the various hydrodynamic modeling outcomes such as cross section profiles at different section, longitudinal river flood profile. Figure 5.20 shows the steady state longitudinal flow profile which has been computed as per RP 200 years.

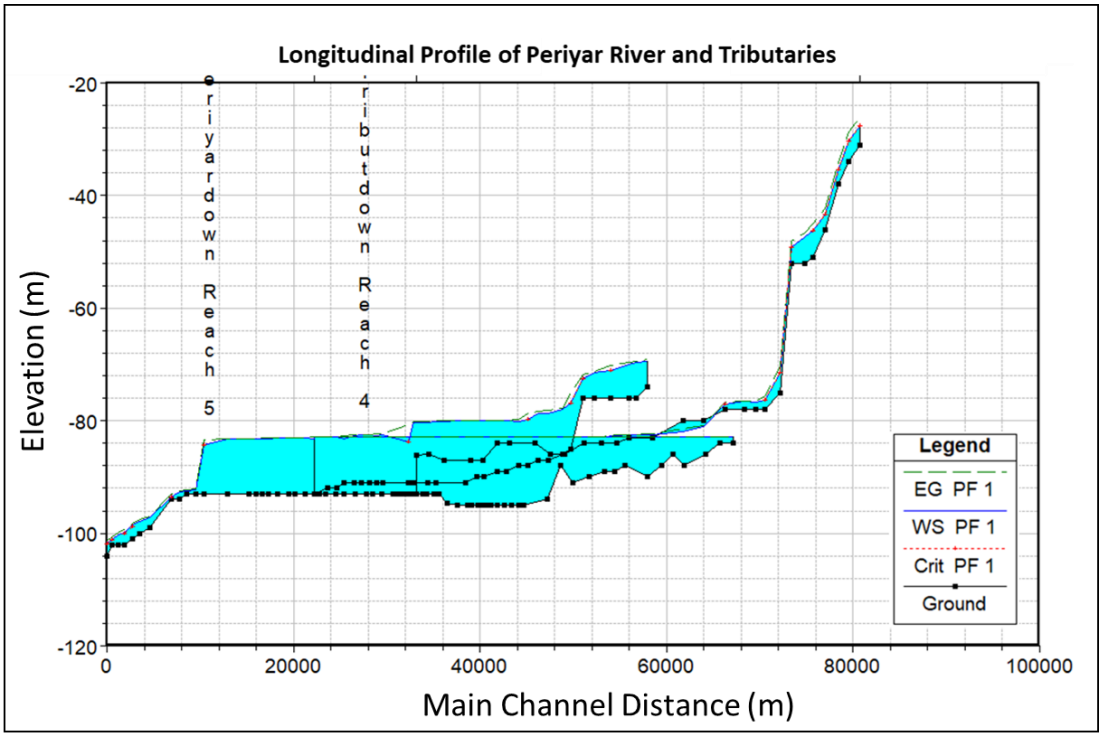

Figure 5.20: 1D Steady state longitudinal profile of river sections as per Gumbel RP200.

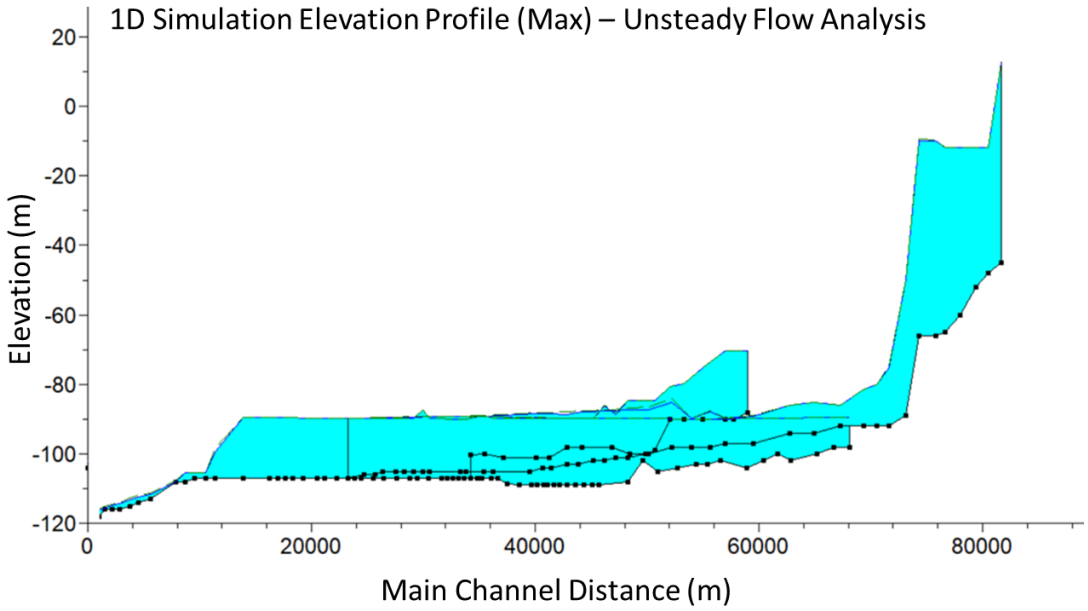

Figure 5.21: 1D Unsteady Steady state longitudinal profile of river sections as per maximum inundation for HE-7.

In 1D HEC-RAS modeling with multiple river reaches, the user can select one or more river reaches to plot. In case of steady state profile (Figure 5.20), The channel distance is computed around 80 km (from upstream to downstream) shown at x-axis (Figures 5.20 and 5.21), whereas y-axis shows the elevation profile along the river reaches. Figure 5.21 shows the longitudinal elevation profile (maximum) for the Periyar river computed as per the 1D unsteady flow simulation for the HE-7 event.

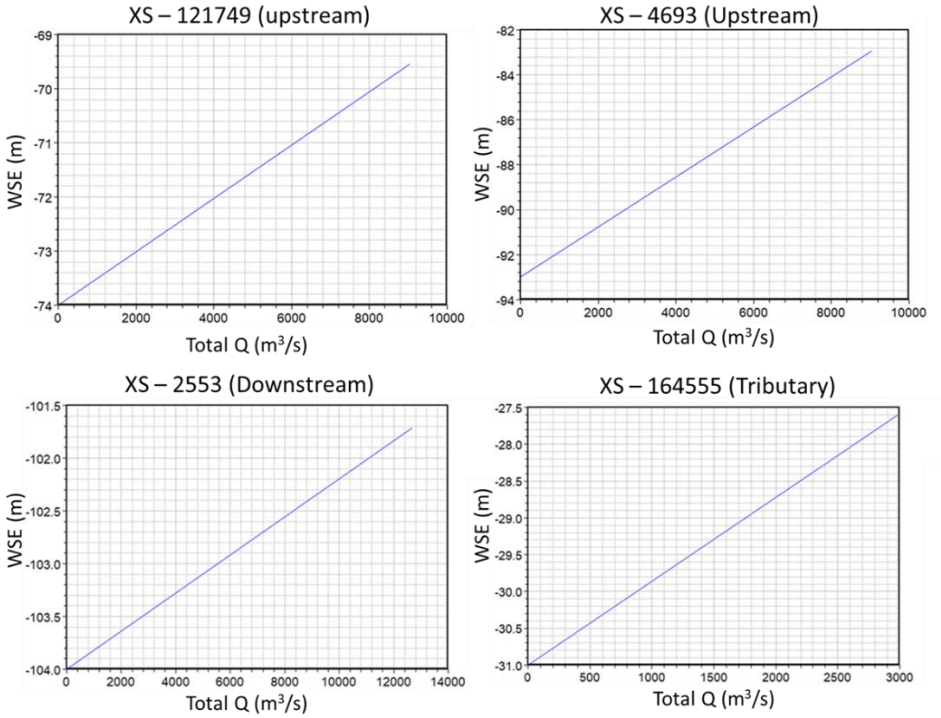

Figure 5.22: RCs generated under 1D Steady state simulation as per Gumbel RP-200 at different cross sections.

Both profiles have shown slight variations in the water level from the upstream to downstream reaches. In case of HE-7 1D unsteady (1-day max for the given duration of the HE-7 event) profile, several high peaks in the water level can be observed. In case of steady flow elevation profile as per RP200 flow, the water level belongs to around -110 m to -30 m, while in case of 1D unsteady flow, the elevation varies from -115 to 10. In HEC-RAS 1D steady and unsteady simulations, various hydraulic variables such as rating curves, flow area in each, water level, channel surface elevation and flooded area. In 1D steady and unsteady flow analysis, these variables can be computed at each river cross section. Similar, variables can also be calculated.

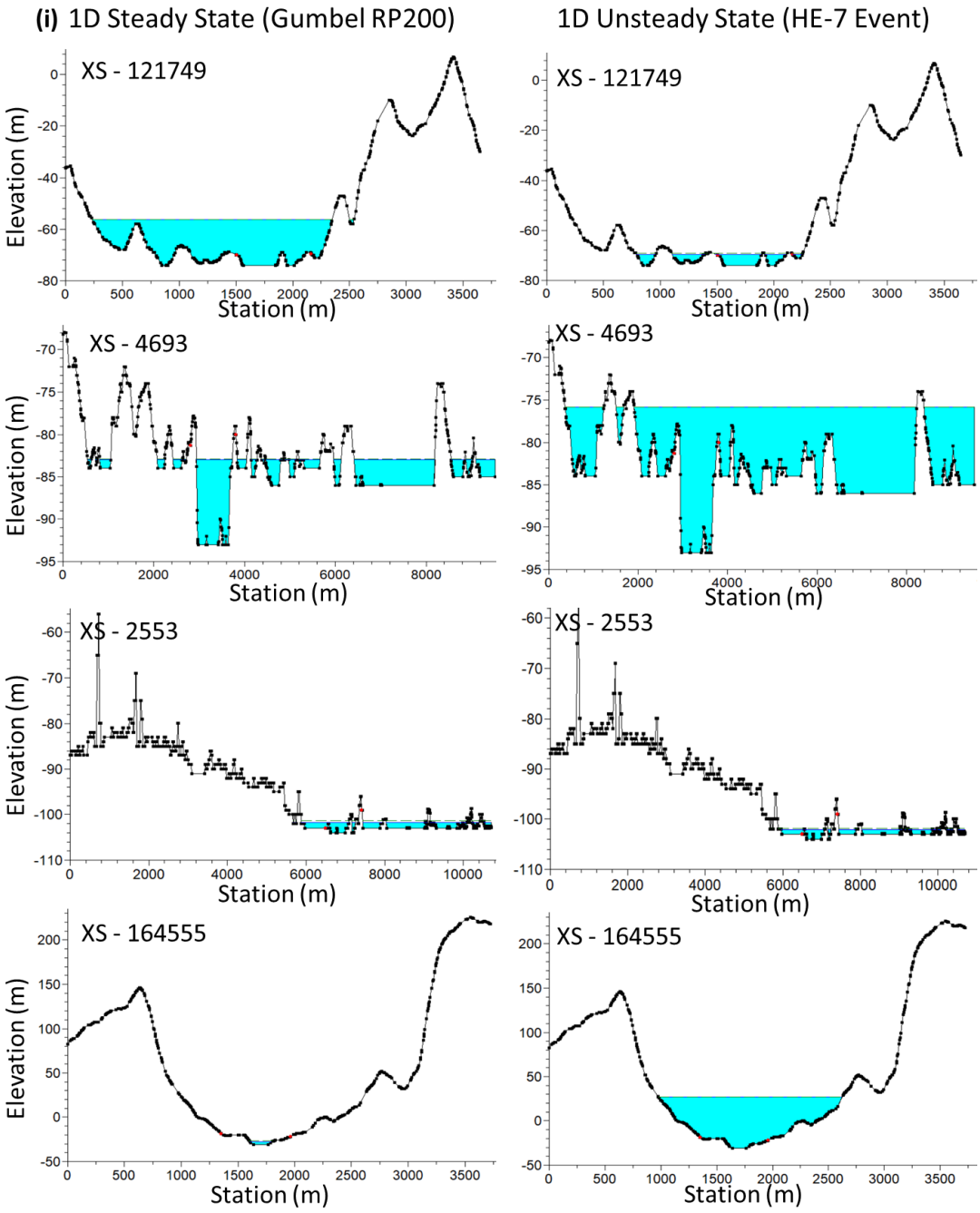

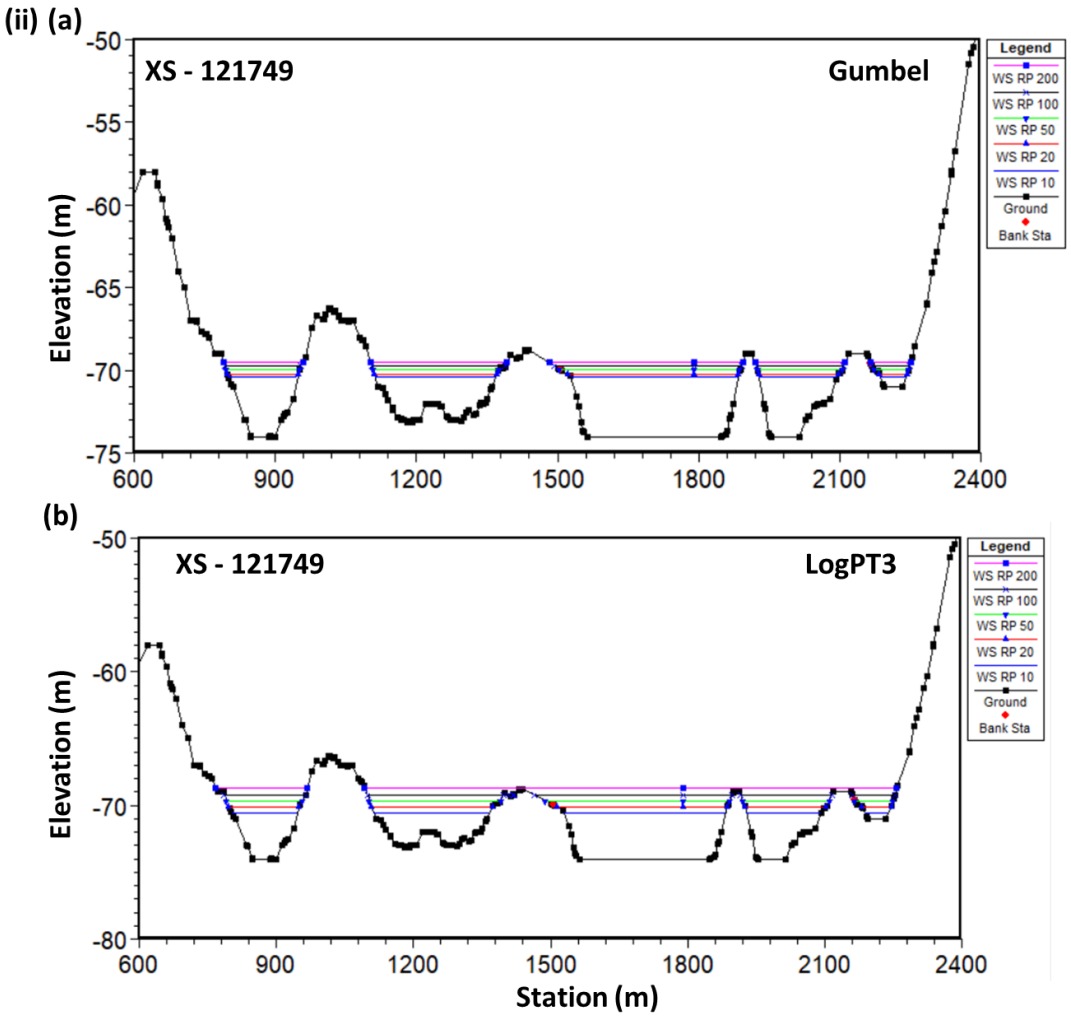

Figure 5.23: (i) Comparison of the water elevation at different cross sections as per the 1D steady state simulation of RP200 (Gumbel) and 1D unsteady flow simulation as per HE-7 event and (ii) Comparison of water surface as per multiple RP floods (e.g. RP10, RP20, RP50, Rp100 and RP200) generated from Gumbel and LogPT3 methods in the upstream cross section.

Figure 5.22 shows the relationship between water level (or water surface elevation: WSE) and Total runoff (Q) (i.e. Rating Curves) at four different locations as per RP200 (Gumbel). This shows the maximum water level at given cross section during RP200 floods. These Hydraulically modelled Rating Curves (RCs) are a promising alternative to calculate the streamflow. The RCs can be utilized in the assessment of extreme flood conditions. Figure 5.23 (i) compares the water elevation at different cross sections as per steady state simulation of RP200 (Gumbel) and 1D unsteady flow simulation as per HE-7 event.

In Figure 5.23 (i), one can clearly observe the variations in the generation and routing of extreme floods as per steady state and unsteady state conditions. Figure 5.23 (ii) shows the comparison of water surfaces as per multiple RP floods (e. g. RP10, RP20, RP50, Rp100 and RP200) generated from Gumbel and LogPT3 methods in an upstream cross section. LogPT3 shows higher water surfaces than Gumbel method (Figure 5.23 ii).

Table 5.6: Results of hydrodynamic variables as per steady state simulation as per Gumbel RP 100.

River	River Station (m)	Gumbel RP100				
		Q (m^3/s)	Min Ch El (m)	W.S. El (m)	Vel Chnl (m/s)	Flow Area (m^2)
Tribut2	120021	932	-84	-82.85	0	78103.98
Tribut2	115460	932	-84	-82.86	0.27	2746.24
Tribut2	110440	932	-86	-82.87	0.23	4450.44
Tribut2	102875	932	-88	-82.87	0.07	11566.19
Tribut2	99035	932	-86	-82.87	0.06	16897.99
Tribut2	94852	932	-88	-82.87	0.03	30363.74
Tribut2	89976	932	-90	-82.87	0.02	32072.08
Tribut2	82131	932	-88	-82.87	0.03	28754.15
Tribut2	78461	932	-89	-82.87	0.03	28800.96
Tribut2	74934	932	-89	-82.87	0.03	33761.61
Tribut2	69424	932	-90	-82.87	0.05	19174.39
Tribut2	63805	932	-91	-82.87	0.02	27500.82
Tribut2	59454	932	-88	-82.87	0.03	22758.08
Tribut1	164555	2683	-31	-27.81	0.01	5.18
Tribut1	145267	2683	-52	-47.59	3.89	690.25
Tribut1	127990	2683	-78	-76.71	0.52	2250.6
Tribut1	124210	2683	-78	-76.68	0.18	6690.7
Tribut1	109577	2683	-80	-81.16	1.23	500.55
Tribut1	102351	2683	-80	-81.96	1.35	294.91
Tribut1	91760	2683	-83	-82.48	0.6	2219.14
Tribut1	83541	2683	-83	-82.51	0.17	8390.68
Tribut1	79041	2683	-84	-82.65	1.15	2193.28
Tribut1	73608	2683	-84	-82.84	0.61	3932.09
Tribut1	67736	2683	-84	-82.83	0.06	14386.88
Tribut1	60973	2683	-86	-82.84	0.14	10210.16
Tribut1	55595	2683	-86	-82.84	0.09	14452.68
Tribut1	50228	2683	-84	-82.84	0.09	13766.03
Tribut1	41509	2683	-84	-82.85	0.14	9601.56
Tribut1	36982	2683	-84	-82.86	0.23	5971.75
Tribut1	32004	2683	-87	-82.86	0.1	17991.67
Tribut1	27900	2683	-87	-82.86	0.11	17800.07
Tribut1	18525	2683	-87	-82.87	0.18	13013.07
Tribut1	12902	2683	-86	-82.87	0.15	11260.97
Tribut1	8874	2683	-86	-82.87	0.1	19914.54
Periyardown	75640	12700	-93	-83.16	2.23	6066.07
Periyardown	57246	12700	-93	-83.16	1.02	14410.64
Periyardown	54972	12700	-93	-83.15	0.73	25462.05
Periyardown	52640	12700	-93	-83.17	0.69	18962
Periyardown	44828	12700	-93	-83.18	0.72	21725.86
Periyardown	33733	12700	-93	-92.24	0.69	7845.03
Periyardown	30680	12700	-93	-92.43	0.59	7626.39
Periyardown	27946	12700	-94	-92.62	1.03	8238.28
Periyardown	17556	12700	-99	-97.19	1.65	6592.33

Periyardown	14112	12700	-100	-97.93	2.41	4817.95
Periyardown	2554	12700	-104	-101.71	0.01	5127.31
Periyardown	6425	12700	-102	-100.22	1.73	5888.22
Periyar	121749	8132	-74	-69.74	2.78	3165.33
Periyar	117746	8132	-76	-69.85	2.19	4674.96
Periyar	115215	8132	-76	-70.09	2.65	3527.44
Periyar	103107	8132	-76	-71.64	1.61	4903.02
Periyar	91857	8132	-86	-78.16	2.2	3722.34
Periyar	86837	8132	-87	-78.69	3.56	2967.98
Periyar	76588	8132	-88	-80.72	3.5	2953.15
Periyar	72053	8132	-89	-80.57	1.93	7199.68
Periyar	68930	8132	-89	-80.65	2.14	7638.33
Periyar	28599	8132	-91	-82.55	1.85	5609.77
Periyar	26510	8132	-91	-82.7	2.3	4553.34
Periyar	23862	8132	-91	-82.64	1.15	8585.68
Periyar	21228	8132	-91	-82.65	1.03	8231.22
Periyar	18529	8132	-91	-82.71	1.32	6567.25
Periyar	14878	8132	-91	-83.1	2.79	3319.33
Periyar	12507	8132	-92	-82.92	1.26	9493.27
Periyar	9168	8132	-92	-82.92	0.87	12287.77
Periyar	4693	8132	-93	-82.93	0.73	16932.12

Table 5.7: Results of hydrodynamic variables as per steady state simulation as per LogPt3 RP 100.

River	River Station (m)	LogPT3 RP 100				
		Q (m^3/s)	Min Ch El (m)	W.S. El (m)	Vel Chnl (m/s)	Flow Area (m^2)
Tribut2	120021	1044	-84	-82.32	0	82684.85
Tribut2	115460	1044	-84	-82.32	0.2	5033.08
Tribut2	110440	1044	-86	-82.33	0.2	6470.04
Tribut2	102875	1044	-88	-82.33	0.07	13830.77
Tribut2	99035	1044	-86	-82.33	0.05	22352.96
Tribut2	94852	1044	-88	-82.33	0.03	36185.13
Tribut2	89976	1044	-90	-82.33	0.02	37829.99
Tribut2	82131	1044	-88	-82.33	0.03	34050.68
Tribut2	78461	1044	-89	-82.33	0.03	33376.59
Tribut2	74934	1044	-89	-82.33	0.03	38417.3
Tribut2	69424	1044	-90	-82.33	0.05	22853.41
Tribut2	63805	1044	-91	-82.33	0.02	31300.03
Tribut2	59454	1044	-88	-82.33	0.03	26146.58
Tribut1	164555	4090	-31	-26.83	0.01	5.76
Tribut1	145267	4090	-52	-46.83	4.86	840.98
Tribut1	127990	4090	-78	-76.4	0.81	2476.78
Tribut1	124210	4090	-78	-76.33	0.29	7454.64
Tribut1	109577	4090	-80	-80.31	3.06	557.73
Tribut1	102351	4090	-80	-81.65	1.14	299.58
Tribut1	91760	4090	-83	-82.01	0.86	3049.77
Tribut1	83541	4090	-83	-82.02	0.23	11865.36

Tribut1	79041	4090	-84	-82.16	1.27	3052.74
Tribut1	73608	4090	-84	-82.28	0.66	5805.34
Tribut1	67736	4090	-84	-82.28	0.1	16828.37
Tribut1	60973	4090	-86	-82.28	0.2	12279.99
Tribut1	55595	4090	-86	-82.28	0.13	17851.3
Tribut1	50228	4090	-84	-82.29	0.13	17006.18
Tribut1	41509	4090	-84	-82.3	0.2	11936.69
Tribut1	36982	4090	-84	-82.32	0.32	7642.27
Tribut1	32004	4090	-87	-82.31	0.14	21778.31
Tribut1	27900	4090	-87	-82.32	0.15	21204.42
Tribut1	18525	4090	-87	-82.32	0.23	15715.75
Tribut1	12902	4090	-86	-82.33	0.21	13564.8
Tribut1	8874	4090	-86	-82.33	0.14	22991.29
Periyardown	75640	16135	-93	-82.69	2.31	7015.63
Periyardown	57246	16135	-93	-82.68	1.16	15942.35
Periyardown	54972	16135	-93	-82.67	0.79	29013.86
Periyardown	52640	16135	-93	-82.69	0.74	21135.88
Periyardown	44828	16135	-93	-82.71	0.77	24691.48
Periyardown	33733	16135	-93	-91.9	0.9	8892.54
Periyardown	30680	16135	-93	-92.1	0.82	8657.34
Periyardown	27946	16135	-94	-92.3	1.2	9386.91
Periyardown	17556	16135	-99	-96.93	1.8	7612.28
Periyardown	14112	16135	-100	-97.7	2.62	5863.56
Periyardown	2554	16135	-104	-101.51	0.001	4240.62
Periyardown	6425	16135	-102	-99.86	1.9	7148.89
Periyar	121749	11031	-74	-69.19	3.15	3800.74
Periyar	117746	11031	-76	-69.31	2.53	5473.53
Periyar	115215	11031	-76	-69.68	3.25	3929.8
Periyar	103107	11031	-76	-71.12	1.89	5679.03
Periyar	91857	11031	-86	-77.59	2.71	4099.57
Periyar	86837	11031	-87	-78.32	4.32	3339.7
Periyar	76588	11031	-88	-78.83	2.58	6694.13
Periyar	72053	11031	-89	-78.75	1.23	15406.1
Periyar	68930	11031	-89	-78.76	1.05	17900.43
Periyar	28599	11031	-91	-81.9	2	6874.43
Periyar	26510	11031	-91	-82.11	2.67	5296.83
Periyar	23862	11031	-91	-82.02	1.37	9988.33
Periyar	21228	11031	-91	-82.05	1.25	9237.52
Periyar	18529	11031	-91	-82.12	1.52	7698.21
Periyar	14878	11031	-91	-82.64	3.28	3873.08
Periyar	12507	11031	-92	-82.4	1.46	11075.58
Periyar	9168	11031	-92	-82.4	0.95	14891.69
Periyar	4693	11031	-92	-82.41	0.85	20088.26

Table 5.8: Results of hydrodynamic variables as per unsteady steady flow simulation as per HE-7 event.

River	River Station (m)	Q	Min Ch El	W.S. El	Vel Chnl	Flow Area
		m^3/s	m	(m)	m/s	m^2
Tributdown	41591	3659.45	-93	-76.53	0.07	66361.95
Tributdown	39752	3616.69	-93	-76.53	0.06	71195.48
Tributdown	38190	3579.22	-93	-76.53	0.06	66390.12
Tributdown	36555	3542.52	-93	-76.53	0.07	55957.65
Tributdown	35002	3517.17	-93	-76.54	0.08	48749.29
Tributdown	31210	3479.53	-93	-76.54	0.1	36129.5
Tributdown	27862	3458.53	-93	-76.54	0.13	28444.48
Tributdown	25672	3445.81	-93	-76.55	0.11	31546.79
Tributdown	21843	3430.72	-93	-76.55	0.09	37793.38
Tributdown	17840	3420.72	-93	-76.55	0.12	33003.47
Tributdown	14924	3418.35	-93	-76.56	0.17	24162.04
Tributdown	11385	3420.11	-93	-76.56	0.08	38390.28
Tributdown	9253	3423.13	-93	-76.56	0.08	39489.56
Tributdown	7521	3427.22	-93	-76.56	0.09	42932.16
Tribut2	115460	1031.82	-84	-76.63	0.03	43200.67
Tribut2	110440	1030.44	-86	-76.63	0.03	39009.6
Tribut2	102875	1030.87	-88	-76.63	0.03	44159.55
Tribut2	99035	1033.94	-86	-76.63	0.01	94176.93
Tribut2	94852	1039.16	-88	-76.62	0.01	113121.4
Tribut2	89976	1047.21	-90	-76.62	0.01	111705.5
Tribut2	82131	1064.98	-88	-76.62	0.01	97012.73
Tribut2	78461	1073.62	-89	-76.62	0.01	96697.68
Tribut2	74934	1083.2	-89	-76.62	0.01	101337.5
Tribut2	69424	1098.13	-90	-76.61	0.02	76972.19
Tribut2	63805	1111.85	-91	-76.61	0.01	83461.61
Tribut2	59454	1123.59	-88	-76.6	0.01	85475.12
Tribut2	54876	1130.71	-94	-76.6	0.02	62890.73
Tribut2	46592	1127.62	-95	-76.59	0.02	78875.48
Tribut2	44590	1125.85	-95	-76.59	0.02	77050.85
Tribut2	42178	1122.23	-95	-76.58	0.02	61237.71
Tribut2	39547	1116.69	-95	-76.58	0.01	85420.38
Tribut2	37170	1110.9	-95	-76.58	0.01	97112.78
Tribut2	34832	1101.17	-95	-76.58	0.01	96947.52
Tribut2	33263	1093.55	-95	-76.58	0.01	88437.62
Tribut2	31381	1084.67	-95	-76.57	0.02	80467.91
Tribut2	30156	1079.43	-95	-76.57	0.02	64358.84
Tribut2	28271	1068.4	-95	-76.57	0.01	81840.62
Tribut2	26658	1057.57	-95	-76.57	0.02	55652.05
Tribut2	19704	1028.06	-94	-76.55	0.05	23854.78
Tribut2	16743	1005	-93	-76.54	0.03	32705.21
Tribut2	14820	981.92	-93	-76.54	0.02	48643.59
Tribut2	12246	935.84	-93	-76.53	0.01	60180.85

Tribut2	10751	902.53	-93	-76.53	0.01	74458.31
Tribut2	8935	857.89	-93	-76.53	0.01	91448.44
Tribut1	164555	2235.8	-31	-15.13	0.36	6547.08
Tribut1	91760	299.68	-83	-76.44	0.01	43103.03
Tribut1	83541	890.74	-83	-76.44	0.01	81862.23
Tribut1	79041	1203.15	-84	-76.45	0.05	22111.5
Tribut1	73608	1409.1	-84	-76.45	0.04	37133.86
Tribut1	67736	1664.32	-84	-76.45	0.02	53923.23
Tribut1	60973	1906.5	-86	-76.46	0.04	41001.79
Tribut1	55595	2189.43	-86	-76.46	0.03	62470.03
Tribut1	50228	2530.91	-84	-76.46	0.04	59242.89
Tribut1	41509	2900.26	-84	-76.47	0.06	43466.21
Tribut1	36982	2976.78	-84	-76.48	0.07	33399.07
Tribut1	32004	3016.64	-87	-76.48	0.04	75497.27
Tribut1	27900	3014.9	-87	-76.49	0.05	64352.72
Tribut1	18525	2947.47	-87	-76.51	0.06	46782.55
Tribut1	12902	2892.52	-86	-76.52	0.06	41097.81
Tribut1	8874	2840.26	-86	-76.53	0.05	56904.77
Periyardown	75640	5658.33	-93	-76.56	0.24	23763.32
Periyardown	72410	5665.08	-93	-76.56	0.1	57028.86
Periyardown	68700	5676.11	-93	-76.56	0.08	73794.38
Periyardown	66494	5685.46	-93	-76.56	0.09	69430.65
Periyardown	62419	5699.88	-93	-76.57	0.17	35834.02
Periyardown	59296	5714.88	-93	-76.57	0.11	55630.7
Periyardown	57246	5730.27	-93	-76.57	0.13	48818.49
Periyardown	54972	5750.08	-93	-76.57	0.08	83291.35
Periyardown	52640	5771.92	-93	-76.57	0.11	55148.82
Periyardown	44828	5803.99	-93	-76.57	0.1	66613.55
Periyardown	33733	5831.12	-93	-91.73	0.33	9416.23
Periyardown	30680	5835.24	-93	-91.75	0.3	9803.29
Periyardown	27946	5839.87	-94	-91.76	0.38	11411.25
Periyardown	25117	5843.49	-94	-94.55	0.01	1115
Periyardown	17556	5850.09	-99	-97.89	1.1	4012.25
Periyardown	14112	5854.68	-100	-98.51	1.79	2792.56
Periyardown	11573	5857.45	-101	-99.28	1.95	2512.23
Periyardown	8584	5859.94	-102	-100.51	2.36	2269.24
Periyardown	6425	5861.92	-102	-100.93	1.07	3575.99
Periyardown	4203	5863.67	-102	-101.74	1.03	2283.03
Periyardown	2554	5864.6	-104	-102.25	0.01	2.66
Periyar	121749	2100	-74	-71.33	1.39	1629.74
Periyar	117746	2105.46	-76	-71.39	1	2572.04
Periyar	115215	2108.58	-76	-71.42	1.01	2384.91
Periyar	108661	2119.63	-76	-71.57	1.52	1964
Periyar	103107	2132.3	-76	-71.58	0.41	4983.35
Periyar	94820	2136.72	-85	-76.59	1.32	1615.47
Periyar	91857	2136.72	-86	-76.56	0.45	4811.96

Periyar	86837	2136.95	-87	-76.56	0.52	5569.34
Periyar	83218	2137.22	-87	-76.56	0.35	7998.36
Periyar	79752	2137.54	-88	-76.56	0.38	7295.69
Periyar	76588	2138.13	-88	-76.56	0.22	15999.55
Periyar	72053	2139.81	-89	-76.56	0.1	29672.29
Periyar	68930	2141.66	-89	-76.56	0.07	32578.37
Periyar	64324	2145.23	-90	-76.56	0.07	36617.18
Periyar	61724	2147.3	-90	-76.56	0.06	43149.76
Periyar	57767	2150.38	-91	-76.56	0.07	38643.69
Periyar	47257	2156.03	-91	-76.56	0.1	24116.55
Periyar	44558	2159.35	-91	-76.56	0.21	12725.84
Periyar	39271	2164.95	-91	-76.56	0.13	22416.18
Periyar	37592	2167.66	-91	-76.57	0.31	9175.63
Periyar	28599	2176.71	-91	-76.57	0.1	21616.53
Periyar	26510	2180.44	-91	-76.57	0.16	16357.93
Periyar	23862	2184.81	-91	-76.57	0.1	25123.9
Periyar	21228	2189.71	-91	-76.57	0.09	25199.58
Periyar	18529	2194.12	-91	-76.56	0.12	20372.79
Periyar	14878	2199.22	-91	-76.56	0.18	15538.51
Periyar	12507	2204.27	-92	-76.56	0.07	35713.95
Periyar	9168	2214.12	-92	-76.56	0.05	49794.48
Periyar	4693	2231.11	-93	-76.56	0.05	64400.45

Tables 5.6, 5.7 and 5.8 show the results of hydrodynamic variables as per steady state simulation (Gumbel RP 100), LogPT3 RP100 and unsteady flow simulation as per HE-7 event, respectively. The hydrodynamic variables such as Q, minimum channel elevation, water surface elevation, velocity and flow area have been computed. Based on these hydrodynamic variables, the extreme flood conditions can be estimated. The discharge vs flow area (flooded area) as shown in all Tables (5.6, 5.7 and 5.8) provide most important information for flood hazard assessment is the flooded area delimitation. In areas, where the flood depth and water velocity are found high, those areas can be critical for extreme flood conditions.

As per one 1D unsteady flood simulation, the 2D flood simulation has been done. In 2D flood simulation using HEC-RAS, all necessary geometric layers and parameters are computed through HEC-RAS mappers. The 2D mesh boundary has been created and for each grid, a computational point has been defined. In this study, the three upstream boundary and one downstream boundary conditions have been given. For 2D and 1 D unsteady flow simulations, the manning's n has been setup between 0.013 to 0.015. In case of 2D simulation, the manning's n values are defined for all grids. The same flow hydrographs for the HE-7 event have been used in 2D simulations as used in 1D unsteady simulation.

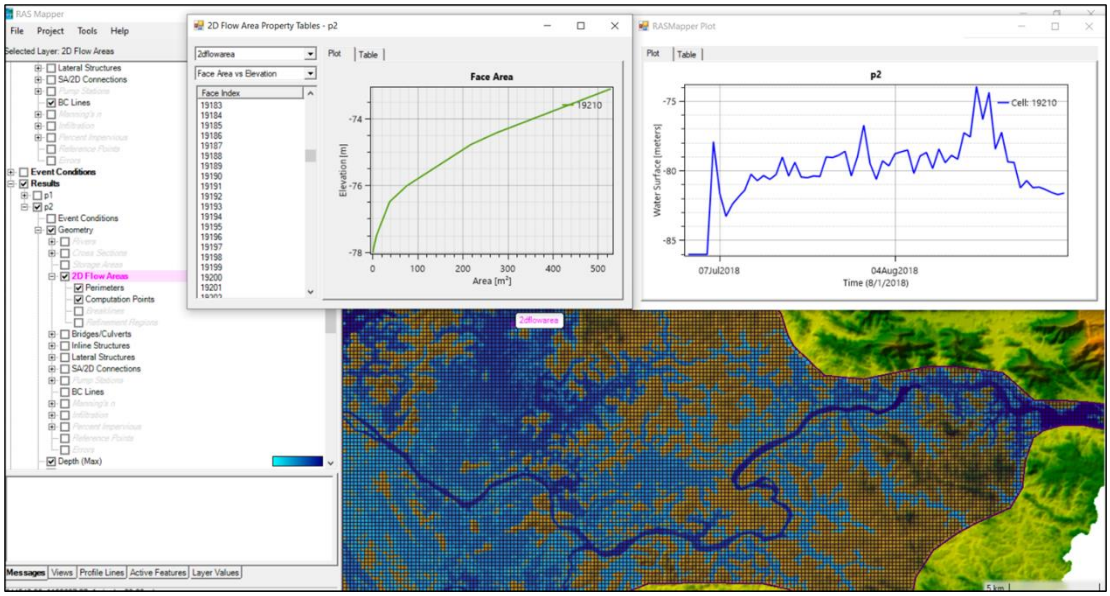

Figure 5.24: RAS mapper showing 2D mesh grid and modeling outcomes (e.g. elevation vs area curve, Surface Water Level for the given time series location) at a grid location.

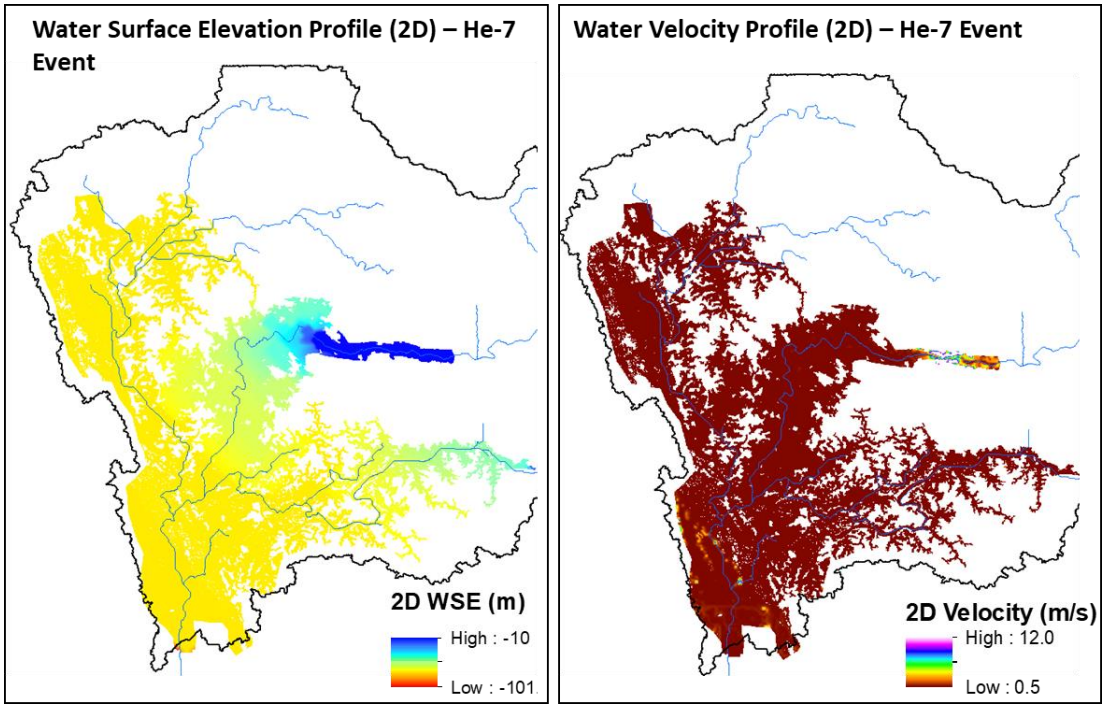

Figure 5.25: Showing water surface elevation profile and water velocity profile in the routed river reaches computed by 2D unsteady flow simulation for the HE-7 (Kerala floods, 2018).

Figure 5.24 highlights the 2D unsteady flow simulation results for HE-7 in RAS mapper. A 2D mesh grid and modeling outcomes (e. g. elevation vs area curve, Surface Water Level for the given time series location) can be visualized at all grid locations. In 1D simulation, the hydrodynamic variables can be calculated at each cross section and the velocity of water cannot be changed with time, however, it can be different at each cross section only. Between two adjacent cross sections, the velocity cannot vary with time.

5.6 1D AND 2D FLOOD DEPTHS AND INUNDATION MAPPING FOR HISTORICAL EVENTS – AN UNSTEADY FLOW ANALYSIS

Figure 5.26 shows the comparison between flood inundation profiles (max of all days) which are computed based on 1D and 2D unsteady flows for the HE-7. There are significant differences can be noticed when to compared 1D vs 2D. The 2D profile looks smoother and fine as compared to 1D profile. In both 1D and 2D profiles, the variations in colour from light to dark highlight the variations in flood depth from lower to higher, respectively.

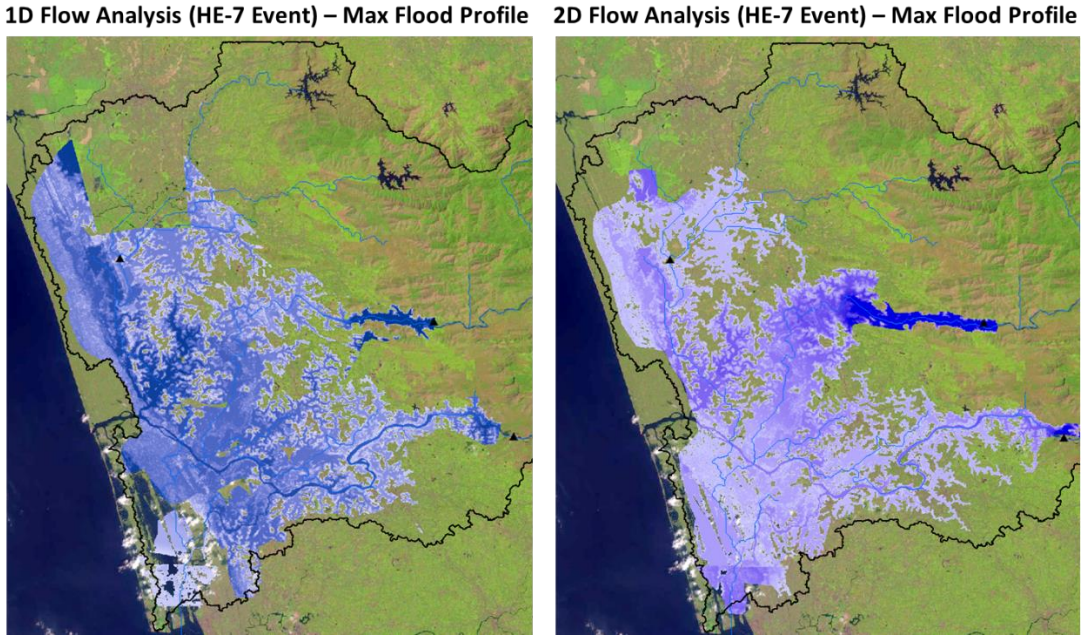

Figure 5.26: Comparison of flood inundation profiles (max inundation) which are computed based on 1D and 2D unsteady flows for the HE-7.

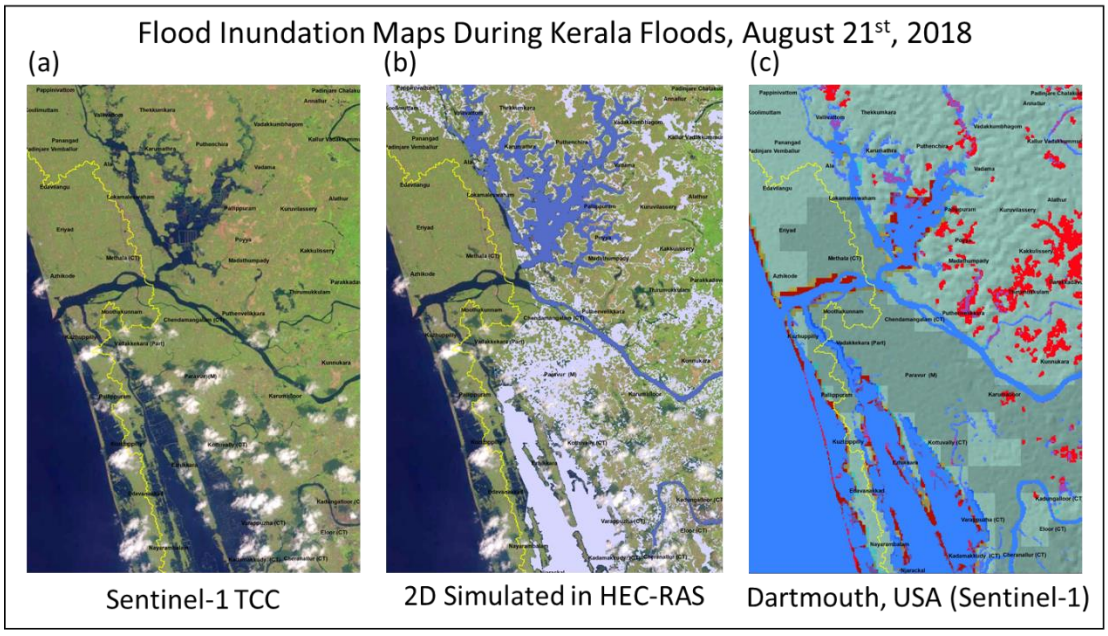

Figure 5.27: A comparison cum validation of HE-7 (Kerala floods, 2018) based floods with reference to the flood pixels as shown by real time Sentinel -1 and flood map derived from DARTMOUT, USA on the dated August 21st, 2018.

However, in case of 1D profile, the visual representation and accuracy of flood inundation can be improved while increasing the numbers of cross sections (Saksena, 2015). The cross-section should be of higher intervals and accurate. Therefore, for 1D modeling, surveyed cross sections should be preferred. One of the drawbacks of this study that in the present work DEM's derived cross sections have been used and thus some errors can be expected in the final modeling outcomes. Although, both simulation steps show a good match between flood inundated maps generated for HE-7 flood event. At the downstream portion, the flood inundation area modelled by 2D unsteady flow simulation for the HE-7 is compared with the Sentinel TCC image (taken on 21st August, 2018) and flood map created by DARTMOUTH, USA (based on Sentinel SAR 21st August 2018). All maps found comparable to each other. The flood map generated by 2D unsteady flow for the HE-7 on the dated August 21st 2018 covered all flooded pixels (or areas) as per the Sentinel TCC image (taken on 21st August, 2018) and flood map created by DARTMOUTH, USA (based on Sentinel SAR 21st August 2018).

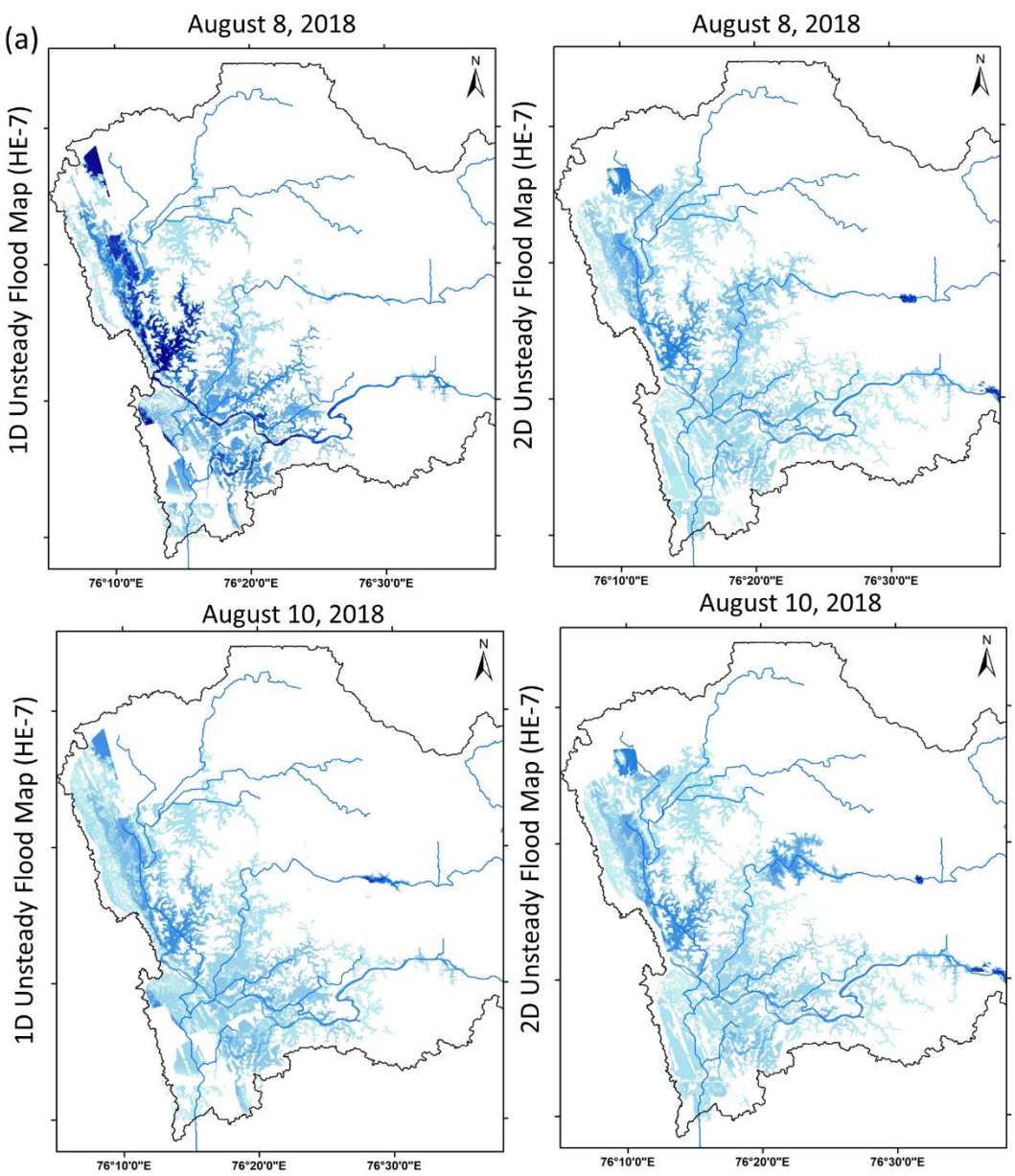

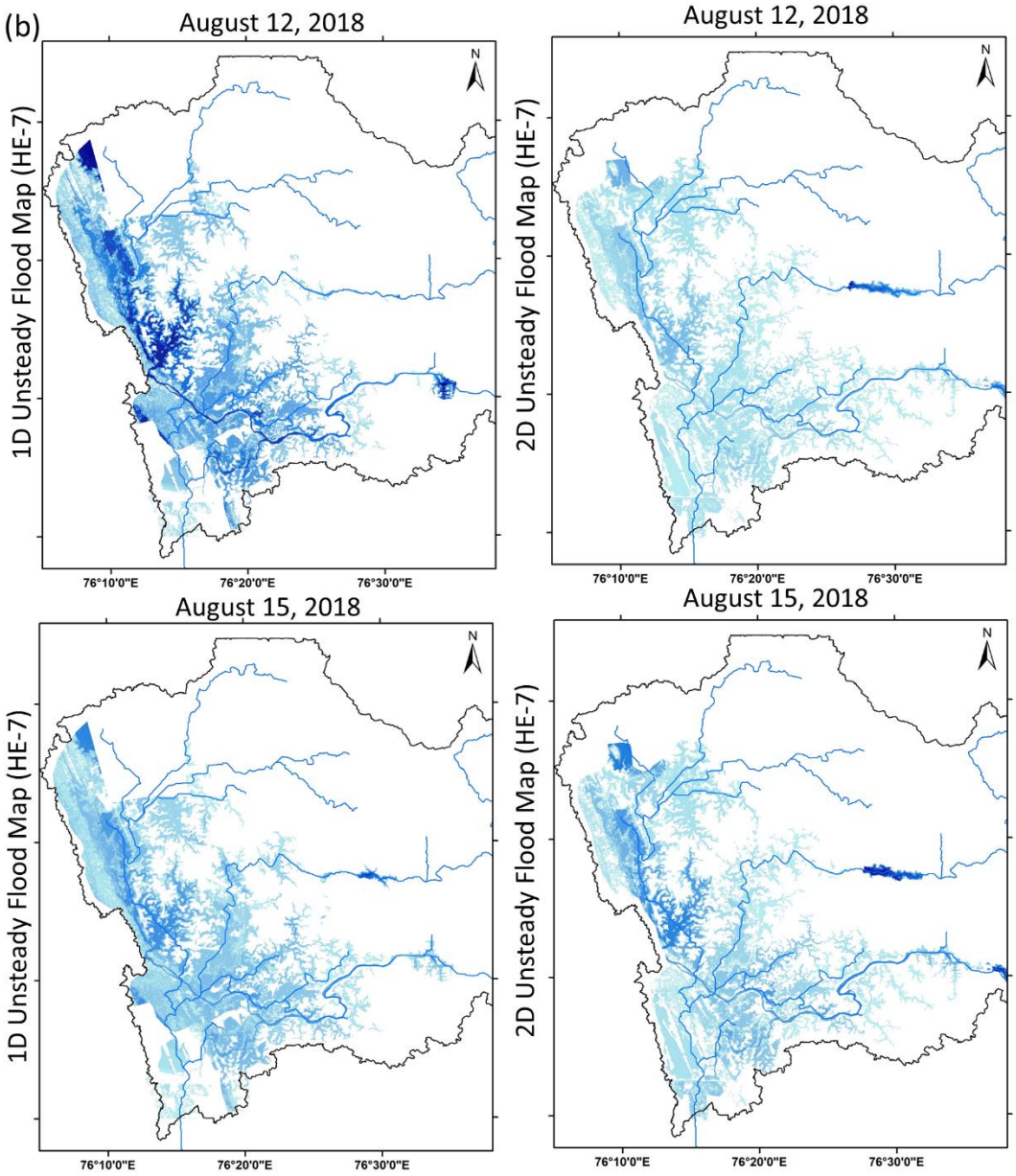
(b)
August 12, 2018
1D Unsteady Flood Map (HE-7)
2D Unsteady Flood Map (HE-7)
August 15, 2018
N
76°10'0"E
76°20'0"E
76°30'0"E

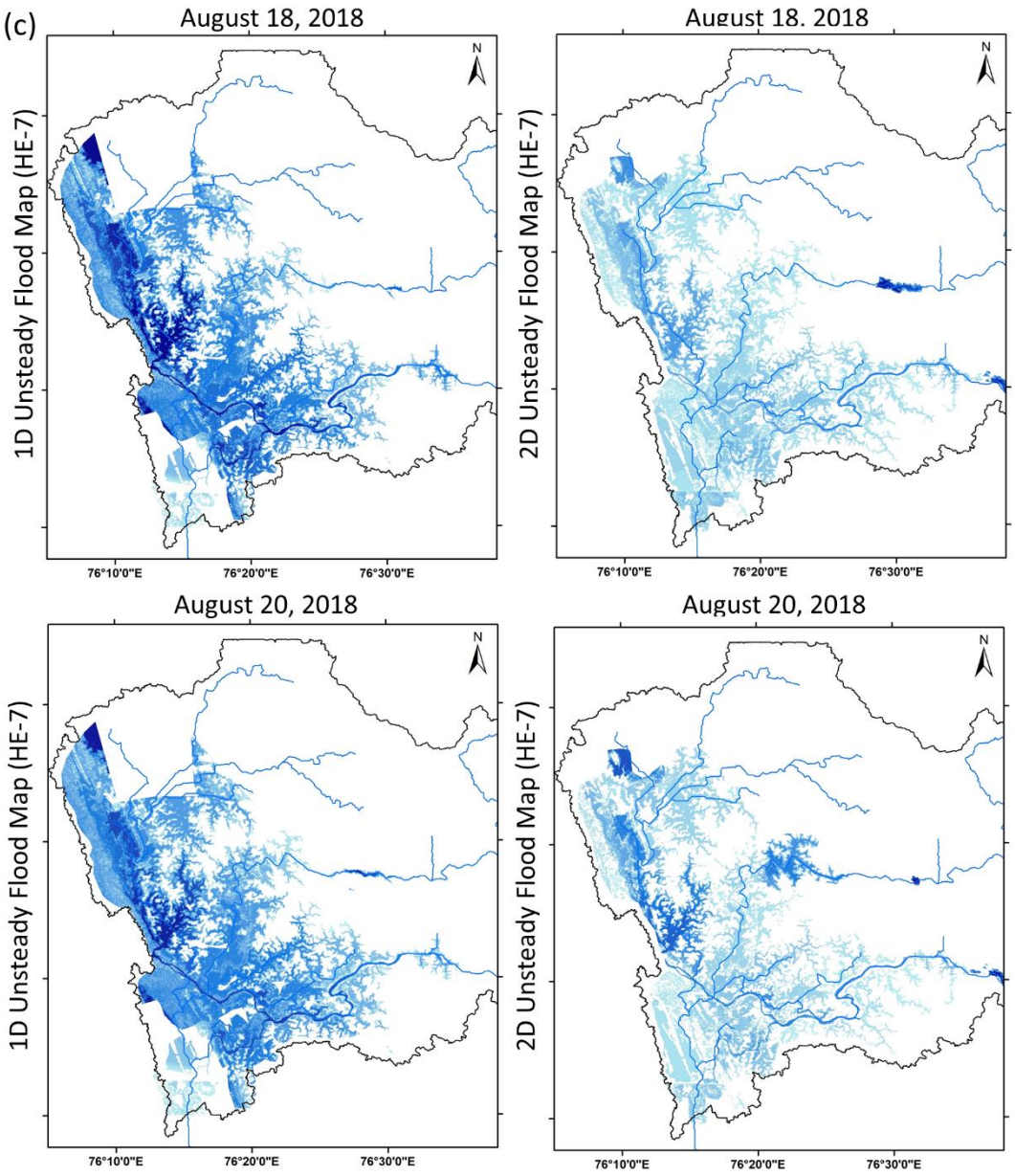
(c)
August 18, 2018
August 18, 2018
1D Unsteady Flood Map (HE-7)
2D Unsteady Flood Map (HE-7)
August 20, 2018
August 20, 2018
1D Unsteady Flood Map (HE-7)
2D Unsteady Flood Map (HE-7)
N
76°10'0"E
76°20'0"E
76°30'0"E

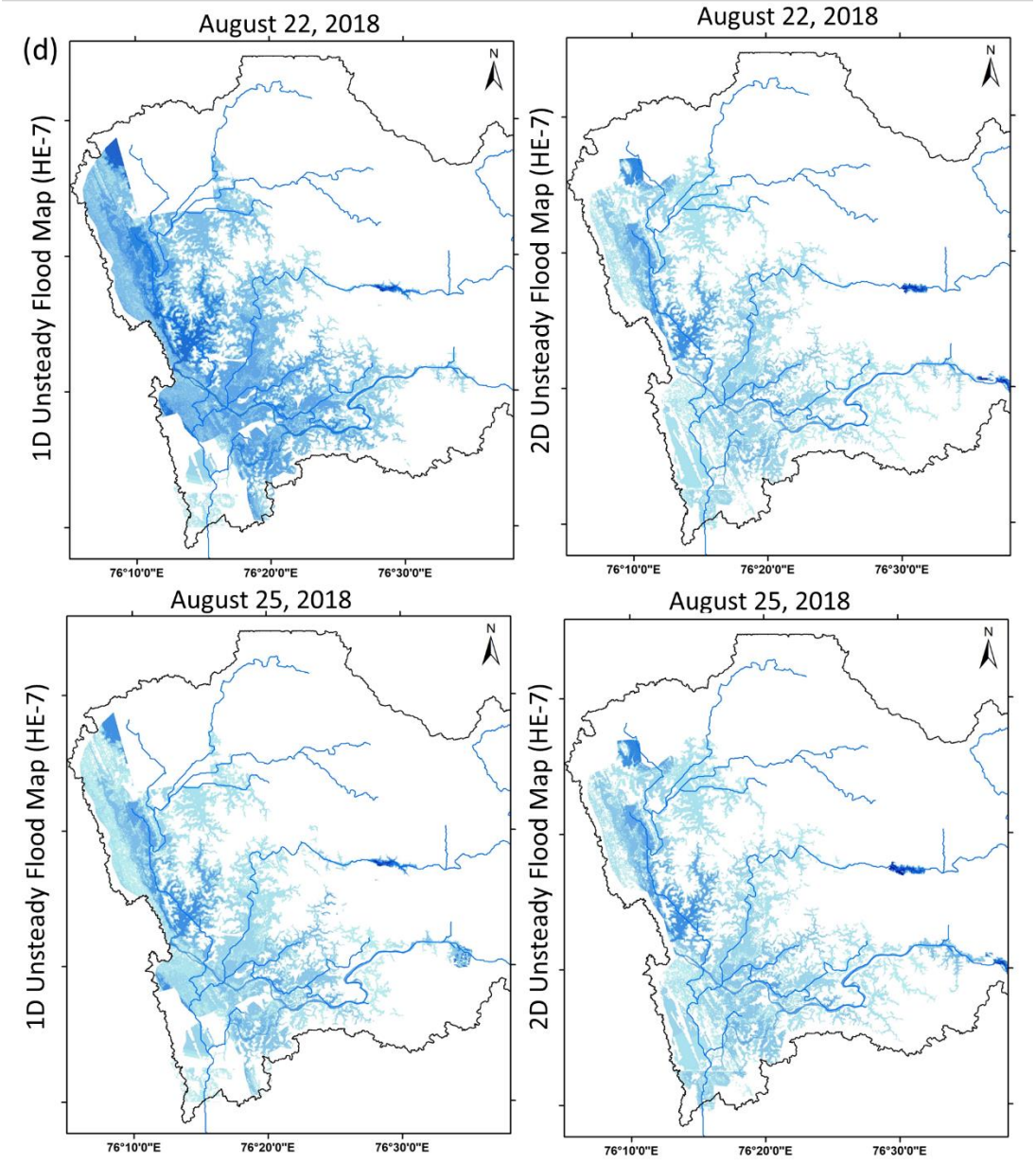

Figure 5.28: Comparisons of flood maps generated as per 1D unsteady flow and 2D unsteady flow simulations for the HE-7 (Kerala Flood, 2018) during (a) 8th and 10th August 2018, (b) 12th and 15th August, (c) 18th and 20th August and (d) 22nd and 25th August, 2018.

Figure 5.28 shows the comparisons of flood maps generated as per 1D unsteady flow and 2D unsteady flow simulations for the HE-7 (Kerala Flood, 2018) during (5.28a) 8th and 10th August 2018, (5.28b) 12th and 15th August, (5.28c) 18th and 20th August and (5.28d) 22nd and 25th August, 2018. A 1D and 2D flood maps showed significant variations in their inundation areas. The inundation areas look more prominent and distributed in 2D based flood maps than 1D maps. As per the temporal variations, both models show almost similar pattern. The main flood starts from 16, 17 and 18 August and thus the maximum flood inundation is recorded in these days. Based on these maps, it is observed that most of the flooded area corresponded to downstream areas, unfortunately

where urban settlement is high. Figure 5.29 shows the 1D unsteady flood inundation maps (max) profiles for different HEs (historical events) such as HE-1, HE-2, HE-5 and HE-7. In these maps, a significant variation can be notified. The darker blue area represents high flood depth. Considering all flood maps, the extreme high floods can be observed in case of HE-7 (i. e. Kerala Floods, 2018).

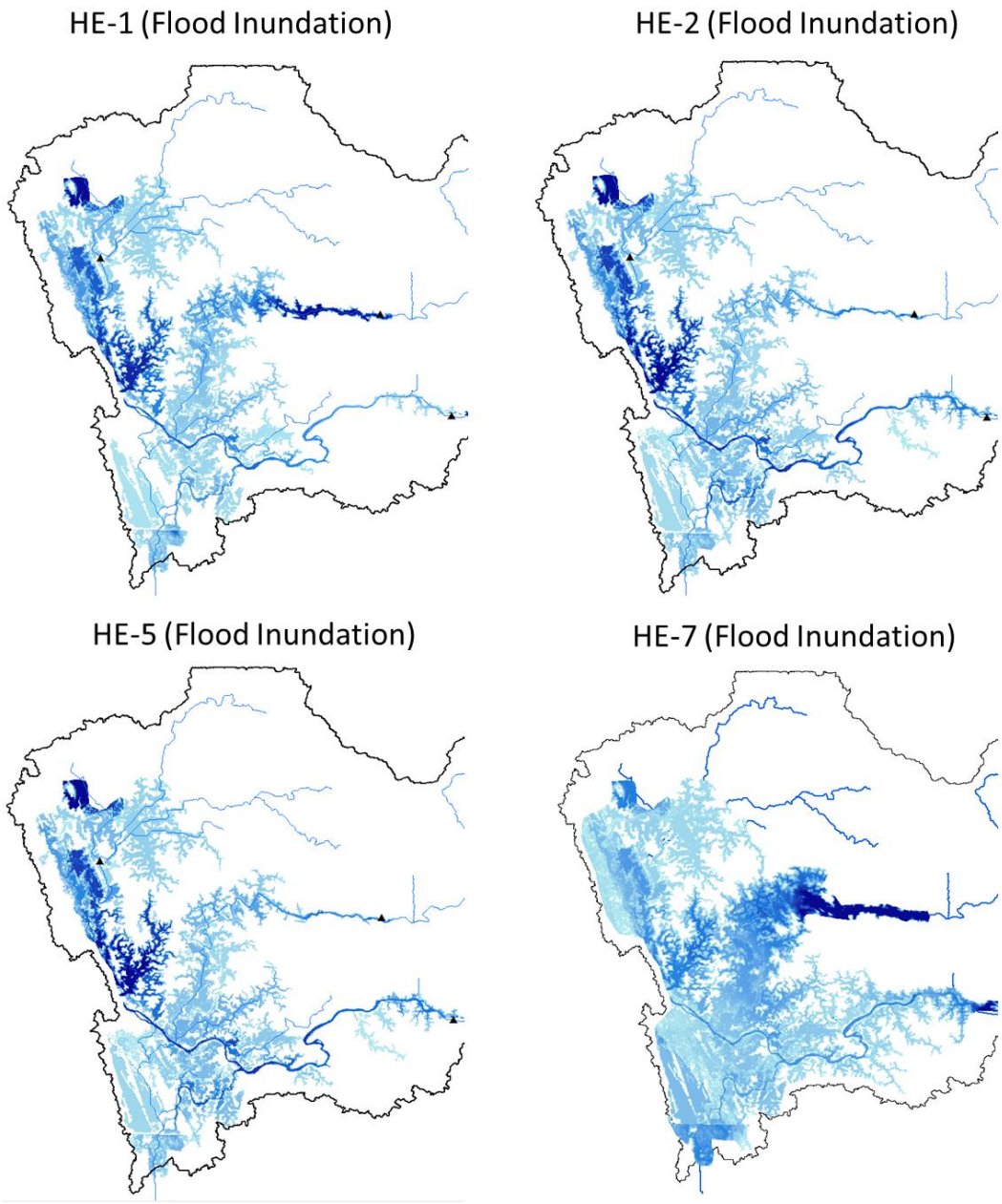

Figure 5.29: Comparison of flood inundation maps during different HEs computed based on 1D unsteady flow analysis in HEC-RAS.

5.7 RAINFALL AND FLOOD FREQUENCY ANALYSIS

5.7.1 Rainfall Frequency Analysis Results

In this study, the rainfall and flood frequency analysis has been done. The main purpose of the rainfall and flood frequency analysis is to generate the return period based extreme rainfalls and flows. These extreme rainfalls were converted into extreme floods and extreme floods based on different return periods (i. e. 20years, 50 years, 100years, 200years etc.) were utilized to generate the return period based different probabilistic flood maps. For rainfall and flood frequency analysis, the evaluation of

different distributed methods has been done. The error estimation has been done to select the best performing distribution method as per the available rainfall and peaks flows over the study area basin. For rainfall frequency analysis (RFA), total 18 years daily rainfall datasets at 23 stations have been utilized. Figures (5.30a to 5.30d) show the station wise evaluation of different distribution methods such Log Normal, Gumbel and Log Pearson Type 3. Figures 5.30 (a to d) show the distribution of rainfall (on the y-axis) and corresponding return period rainfall value (on the x-axis) at each station. Some variations ca be observed in all distribution methods. In majority of rainfall stations, the Log Pearson Type 3 (LogPT3) based CDF curve is found more closure to the observed data points and this is clearly visible in the Figures 5.30 (a to d).

(a)

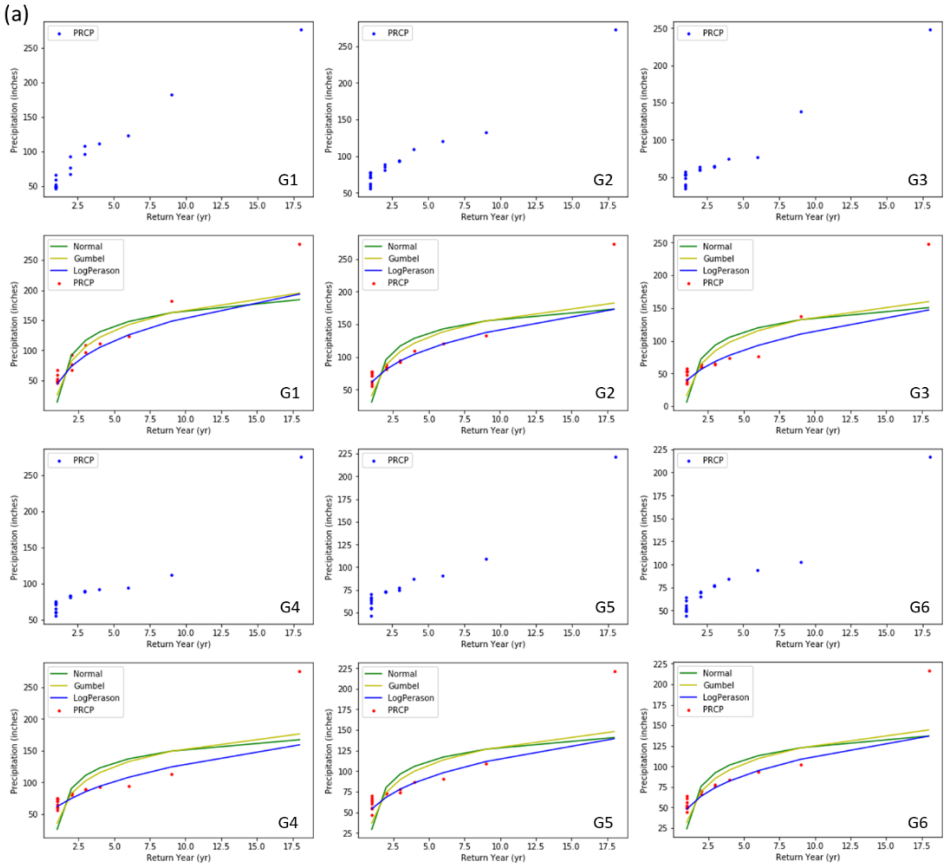

(b)

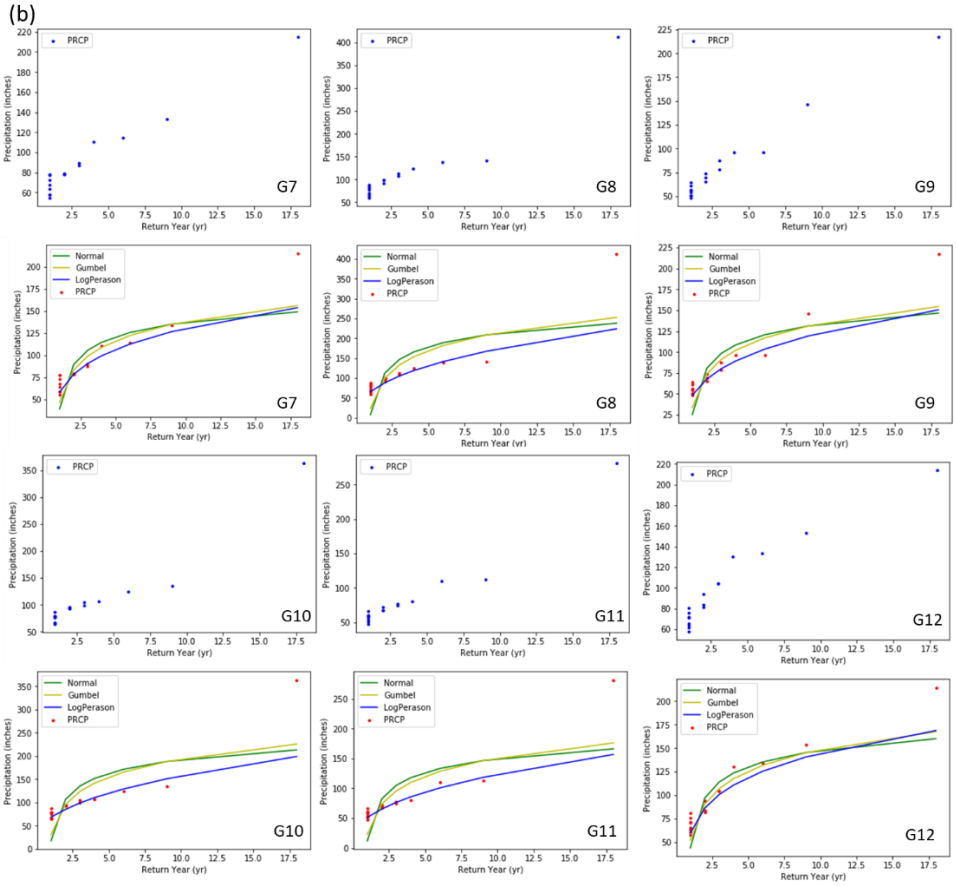
PRCP
Normal
Gumbel
LogPerason
Precipitation (inches)
Return Year (yr)
G7
G8
G9
G10
G11
G12

(c)

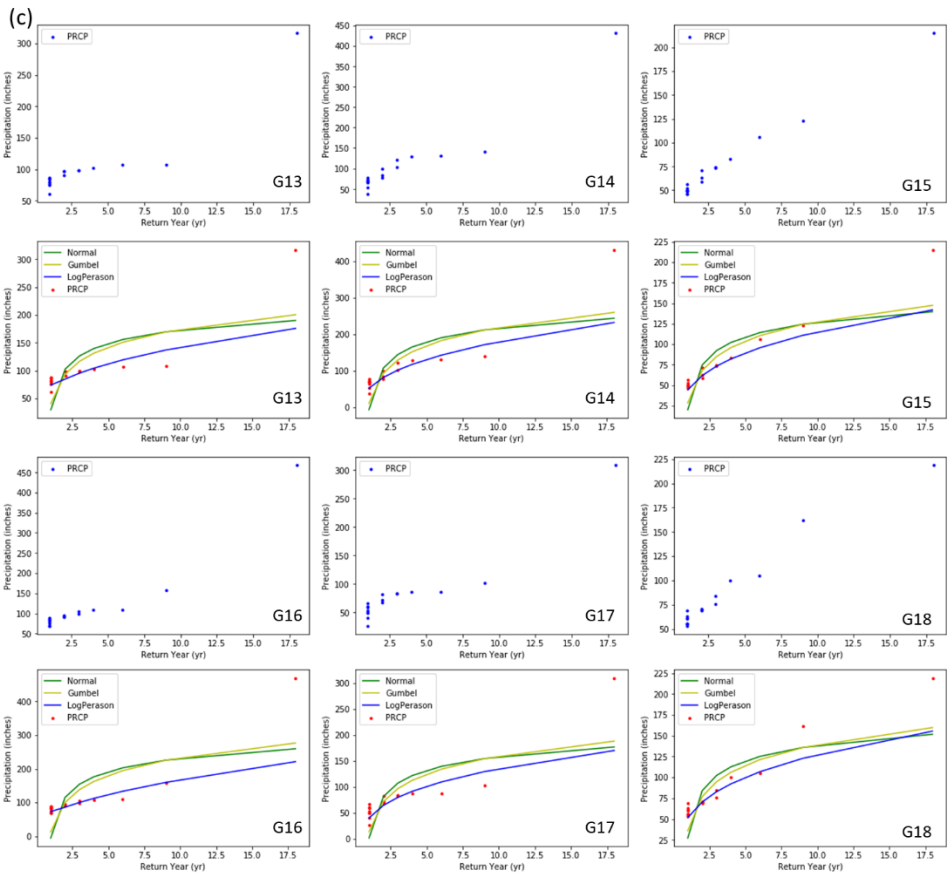
PRCP
Normal
Gumbel
LogPerason
Precipitation (inches)
Return Year (yr)
G13
G14
G15
G16
G17
G18

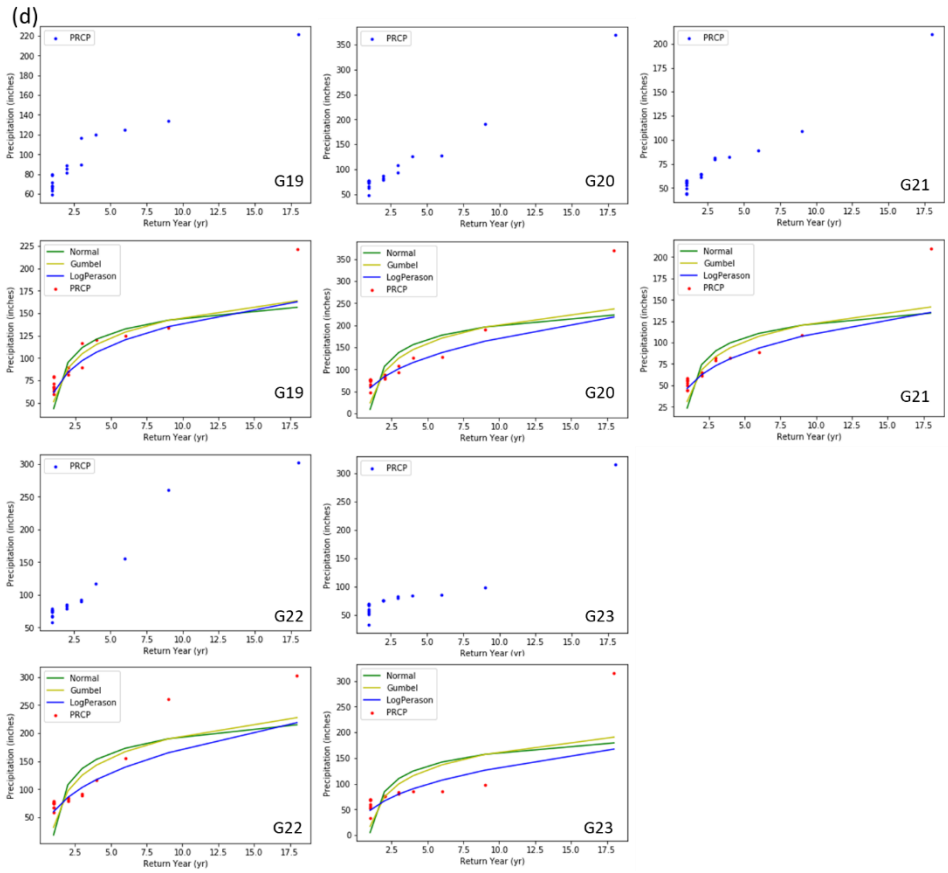

Figure 5.30: Station wise evaluation of rainfall using different distribution methods such Log Normal, Gumbel and Log Pearson Type 3. The distribution of rainfall has shown on the y-axis and corresponding return period rainfall value has shown on the x-axis.

Table 5.9 shows the results of the best performing extreme value distribution method over Periyar river basin. Three methods which are mostly used for the computation of extreme values, especially to generate the return period based extreme value, evaluated in this study. The Mean Squared Error (MSE) and Root Mean Squared Error (RMSE) statistical evaluation methods have been utilized to check the applicability of the three selected extreme value distribution methods such as Log Normal, Gumbel, Log Pearson Type 3. As per the results as shown in Table 5.9, the LogPT3 method performed superior to other methods. The Log Normal gave maximum error across all rainfall stations. Therefore, finally, the Gumbel and LogPT3 methods have been selected for the rainfall and flood frequency analysis.

Table 5.9: Evaluation of best performing extreme distribution method.

Stations	MSE			RMSE		
	Log Normal	Gumbel	Log Pearson	Log Normal	Gumbel	Log Pearson
Grid75	1377	825	571	37.1	28.7	23.9
Grid120	1808	1272	855	42.5	35.7	29.2
Grid136	1453	963	649	38.1	31.0	25.5
Grid137	993	675	444	31.5	26.0	21.1
Grid138	1661	1106	723	40.8	33.3	26.9
Grid148	901	601	413	30.0	24.5	20.3
Grid149	699	437	296	26.4	20.9	17.2
Grid151	3449	2412	1652	58.7	49.1	40.6

Grid152	4592	3201	2224	67.8	56.6	47.2
Grid153	2054	1404	948	45.3	37.5	30.8
Grid164	835	515	347	28.9	22.7	18.6
Grid165	519	301	224	22.8	17.3	15.0
Grid166	2660	1931	1284	51.6	43.9	35.8
Grid167	7448	5307	3676	86.3	72.8	60.6
Grid168	5287	3675	2559	72.7	60.6	50.6
Grid169	2729	1943	1358	52.2	44.1	36.9
Grid179	847	525	354	29.1	22.9	18.8
Grid180	921	564	367	30.3	23.7	19.2
Grid181	639	400	291	25.3	20.0	17.1
Grid182	2556	1601	1060	50.6	40.0	32.6
Grid183	3469	2270	1496	58.9	47.6	38.7
Grid184	3066	2214	1480	55.4	47.1	38.5
Grid195	818	533	364	28.6	23.1	19.1

The second important step in the frequency analysis is to compute the parameters for the selected extreme value distribution methods such as Gumbel and LogPT3. Based on the literature survey (Anwat et al., 2021; Bezak et al., 2014), it is concluded that methods such as Method of Moments, L-Moments and Maximum Likelihood can have a significant impact on the computed extreme values as per their parameters. However, it depends on the data length and quality. Many studies suggested to use Method of Moments (MoM) for the computation of parameters for these selected methods (References). Table 5.10 shows the parameters values for rainfall for two methods such as Gumbel and LogPT3. For Gumbel four parameters viz. $\bar{x}$, sx, u, a and for LogPT3, variance, standard deviation (Std dev), skewness coefficient (Sk C) and K have been computed as per the work done by Bharadwaj et. al (2019) and Hunt and Menon (2018). The values of K for different return periods at each rainfall station have shown in Table 5.11. These parameters have played significant and crucial role in the computation of return period rainfall value.

Table 5.10: Parameters computation for rainfall frequency analysis (RFA) as per Gumbel and LogPT3

Stations	**Gumbel**				**Log PT3**		
	$\bar{x}$	**sx**	**u**	**α**	**Variance**	**Std dev**	**Sk C**
Grid75	91.62	59.89	64.65	46.72	0.0500	0.2235	1.0347
Grid120	90.37	49.77	67.97	38.82	0.0241	0.1552	2.4343
Grid136	95.84	50.04	73.31	39.04	0.0262	0.1619	1.7841
Grid137	80.16	39.25	62.49	30.62	0.0225	0.1499	1.9968
Grid138	72.07	50.79	49.20	39.62	0.0421	0.2051	1.7294
Grid148	75.53	39.81	57.61	31.05	0.0267	0.1635	1.7521
Grid149	89.13	38.65	71.72	30.15	0.0223	0.1493	1.3791
Grid151	106.64	68.82	75.65	53.69	0.0304	0.1745	2.3853
Grid152	112.71	81.03	76.22	63.21	0.0382	0.1955	2.0222
Grid153	82.22	54.20	57.82	42.28	0.0328	0.1811	2.2619
Grid164	80.57	42.76	61.31	33.36	0.0306	0.1748	1.4845
Grid165	96.92	40.85	78.53	31.86	0.0247	0.1571	0.9389
Grid166	102.67	56.50	77.23	44.07	0.0221	0.1488	2.8348
Grid167	115.41	93.13	73.48	72.65	0.0368	0.1918	2.9229
Grid168	107.51	88.22	67.78	68.82	0.0528	0.2297	1.4503

Grid169	81.09	61.81	53.26	48.22	0.0487	0.2208	1.1874
Grid179	74.55	42.15	55.57	32.88	0.0325	0.1804	1.5919
Grid180	84.01	43.82	64.28	34.18	0.0291	0.1707	1.6324
Grid181	94.98	39.85	77.03	31.09	0.0406	0.2015	1.7078
Grid182	107.91	69.24	76.73	54.02	0.0406	0.2015	1.7078
Grid183	106.71	75.22	72.84	58.68	0.0426	0.2063	1.6951
Grid184	84.41	61.44	56.74	47.93	0.0383	0.1956	1.8484
Grid195	74.06	39.04	56.48	30.46	0.0276	0.1663	1.6682

Table 5.11: K values computed for different return periods and rainfall stations.

Stations	**K for Log PT3**				
	RP10	**RP20**	**RP50**	**RP100**	**RP200**
Grid75	1.34	2.051	2.557	3.044	3.519
Grid120	1.258	2.258	3.031	3.815	4.607
Grid136	1.319	2.191	2.843	3.49	4.135
Grid137	1.302	2.219	2.911	3.603	4.394
Grid138	1.322	2.182	2.824	3.46	4.092
Grid148	1.321	2.186	2.832	3.472	4.109
Grid149	1.337	2.124	2.698	3.258	3.811
Grid151	1.264	2.255	3.019	3.747	4.574
Grid152	1.3	2.221	2.918	3.546	4.403
Grid153	1.277	2.245	2.986	3.299	4.487
Grid164	1.334	2.143	2.737	3.32	3.896
Grid165	1.339	2.028	2.515	2.982	3.435
Grid166	1.205	2.276	3.121	3.987	4.868
Grid167	1.192	2.277	3.137	4.021	4.923
Grid168	1.335	2.137	2.725	3.3	3.869
Grid169	1.34	2.084	2.621	3.141	3.65
Grid179	1.329	2.162	2.777	3.383	3.983
Grid180	1.327	2.168	2.791	3.406	4.015
Grid181	1.339	2.096	2.643	3.175	3.696
Grid182	1.323	2.179	2.817	3.448	4.075
Grid183	1.324	2.177	2.812	3.441	4.065
Grid184	1.314	2.199	2.863	3.525	4.208
Grid195	1.325	2.173	2.803	3.426	4.044

Table 5.12 shows the return period rainfall values as per the Gumbel and LogPT3 methods across all rainfall stations. In Table 5.2, in case of RP 10 the Gumbel has shown high rainfall values than LogPT3. However, in case of other return periods (e. g. RP20, RP50, RP100, RP100), the LogPT3 has shown higher rainfall values.

Table 5.12: Return periods-based rainfall values as per the Gumbel and LogPT3 methods across all rainfall stations

Stations	Gumbel	Log PT3	Gumbel	Log PT3	Gumbel	Log PT3	Gumbel	Log PT3	Gumbel	Log PT3
	RP10	RP10	RP20	RP20	RP50	RP50	RP 100	RP100	RP 200	RP 200
Grid75	170	158	203	228	247	296	280	380	312	486
Grid120	155	131	183	187	219	247	247	327	274	434
Grid136	161	145	189	200	226	255	253	325	280	413
Grid137	131	117	153	161	182	204	203	259	225	341
Grid138	138	118	167	177	204	239	231	323	259	435
Grid148	127	114	150	158	179	202	200	257	222	327
Grid149	140	132	161	173	189	211	210	256	231	310
Grid151	196	160	235	238	285	324	323	434	360	605
Grid152	218	178	264	270	323	369	367	490	411	721
Grid153	153	126	183	188	223	256	252	292	282	479
Grid164	136	126	160	174	191	221	215	280	238	353
Grid165	150	147	173	189	203	225	225	266	247	314
Grid166	176	144	208	208	249	277	280	373	311	505
Grid167	237	170	289	275	357	402	408	595	458	885
Grid168	223	184	272	281	336	384	384	521	432	703
Grid169	162	138	196	201	241	264	275	344	309	446
Grid179	130	117	153	166	184	214	207	275	230	353
Grid180	141	130	166	181	198	231	222	294	245	373
Grid181	147	141	169	183	198	220	220	265	242	316
Grid182	198	176	237	262	287	352	325	471	363	630
Grid183	205	175	247	262	302	355	343	478	384	643
Grid184	165	134	199	200	244	270	277	364	311	495
Grid195	125	113	147	157	175	199	197	253	218	320

Figure 5.31 shows the distribution of computed extreme rainfall values with respect to the given return period as per Gumbel and LogPT3 across all precipitation stations (23 numbers). Figure 5.30 (a) shows the distribution of computed extreme rainfall values as per Gumbel method and Figure 5.31 (b) shows the distribution of computed extreme rainfall values based on the LogPT3 method.

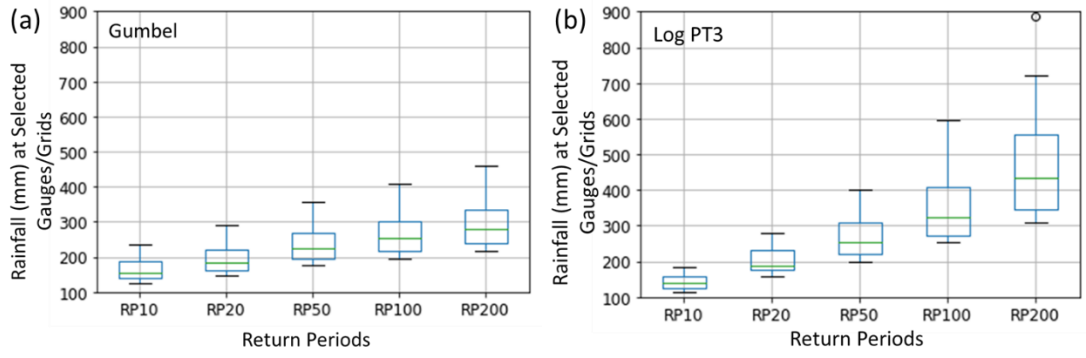

Figure 5.31: Distribution of computed extreme rainfall values with respect to the given return period as per Gumbel and LogPT3 across all precipitation stations (23 numbers).

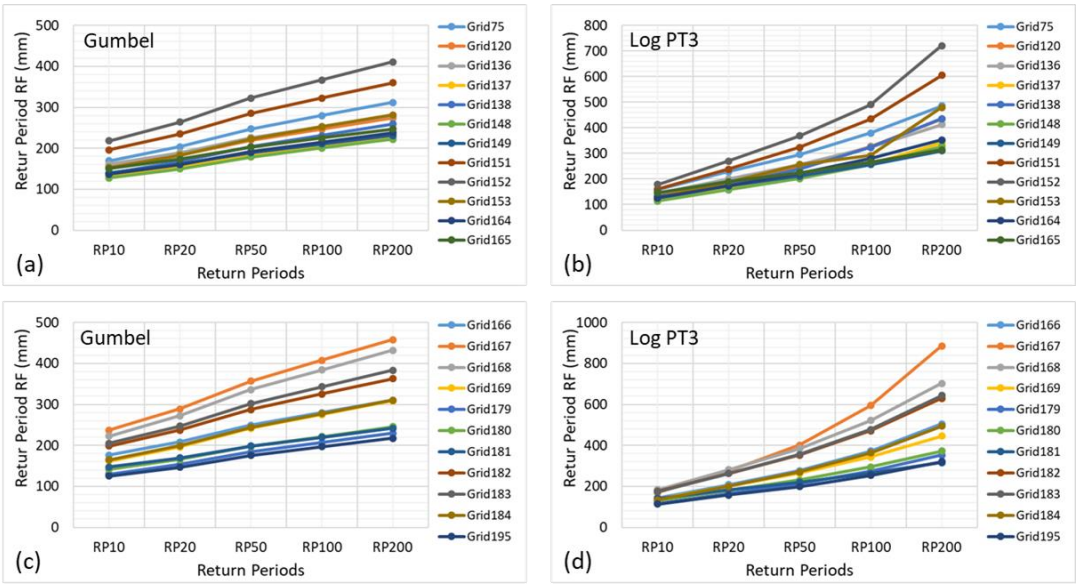

Figures 5.32: Station wise return period rainfall corresponding to the given return period as per Gumbel and LogPT3 methods.

In Figures (5.31 and 5.32), in case of Gumbel, a gradual increase in rainfall values can be seen from RP 10 to RP 200; while in case of LogPT3, a sharp increase can be observed in rainfall as per RP 10 to RP 200. In case of Gumbel, the maximum rainfall value is computed around 490 mm (as per RP 200), whereas in case of LogPT3, the maximum rainfall is computed 900 mm (for RP 200 and i. e. one day maximum). However, LogPT3 based computed one day maximum rainfall looks slightly high (Figure 5.33). In both methods, if one can see that so RP10 and RP 20 based computed rainfall are found comparable but when RP time increases the rainfall variation increases in both methods (Figure 5.33).

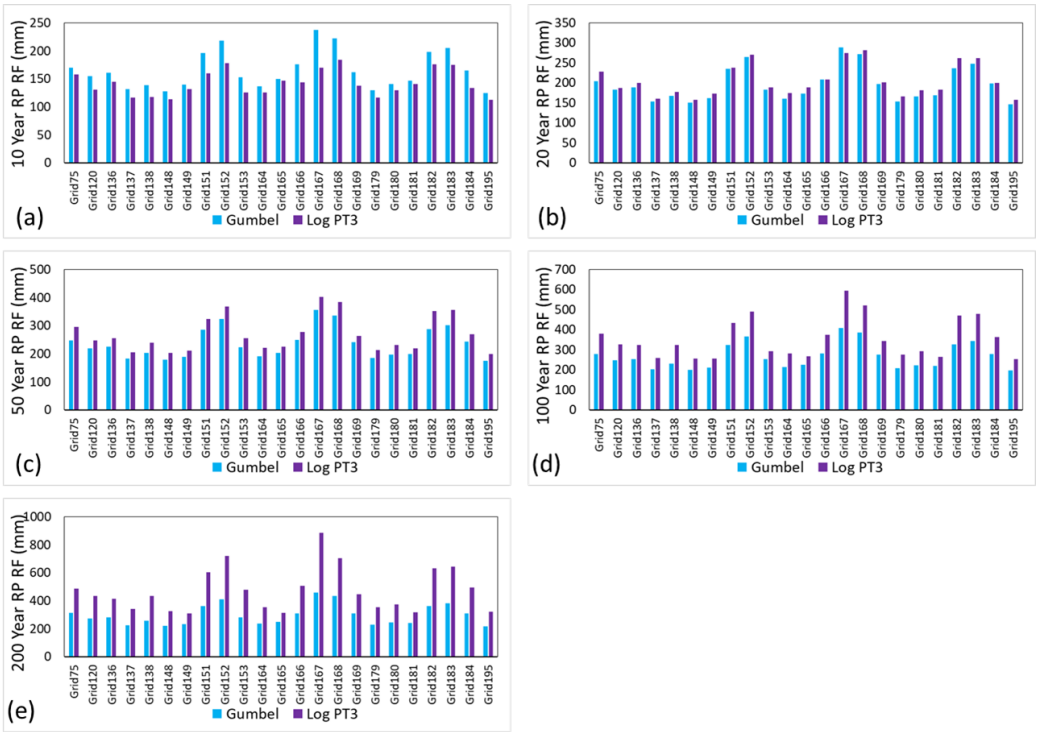

Figure 5.33: Comparison of Gumbel and LogPT3 based computed different return period-based rainfall.

Figure 5.33 (a-c) shows the annual exceedance probability (%) against annual maximum rainfall shown at all rainfall stations. To see the chances are over a given time that a flood will reach or exceed a specific magnitude, and this is called the probability of occurrence or the exceedance probability (Tanaka et al., 2017). All figures (5.33a, 5.33b and 5.33c) plotted for different grids showed a significant variation in the extreme peak rainfall. In figure (5.33), higher rainfall events have less probability of occurrence. The exceedance probability may be formulated simply as the inverse of the return period.

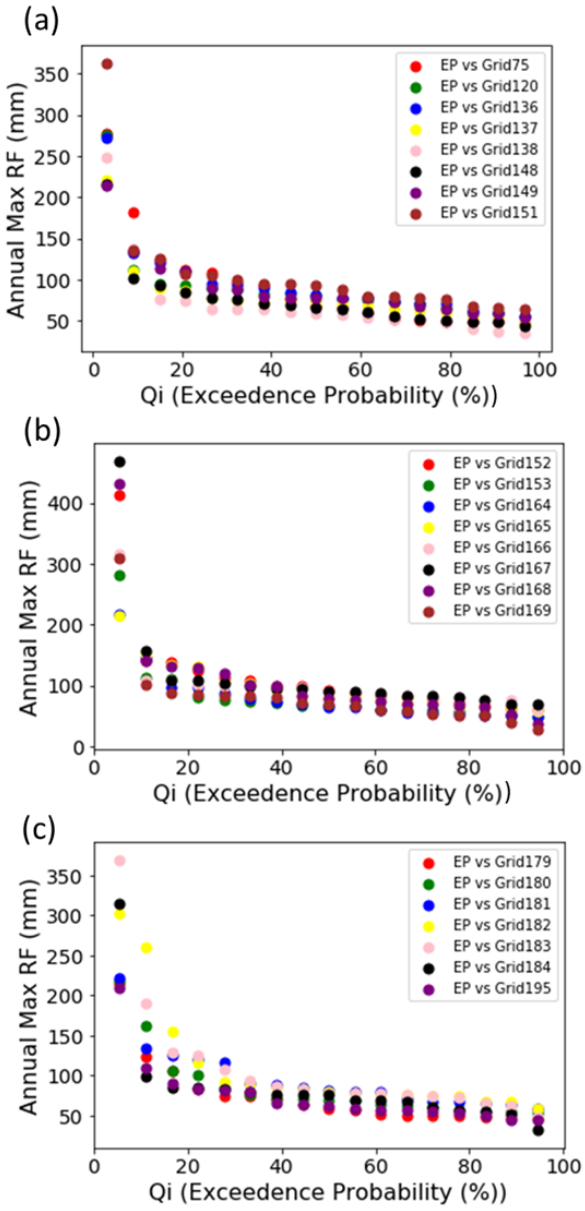

Figure 5.34 (a-c): Annual exceedance probability vs. Annual maximum rainfall at all grids.

5.7.2 Flood Frequency Analysis Results

In this study, the FFA has been performed to compute the flood flows and inundation mapping though HEC-RAS in the downstream portion (flood plain areas) of the Periyar river basin. FFA has been performed at each Subbasin (flood only corresponded to individual subbasin) and Junction (cumulative floods for upstream portions) utilizing daily timeseries discharge (2002-2018). This time series discharge has been generated from HEC-HMS after detailed calibration and optimization. For the generation of return period floods as per Gumbel and LogPT3 methods, the non-structured (or virgin)

flows have been computed, because the regulated flow may restrict to capture the real time extreme high flood values.

(a)

RP Floods	Gumbel			LP Type 3		
	Neeleswaram	Junction 16	Junction 21	Neeleswaram	Junction 16	Junction 21
10	5015.93	1668.59	656.14	4707.16	1592.32	666.43
20	5970.77	1979.40	740.49	6686.26	2336.40	807.11
50	7206.71	2381.70	849.67	8645.55	3110.68	922.76
100	8132.87	2683.17	931.48	11031.36	4090.88	1044.68
200	9055.66	2983.54	1013.00	13825.07	5277.81	1170.56

(b)

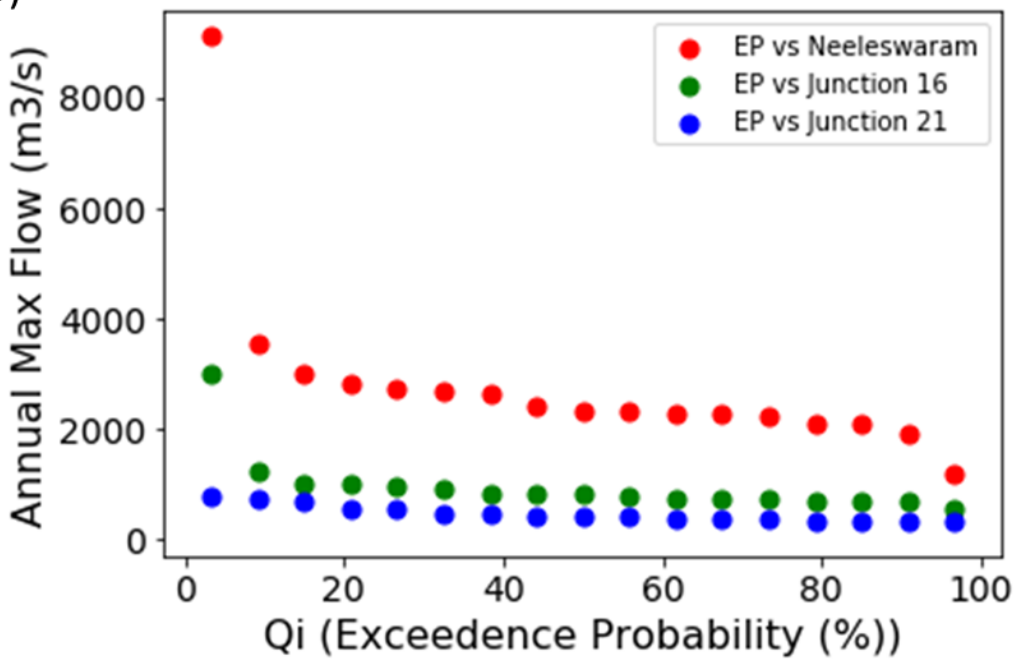

Figure 5.35: (a) Return periods-based flows at Neeleswaram gauge (Junction 7), Junction 16 and Junction 21 computed based on Gumbel and LogPT3 methods and **(b)** computation of annual exceedance probability for annual max flow.

Figure 5.35(a) shows different RP-based flows at Neeleswaram gauge (Junction 7), Junction 16 and Junction 21 computed based on Gumbel and LogPT3 methods and (b) computation of annual exceedance probability for annual max flow. In Figure 5.35(a), similar to rainfall frequency analysis (RFA), the extreme high flood values can be computed. In Figure (5.35b), the maximum flood values corresponded to Neeleswaram gauge, while Junction 21 (tributary 2), shows the lower values in all return period. Figures 5.36 shows the flow values on the y-axis and their RP floods have shown in the x-axis.

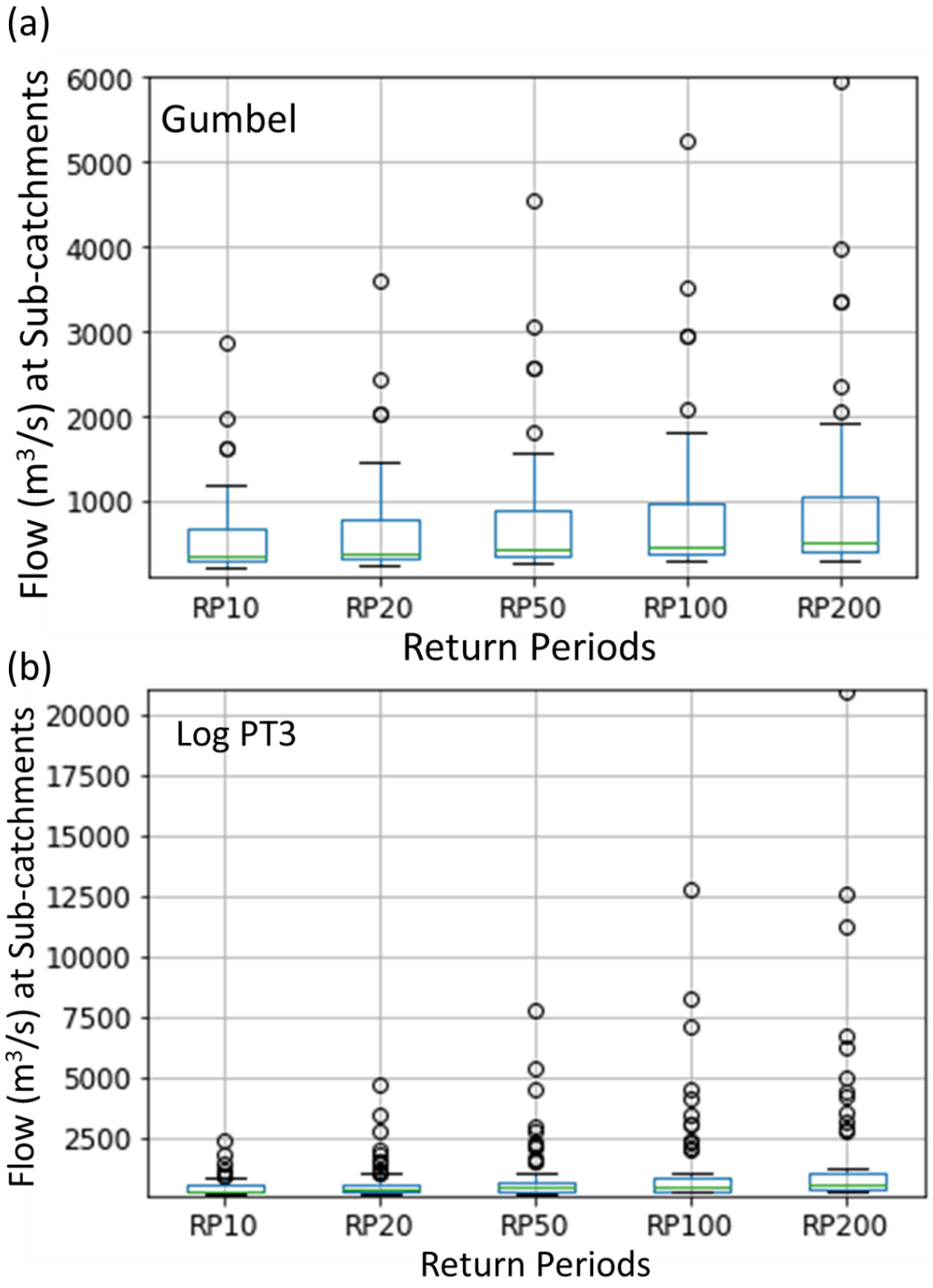

Figure 5.36: Computation of extreme flow values for different return periods as per (a) Gumbel and (b) LogPT3.

Figure 5.36 shows the extreme flow values computed for different return periods as per Gumbel (Figure 5.36a) and LogPT3 (Figure 5.36b) methods. The box plots show the variations in extreme flow values as per different return periods. In both Figures (5.36a and 5.36b), a steady increase has been observed. In case of LogPT3, the computed flows for different return periods are higher than Gumbel method. For the computation of flow values for different return periods at each subbasin and Junction, the

parameters of Gumbel and LogPT3 are computed using Method of Moments as shown in Tables 5.13 and 5.14.

Table 5.13: Parameters of Gumbel and LogPT3 for the computation of flood flows at different subbasins.

GRIDS	Gumbel				Log PT3		
	$\bar{x}$	Sx	u	α	Variance	Std dev	Sk C
Mullaperiyar	682.74	723.42	357.00	564.33	0.13	0.36	1.33
Sub39	852.00	849.70	469.41	662.84	0.13	0.36	1.17
Sub37	527.96	491.44	306.68	383.37	0.11	0.34	1.21
Sub36	409.65	350.74	251.72	273.61	0.09	0.31	1.24
Idukki	1151.36	1303.78	564.31	1017.07	0.13	0.36	1.57
Sub34	507.61	379.82	336.59	296.29	0.07	0.27	1.26
Sub35	376.98	263.11	258.51	205.25	0.06	0.25	1.28
Sub29	167.50	117.56	114.57	91.71	0.06	0.25	1.26
Sub31	221.16	46.98	200.01	36.65	0.01	0.11	-1.92
Sub23	377.15	368.15	211.39	287.19	0.14	0.37	0.94
Sub30	231.21	57.69	205.24	45.00	0.01	0.10	1.50
Sub38	204.35	52.81	180.57	41.19	0.01	0.09	2.45
Sub67	222.44	60.44	195.22	47.15	0.01	0.10	2.64
Sub28	682.74	723.42	357.00	564.33	0.01	0.09	1.88
Sub24	330.24	280.84	203.78	219.08	0.09	0.31	1.27
Sub27	249.89	66.51	219.94	51.89	0.01	0.09	2.51
Sub20	227.35	73.78	194.13	57.55	0.01	0.12	2.00
Sub43	301.51	78.91	265.98	61.56	0.02	0.13	-1.74
Sub17	435.61	438.24	238.29	341.87	0.15	0.39	0.91
Sub68	249.79	66.57	219.81	51.93	0.01	0.09	2.54
Sub32	233.98	91.96	192.57	71.73	0.02	0.14	1.77
Sub21	254.40	62.08	226.45	48.43	0.01	0.10	0.15
Sub69	514.58	161.65	441.79	126.10	0.06	0.24	-2.79
Sub70	226.65	74.81	192.96	58.36	0.01	0.12	2.00
Sub16	231.78	49.48	209.49	38.60	0.01	0.09	1.11
Sub71	188.56	29.64	175.21	23.13	0.00	0.06	1.55
Sub25	198.04	45.07	177.74	35.16	0.02	0.13	-2.56
Sub18	179.26	42.52	160.12	33.17	0.01	0.09	1.21
Sub72	275.06	51.76	251.76	40.37	0.01	0.10	-2.69
Sub19	194.38	41.16	175.84	32.10	0.01	0.10	-0.93
Sub9	348.53	284.39	220.47	221.85	0.09	0.31	0.99
Sub40	243.64	114.78	191.95	89.54	0.03	0.17	1.40
Sub2	243.59	57.87	217.53	45.14	0.01	0.09	1.63
Sub4	264.55	65.57	235.02	51.15	0.01	0.09	1.60

Sub11	256.33	66.23	226.51	51.66	0.01	0.09	2.41
Sub46	390.71	127.06	333.50	99.11	0.06	0.25	-2.76
Sub5	242.34	115.88	190.16	90.40	0.03	0.18	1.28
Sub14	340.96	268.34	220.14	209.33	0.09	0.29	0.97
Sub22	397.09	116.58	344.59	90.94	0.04	0.19	-2.53
Sub56	227.53	62.08	199.57	48.42	0.01	0.10	2.63
Sub13	223.79	51.11	200.78	39.87	0.01	0.10	-0.03
Sub62	272.85	135.32	211.92	105.56	0.05	0.21	0.25
Sub6	165.55	37.55	148.64	29.29	0.01	0.10	0.18
Sub10	166.49	39.64	148.64	30.92	0.01	0.10	-0.19
Sub33	217.99	65.79	188.37	51.32	0.05	0.21	-2.72
Sub8	165.48	37.54	148.57	29.28	0.01	0.09	0.91
Sub42	274.71	94.02	232.38	73.35	0.09	0.30	-2.81
Sub1	210.41	74.63	176.81	58.22	0.02	0.16	-0.04
Sub3	172.91	40.80	154.54	31.83	0.01	0.10	0.47
Sub12	183.06	36.97	166.42	28.84	0.01	0.09	-1.03
Sub41	190.34	41.37	171.71	32.27	0.01	0.11	-1.83
Sub61	185.44	38.66	168.03	30.16	0.01	0.09	0.68
Sub15	222.55	66.45	192.63	51.84	0.04	0.21	-2.71
Sub63	266.83	84.07	228.97	65.58	0.06	0.24	-2.76
Sub44	269.78	86.86	230.66	67.76	0.07	0.26	-2.81
Sub26	179.54	37.33	162.73	29.12	0.01	0.10	-0.65
Sub76	183.00	38.38	165.72	29.94	0.01	0.11	-2.24
Sub77	659.40	239.32	551.64	186.69	0.13	0.36	-2.81

Table 5.14: K values computed for different return periods and flood flows stations.

GRIDS	**K for Log PT3**				
	RP10	**RP20**	**RP50**	**RP100**	**RP200**
Mullaperiyar	1.338	2.114	2.679	3.23	3.772
Sub39	1.34	2.081	2.614	3.131	3.637
Sub37	1.34	2.088	2.628	3.152	3.666
Sub36	1.339	2.095	2.642	3.174	3.695
Idukki	1.33	2.158	2.77	3.372	3.968
Sub34	1.339	2.098	2.648	3.183	3.707

Sub35	1.339	2.102	2.656	3.195	3.724
Sub29	1.339	2.1	2.651	3.188	3.714
Sub31	0.915	0.99	1.016	1.029	1.036
Sub23	1.339	2.029	2.516	2.984	3.438
Sub30	1.333	2.145	2.742	3.327	3.906
Sub38	1.257	2.258	3.034	3.82	4.614
Sub67	1.233	2.268	3.079	3.904	4.741
Sub28	1.312	2.203	2.873	3.541	4.246
Sub24	1.339	2.101	2.652	3.189	3.716
Sub27	1.249	2.262	3.049	3.848	4.656
Sub20	1.302	2.219	2.912	3.605	4.398
Sub43	0.96	1.06	1.099	1.121	1.134
Sub17	1.338	2.02	2.502	2.963	3.409
Sub68	1.245	2.264	3.057	3.863	4.679
Sub32	1.32	2.188	2.837	3.48	4.121
Sub21	1.297	1.802	2.135	2.438	2.72
Sub69	0.704	0.715	0.717	0.717	0.717
Sub70	1.302	2.219	2.912	3.604	4.396
Sub16	1.34	2.068	2.59	3.094	3.587
Sub71	1.331	2.155	2.762	3.36	3.952
Sub25	0.756	0.775	0.78	0.781	0.781
Sub18	1.34	2.089	2.63	3.155	3.669
Sub72	0.728	0.742	0.745	0.745	0.745
Sub19	1.142	1.396	1.533	1.641	1.727
Sub9	1.34	2.04	2.536	3.014	3.478
Sub40	1.337	2.127	2.705	3.269	3.826
Sub2	1.328	2.167	2.789	3.402	4.01
Sub4	1.329	2.163	2.78	3.388	3.99
Sub11	1.26	2.257	3.026	3.806	4.593
Sub46	0.712	0.723	0.726	0.726	0.726
Sub5	1.339	2.104	2.659	3.199	3.729
Sub14	1.339	2.036	2.53	3.004	3.465
Sub22	0.763	0.783	0.788	0.79	0.79
Sub56	1.233	2.268	3.078	3.903	4.739
Sub13	1.278	1.74	2.037	2.303	2.547
Sub62	1.305	1.834	2.186	2.51	2.812
Sub6	1.299	1.811	2.148	2.457	2.743
Sub10	1.259	1.682	1.948	2.182	2.393
Sub33	0.72	0.733	0.735	0.736	0.736
Sub8	1.338	2.02	2.501	2.962	3.408
Sub42	0.701	0.711	0.713	0.713	0.713
Sub1	1.277	1.737	2.032	2.296	2.538
Sub3	1.321	1.899	2.293	2.661	3.009
Sub12	1.121	1.352	1.474	1.566	1.638
Sub41	0.939	1.025	1.058	1.075	1.084
Sub61	1.331	1.961	2.398	2.811	3.206

Sub15	0.722	0.735	0.738	0.738	0.738
Sub63	0.71	0.721	0.724	0.724	0.724
Sub44	0.7	0.71	0.712	0.712	0.712
Sub26	1.191	1.507	1.691	1.842	1.97
Sub76	0.835	0.876	0.887	0.891	0.893
Sub77	0.699	0.709	0.711	0.711	0.711

Figure 5.37 shows the subbasin wise computation of extreme flood flows using Gumbel method (Figure 5.37 a to f) and LogPT3 (Figure 5.37 d to l). As per the comparison of extreme flood flows computed for different RPs, the LoGPT3 contain higher flood values than Gumbel. For example: in case of Gumble, for RP 100 and RP 200, the flood values range from 600-1300 and 600-6000 m^3/s, respectively. Whereas, in case of LogPT3, for RP 100 and RP 200, the flood values range from 600-12000 and 600-22000 m^3/s, respectively. Although, at each subbasin scale due to the variation in the size of subbasin and variability in rainfall, corresponding discharge or flood flows vary.

In Figure 5.38, the flood flows extremity has been compared based on different period (RPs) floods computed by Gumbel and LogPT3 methods. In case of RP 10, Gumbel and LogPT3 have shown almost a similar peak, expect one value where Gumbel looks high. While in case of RP20, RP50, RP100 and RP200, the LogPT3 showed consistent high flow values than Gumbel. The difference in flow values between Gumbel and LogPT3 increases as the RP time progresses. For Example: in case of RP 200, the Gumbel method calculated maximum flow peak around 6000 m^3/s, whereas in case of LogPT3, the maximum values corresponded around 22000 m3/s.

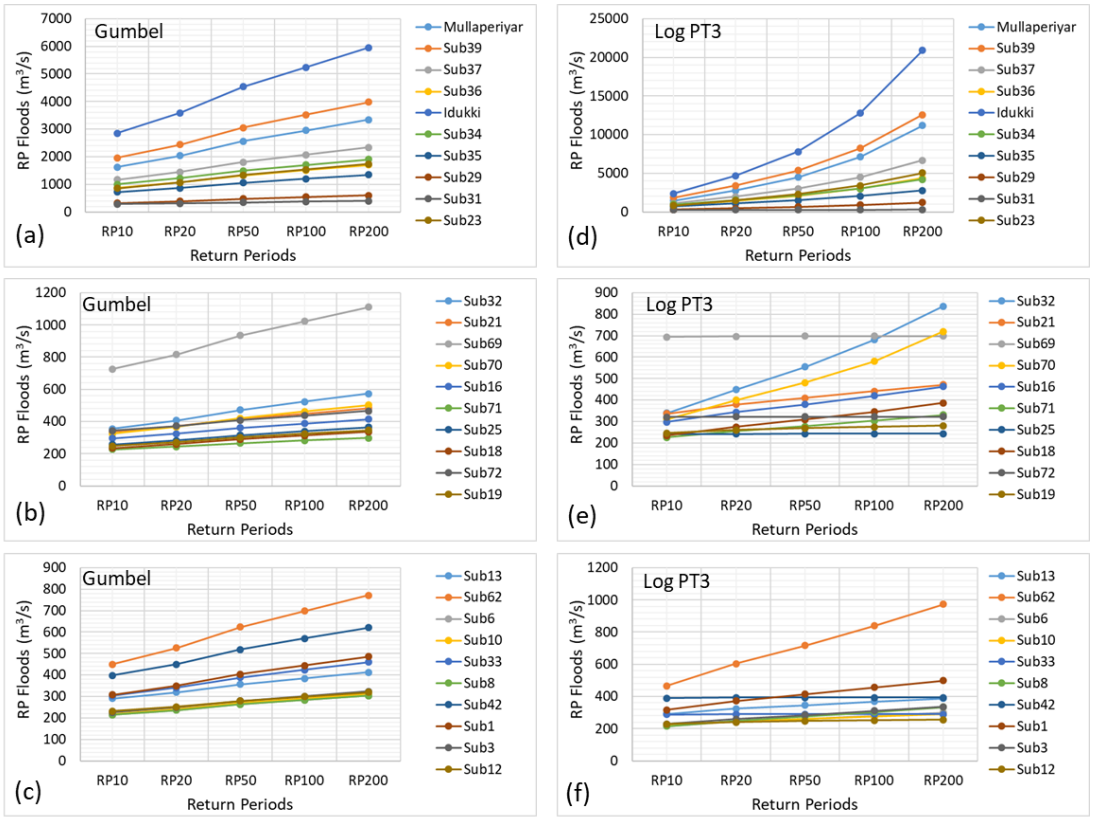

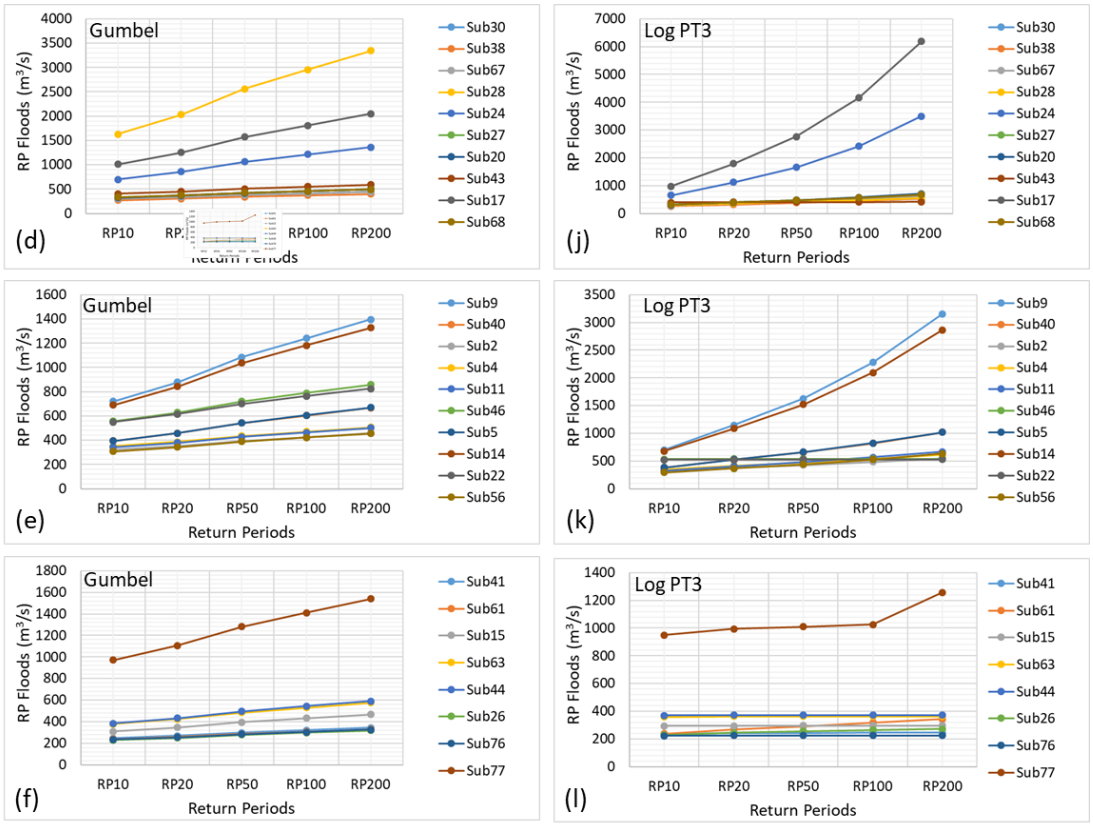

Figure 5.37: Computation of extreme flood flows for different RPs at each subbasin utilizing Gumbel and LogPT3 methods.

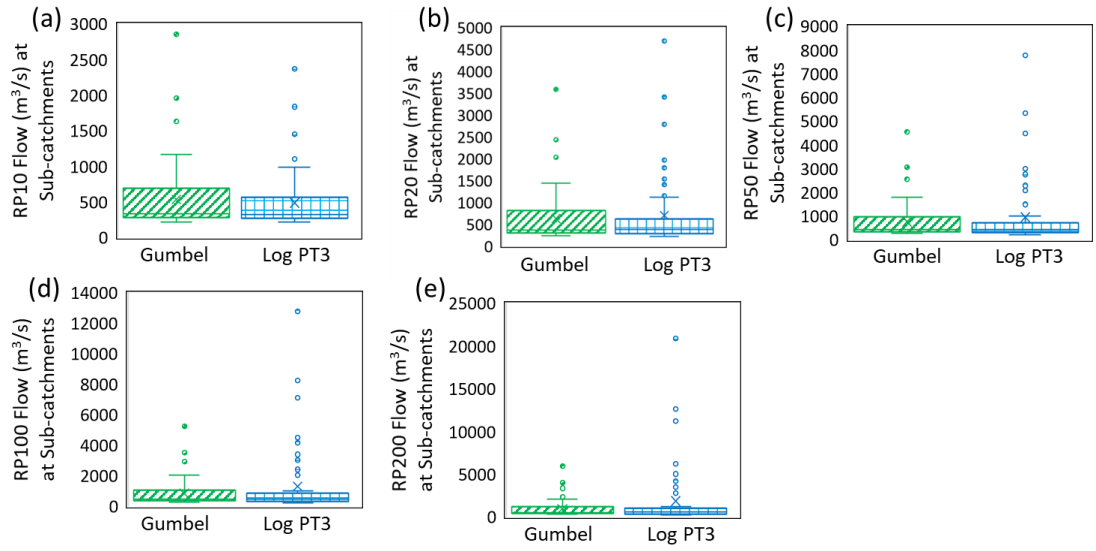

Figure 5.38: Comparison of flood flows extremity as per different RPs at each subbasin utilizing Gumbel and LogPT3.

5.8 GENERATION OF PROBABILISTIC RETURN PERIOD FLOOD MAPS – STEADY STATE FLOW ANALYSIS

In this study, the probabilistic flood inundation maps with depths have been generated after a detailed hydraulic modeling performed in HEC-RAS. For the generation of flood depth maps for a given return period, the flood flows generated at subbasin and Junctions have been utilized. Figures 5.39 (a) and 5.39 (b) show the flood inundation maps computed by LogPT3 and Gumbel, respectively. The main purpose of the creation of probabilistic return period flood maps is to perform a flood plain zoning. Figures 5.40 (a-c) shows the comparison of different RPs based flood inundation areas and their depth as per Gumbel and LogPT3. As per Figure 5.40a, the RP50 based flood maps corresponded flood depth varies from 0.1 to 8 m. Whereas as per RP100 and RP 200, the flood depths vary from 0.01 m to 9.0 (Figure 5.40b) and 0.01 to 10.0 m (Figure 5.40c), respectively for both Gumbel and LogPT3 methods. As per the comparison between Gumbel and LogPT3, a slight variation in the spread areas and flood depths can be observed.

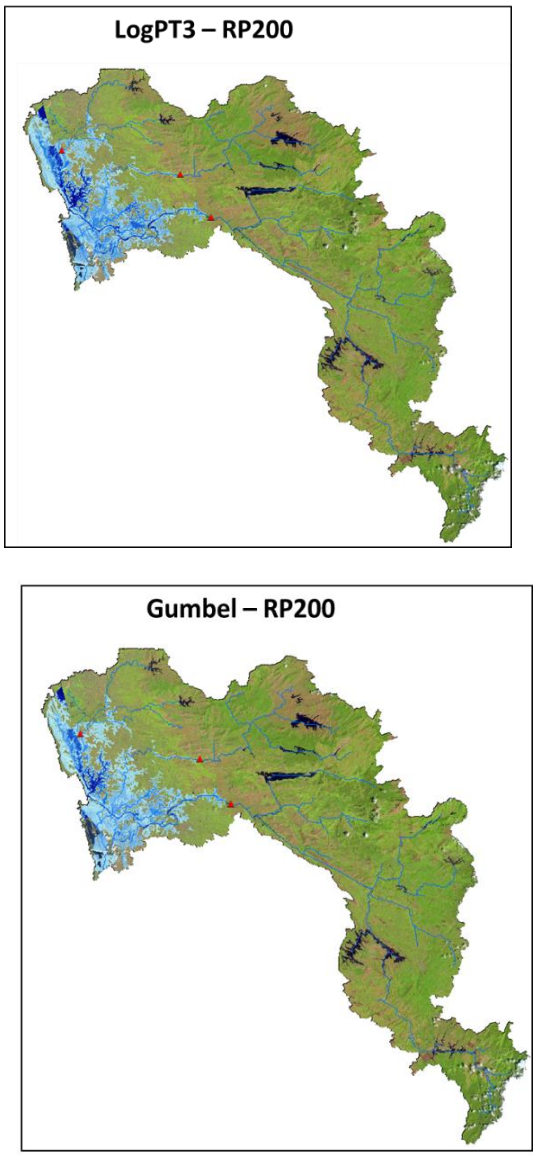

Figure 5.39: Flood maps as per RP 200 computed by (a) LogPT3 and (b) Gumbel methods.

(a)

Gumbel – RP50

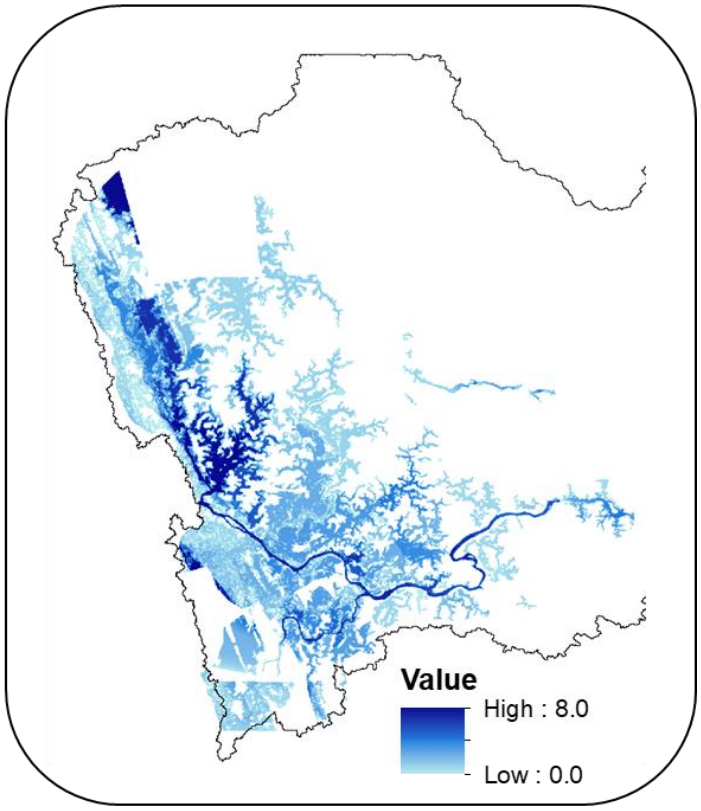

LogPT3 – RP50

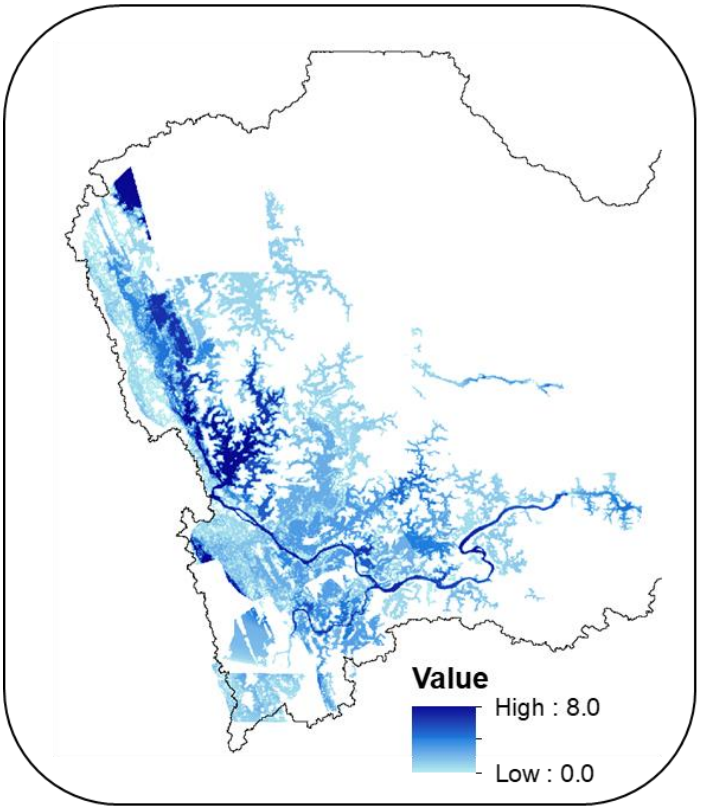

(b) Gumbel – RP100

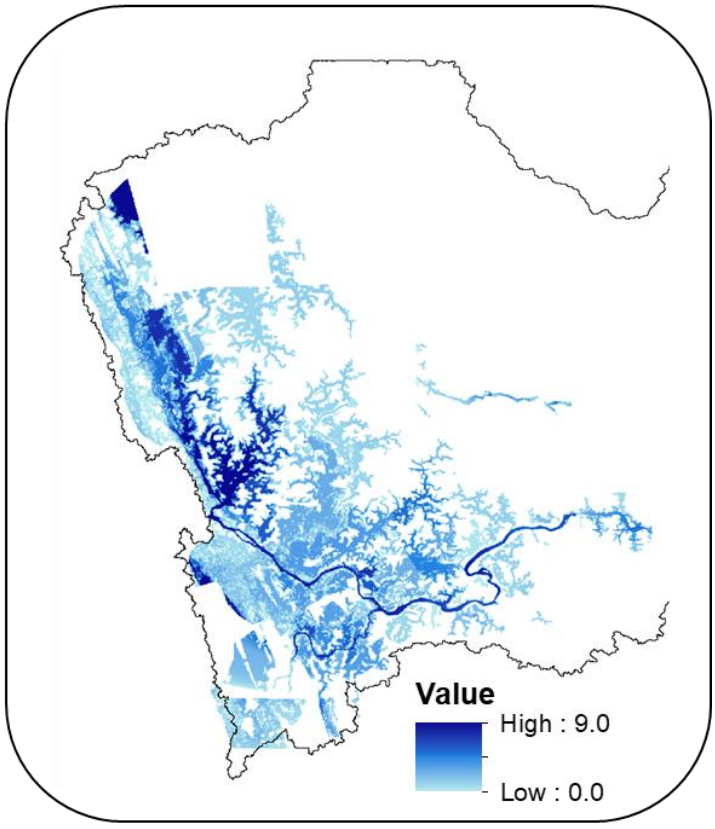

LogPT3 – RP100

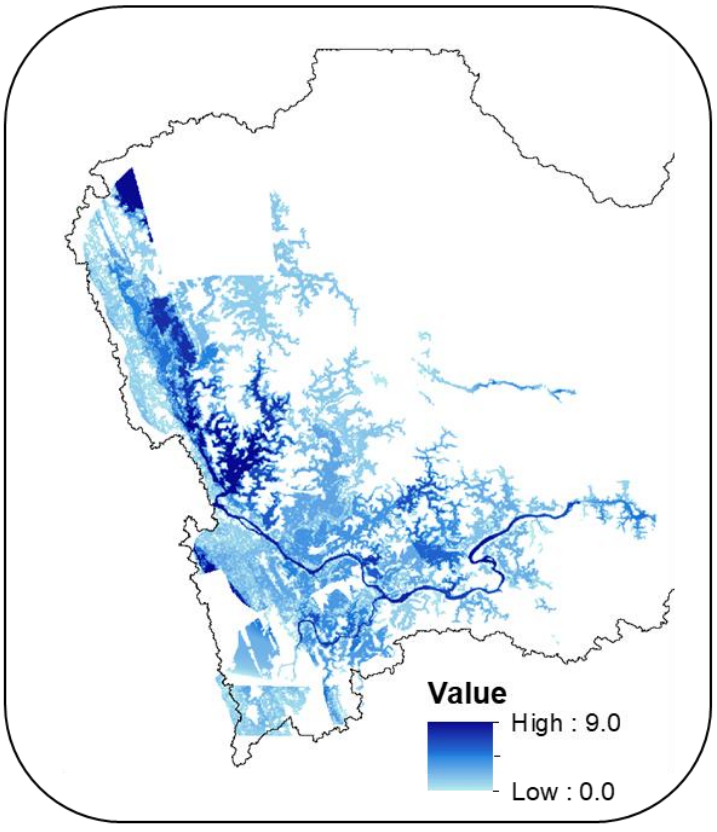

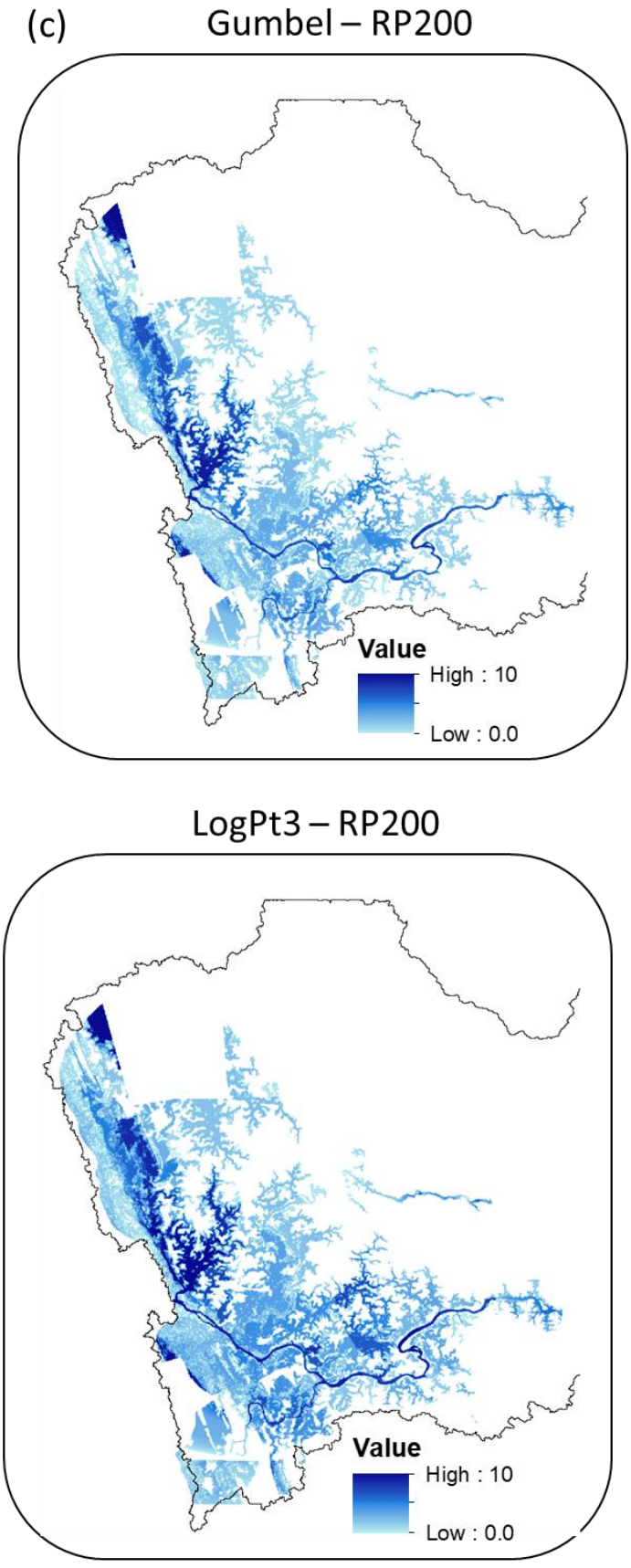

Figures 5.40: Flood inundation and depths as per RP50, (b) RP 100 and (c) RP 200 computed based on Gumbel and LogPT3 methods.

CHAPTER 6: CONCLUSION AND RECOMMENDATION

6.1 MAJOR FINDINGS AND CONCLUSIONS

This study utilized HEC-RTS framework to perform an integrated hydrological – hydrodynamic modeling approach to compute steady and unsteady flood flows as per identified historical flood events and based on long-term simulation. The main components of HEC-RTS such as HEC-DSSVue, HEC-GeoRAS, HEC-HMS and HEC-RAS have been utilized. For hydrodynamic study, 1D and 2D modeling were performed to rout the flood flows. In this study, various kind of thematic, real time meteorological and hydro-observation and remote sensing datasets have been used. A high spatial resolution (12.5m) ALOS PALSAR digital elevation model (DEM) has been used to derive the watershed and channel properties, like area, subbasins, slope, flow direction, cross sections, flow path, riverbanks etc. All these parameters have been derived successfully utilizing HEC-GeoRAS tool on ARCGIS platform. HEC-DSSVue has been used to organize the time series and other datasets which were required to setup the HEC-HMS, HEC-RESSIM and HECRAS tools in HEC-RTS system. HEC-HMS has been successfully setup at event basis and continuous simulation steps to compute the historical and real time flood discharge at different locations of the Periyar river basin. HEC-RESSIM was utilized to re-construct the historical event that is happened in August 2018 (i.e. well known as Kerala Floods 2018). The minimum and maximum reservoir release rules are applied to Mullaperiyar and Idukki reservoirs to regulate the floods and attenuate the extreme flood peaks before releasing flood discharge in the downstream portion. The results obtained in the study have been compared with (i) CWC based datasets (ii) satellite (Sentinel) derived flood maps prepared by DARTMOUTH Flood Agency USA. The results of this study compared well with the above two results. After that Rainfall and Flood Frequency Analysis has been done to generate the different return period-based floods to generate the probabilistic flood inundation maps. HEC-RAS 1D and 2D unsteady simulations were performed to generate the historical floods and real time floods. Other hydrodynamic variables such as rating curves, flood depth, velocity, water surface elevation etc. have been computed as per steady and unsteady flow analysis through HEC-RAS. The main conclusions drawn from this study are as follows:

- The bias corrected rainfall datasets (TRMM+GPM) were generated to construct the historical greatest Kerala Flood event 2018 on a three-hourly basis. The same event is also generated in using the daily rainfall datasets. Both observations show a slight variation in flood extreme high peaks and the 3-hourly rainfall datasets found more reliable to construct the real time extreme flood event. The same bias correction methodology can be applied in other studies.
- HEC-HMS has been constructed on event basis and continuous simulation basis. Initially, the HE-7 (i. e. Kerala flood event 2018) has been performed utilizing CN method and the extreme flood conditions and parameters were optimized. The optimized parameters as per HE-7 were used for the simulation of other HEs. The flood flows generated at each Subbasin and Junctions. The flood discharge generated based on the event wise and continuous time step simulations were used for the flood frequency analysis
- This study also performed Rainfall and Flood frequency analysis to generate flood discharges for different return periods (RPs). For the FFA, the three extreme value distribution methods were evaluated by RMSE and MSE and then worst performing method was removed and Gumbel and Log Pearson Type 3 methods were utilized.
- In this study, the RESSIM module of HEC-RTS is mainly used for the construction of HE-7 (Kerala Floods, 2018). For reservoir simulation, two reservoirs such as Mullaperiyar and Idukki which are situated at the upstream portion were considered for the routing of flood discharge in the downstream portion. Considering extreme flood conditions, the minimum and maximum reservoir release rules were formulated, and the extreme flood peaks are attenuated. The

reservoir released floods were compared at the downstream discharge gauge i. e. Neeleswaram. The flood discharge which was computed and reported by CWC is found comparable to the present study observations.

- Finally, flood inundation maps were prepared for different RPs computed by Gumbel and LogPT3. These maps can be utilized for flood plain zoning and making guidelines for flood management plans.

6.2 RECOMMENDATIONS

In this study, all the components of HEC-RTS system such as HEC-DSSVue, HEC-HMS, HEC-RESSIM and HEC-RAS have been successfully setup, simulated and tested based on different flood conditions such as short term (event wise simulation for HEs) and continuous long-term simulations. The long-term simulation of floods can be utilized to generate virgin flood flows at each subbasin scale. Based on that subbasin wise and small-scale flood protection and management practices can be developed. Based on event wise and continuous simulations, the modelled parameters and variables which are required to perform hydrologic and hydrodynamic flood modeling optimized successfully and thus they can be utilized for similar event based future extreme flood conditions. The long-term flood flows can also be generated and then flood modeling can be performed to generate probabilistic flood inundation maps as per consideration of future climate model datasets. In this way, the impact of climate change can be incorporated while making the long-term flood protection and management policies.

ACKNOWLEDGEMENT

We sincerely thanks to National Institute of Hydrology Roorkee for granting us permission to carry out this research work and for providing necessary facilities and services to complete this work. We thank to the Dr. Sanjay. K. Jain (Scientist G and Head WRSD NIH) and Dr. M.K. Goel (Scientist G and Head GWHD NIH) for providing their sincere guidance and every kind of help. We also thankful to our Ex-Director NIH Dr. Sharad K Jain, and present Director NIH Dr. J.V. Tyagi for giving their full cooperation and support for the completion of this research study. We thank to Earth explorer NASA, Bhuvan ISRO India, IMD India, IITM Pune India, CWC India, CEIWR-HEC USA for providing the necessary datasets and software to carry out the research works.

BIBLIOGRAPHY

- Ali, H., Modi, P. and Mishra, V., 2019. Increased flood risk in Indian sub-continent under the warming climate. *Weather and Climate Extremes*, *25*, p.100212.
- Anwat, V.K., Hire, P.S., Pawar, U.V. and Gunjal, R.P., 2021. Analysis of Magnitude and Frequency of Floods in the Damanganga Basin: Western India.
- Ashrit, R., Indira Rani, S., Kumar, S., Karunasagar, S., Arulalan, T., Francis, T., Routray, A., Laskar, S.I., Mahmood, S., Jermey, P. and Maycock, A., 2020. IMDAA Regional Reanalysis: Performance Evaluation During Indian Summer Monsoon Season. *Journal of Geophysical Research: Atmospheres*, *125*(2), p.e2019JD030973.
- Bekele, D.M., Ayana, M.T., Mohammed, A.K., Lohani, T.K. and Shabaz, M., 2021. Prophesying the stream flow and perpetrating the performance of Halele-Werabessa reservoirs of Ethiopia using HEC-HMS and HEC-ResSim. *World Journal of Engineering*.
- Bezak, N., Brilly, M. and Šraj, M., 2014. Comparison between the peaks-over-threshold method and the annual maximum method for flood frequency analysis. *Hydrological Sciences Journal*, *59*(5), pp.959-977.
- Bharadwaj, R.S., Thube, A.D., Vivekanandan, N. and Srishailam, C., 2019. Intercomparison of Estimators of Gumbel Distribution using Goodness-of-Fit Tests for Estimation of Extreme Rainfall.
- Cheng, X., Ma, X., Wang, W., Xiao, Y., Wang, Q. and Liu, X., 2021. Application of HEC-HMS Parameter Regionalization in Small Watershed of Hilly Area. *Water Resources Management*, pp.1-16.
- Devia, G.K., Ganasri, B.P. and Dwarakish, G.S., 2015. A review on hydrological models. *Aquatic Procedia*, *4*, pp.1001-1007.
- Dubey, S. and Goyal, M.K., 2020. Glacial lake outburst flood hazard, downstream impact, and risk over the Indian Himalayas. *Water Resources Research*, *56*(4), p.e2019WR026533.
- Grimaldi, S., Nardi, F., Piscopia, R., Petroselli, A. and Apollonio, C., 2020. Continuous hydrologic modelling for design simulation in small and ungauged basins: A step forward and some tests for its practical use. *Journal of Hydrology*, p.125664.
- Gupta, V., Jain, M.K., Singh, P.K. and Singh, V., 2020. An assessment of global satellite-based precipitation datasets in capturing precipitation extremes: A comparison with observed precipitation dataset in India. *International Journal of Climatology*, *40*(8), pp.3667-3688.
- Hunt, K.M. and Menon, A., 2020. The 2018 Kerala floods: a climate change perspective. *Climate Dynamics*, *54*(3), pp.2433-2446.
- Maneshdavi, A., NIKBAKHT SHAHBAZI, A.L.I.R.E.Z.A. and Fathian, H., 2018. Rainfall-Runoff continuous simulation in Abolabbas watershed using SMA by HEC-HMS. *Iranian Journal of Soil and Water Research*, *49*(2), pp.317-327.
- Mishra, V., Shah, R., Azhar, S., Shah, H., Modi, P. and Kumar, R., 2018. Reconstruction of droughts in India using multiple land-surface models (1951–2015). *Hydrology and Earth System Sciences*, *22*(4), pp.2269-2284.
- Mohammed, K., Saiful Islam, A.K.M., Tarekul Islam, G.M., Alfieri, L., Bala, S.K. and Uddin Khan, M.J., 2017. Impact of high-end climate change on floods and low flows of the Brahmaputra River. *Journal of Hydrologic Engineering*, *22*(10), p.04017041.
- Mohanty, M.P., Mudgil, S. and Karmakar, S., 2020. Flood management in India: a focussed review on the current status and future challenges. *International Journal of Disaster Risk Reduction*, p.101660.
- Mukherjee, S., Aadhar, S., Stone, D. and Mishra, V., 2018. Increase in extreme precipitation events under anthropogenic warming in India. *Weather and climate extremes*, *20*, pp.45-53.
- Otkin, J.A., Svoboda, M., Hunt, E.D., Ford, T.W., Anderson, M.C., Hain, C. and Basara, J.B., 2018. Flash droughts: A review and assessment of the challenges imposed by rapid-onset

droughts in the United States. *Bulletin of the American Meteorological Society*, *99*(5), pp.911-919.

- Ouédraogo, W.A.A., Raude, J.M. and Gathenya, J.M., 2018. Continuous modeling of the Mkurumudzi River catchment in Kenya using the HEC-HMS conceptual model: Calibration, validation, model performance evaluation and sensitivity analysis. *Hydrology*, *5*(3), p.44.
- Refsgaard, J.C. and Knudsen, J., 1996. Operational validation and intercomparison of different types of hydrological models. *Water Resources Research*, *32*(7), pp.2189-2202.
- Saksena, S., 2015. Investigating the role of DEM resolution and accuracy on flood inundation mapping. In *World Environmental and Water Resources Congress 2015* (pp. 2236-2243).
- Salami, R.O., Giggins, H. and Von Meding, J.K., 2017. Urban settlements' vulnerability to flood risks in African cities: A conceptual framework. *Jàmbá: Journal of Disaster Risk Studies*, *9*(1), pp.1-9.
- Schiermeier, Q., 2019. Eat less meat: UN climate-change report calls for change to human diet. *Nature*, *572*(7769), pp.291-292.
- Singh, V. and Goyal, M.K., 2017. Spatio-temporal heterogeneity and changes in extreme precipitation over eastern Himalayan catchments India. *Stochastic Environmental Research and Risk Assessment*, *31*(10), pp.2527-2546.
- Sood, A. and Smakhtin, V., 2015. Global hydrological models: a review. *Hydrological Sciences Journal*, *60*(4), pp.549-565.
- Srinivas, R., Singh, A.P. and Deshmukh, A., 2018. Development of a HEC-HMS-based watershed modeling system for identification, allocation, and optimization of reservoirs in a river basin. *Environmental monitoring and assessment*, *190*(1), pp.1-18.
- Sudheer, K.P., Bhallamudi, S.M., Narasimhan, B., Thomas, J., Bindhu, V.M., Vema, V. and Kurian, C., 2019. Role of dams on the floods of August 2018 in Periyar River Basin, Kerala. *Current Science (00113891)*, *116*(5).
- Swain, A. and Vyas, N., 2020. An Analysis of Preparedness and The Impact of Floods in India. *Indian Journal of Public Health Research & Development*, *11*(6).
- Tanaka, T., Tachikawa, Y., Ichikawa, Y. and Yorozu, K., 2017. Impact assessment of upstream flooding on extreme flood frequency analysis by incorporating a flood-inundation model for flood risk assessment. *Journal of hydrology*, *554*, pp.370-382.
- Thakur, B., Parajuli, R., Kalra, A., Ahmad, S. and Gupta, R., 2017. Coupling HEC-RAS and HEC-HMS in precipitation runoff modelling and evaluating flood plain inundation map. In *World Environmental and Water Resources Congress 2017* (pp. 240-251).
- Wang, Y., Sang, G., Jiao, C., Xu, Y. and Zheng, H., 2018, July. Flood simulation and parameter calibration of small watershed in hilly area based on HEC-HMS model. In *IOP Conference Series: Earth and Environmental Science* (Vol. 170, No. 3, p. 032093). IOP Publishing.
- Yang, W., Chen, H., Xu, C.Y., Huo, R., Chen, J. and Guo, S., 2020. Temporal and spatial transferabilities of hydrological models under different climates and underlying surface conditions. *Journal of Hydrology*, *591*, p.125276.